Radiolytic degradation of 2-methylisoborneol and geosmin in water: reactive radical species and transformation pathways.

CHRISTOPHORIDIS, C., PESTANA, C.J., KALOUDIS, T., LAWTON, L.A., TRIANTIS, T.M. and HISKIA, A.

2021

Chemical Engineering Journal Advances 8 (2021) 100196

Contents lists available at ScienceDirect

Chemical Engineering Journal Advances

journal homepage: www.sciencedirect.com/journal/chemical-engineering-journal-advances

Radiolytic degradation of 2-methylisoborneol and geosmin in water: Reactive radical species and transformation pathways

C. Christophoridis [a], C.J. Pestana [b], T. Kaloudis [a,c], L.A. Lawton [b], T.M. Triantis [a], A. Hiskia [a,*]

[a] Laboratory of Photo-Catalytic Processes and Environmental Chemistry, Institute of Nanoscience & Nanotechnology, NCSR "Demokritos", Patr. Gregoriou E' & 27 Neapoleos Str, Agia Paraskevi, Athens 15341, Greece

[b] School of Pharmacy and Life Sciences, Robert Gordon University, Aberdeen, United Kingdom

[c] Water Quality Control Department, Athens Water Supply and Sewerage Company (EYDAP SA), Athens, Greece

ARTICLE INFO

Keywords:
Water radiolysis
Gamma irradiation
Taste and odor
Transformation products
Reactive species
Degradation rate

ABSTRACT

Water radiolysis can serve as a useful tool to study the degradation of organic pollutants in water. Manipulation of the radiolytic system enables the selective production of reactive species (RS) with known yields. Our aim was to explore the effects of the radiolytically produced RS on commonly occuring water taste and odor compounds (T&O), 2-methylisoborneol (MIB) and geosmin (GSM). Observed degradation rate constants differ among experimental conditions/dominant RS and follow the order: $HO^{\bullet}>H^{\bullet}>>e_{aq}^{-}>(O_2^{-\bullet}/HO_2^{\bullet})$, ranging from 0.002 Gy^{-1} $(O_2^{-\bullet}/HO_2^{\bullet})$ to 0.083 Gy^{-1} $(HO^{\bullet})$ for MIB and from 0.006 Gy^{-1} $(O_2^{-\bullet}/HO_2^{\bullet})$ to 0.068 Gy^{-1} $(HO^{\bullet})$ for GSM. Degradation by $HO^{\bullet}$ was very efficient, requiring 1.14 and 1.49 μmoles of $HO^{\bullet}$ for each degraded μmole of MIB and GSM, respectively. The oxidative degradation of MIB by $HO^{\bullet}$ proceeds with the production of carbonyl- and hydroxyl-containing transformation products (TPs), leading to linear structures, while for GSM degradation proceeds with ring opening, followed by formation of carboxyl-groups. Fewer TPs are produced by $HO_2^{\bullet}$, while degradation with $H^{\bullet}$ led to numerous TPs, via dehydroxylation, dehydration and ring opening. Degradation with e_{aq}^{-}, yielded demethylated and rearranged TPs with formation of double bonds.

Introduction

Taste and odor (T&O) are important esthetic parameters of water quality that largely determine its acceptability by consumers [1]. A plethora of compounds of natural or anthropogenic origin can be responsibe for water T&O, while some compounds are sensed by the human nose at low ng L^{-1} concentrations [2]. In surface waters, a major source of T&O are cyanobacteria (prokaryotic organisms) as well as eukaryotic microorganisms, commonly known as "algae" that produce a range of volatile metabolites with diverse chemical structures and odor characteristics [3]. Their occurrence in water often causes consumer complaints, making water unacceptable for esthetic reasons, with serious negative socioeconomic impacts for water supplies, aquaculture and tourism [3,4].

The most widely known and frequently occurring T&O compounds are the terpenoids 2-methylisoborneol (MIB) and geosmin (GSM) (Fig. 1). MIB (1,6,7,7-tetramethylbicyclo[2.2.1]heptan-6-ol, $C_{11}H_{20}O$) has a strong "musty" odor, with an odor threshold at 6 ng L^{-1} in water [2]. GSM (4*S*,4a*S*, 8a-4,8a-dimethyl-1,2,3,4,5,6,7,8-octahydronaphthalen-4a-ol, $C_{12}H_{22}O$) has a strong "muddy/earthy" smell with an odor threshold at 4 ng L^{-1} in water [2]. MIB and GSM are mostly associated with cyanobacteria in water but they are also produced by actinomycetes in soil and water [5].

Conventional treatment processes such as coagulation, sedimentation, filtration [6], granulated activated carbon (GAC) [7,8] and powered activated carbon (PAC) [9,10] have presented limitations in the removal of MIB and GSM from water, since the removal efficiency is affected by several parameters, e.g. the type of adsorbent, the contact time of application, etc. [11,12]. Air-stripping has been proven ineffective and not economical as well, due to the moderately volatile nature and low Henry's constants of MIB and GSM [13,14]. Biodegradation has been shown to be effective, but it requires the constant operation of biologically active sand filters [15] or dual medium biological filters [16], while occurrence of MIB and GSM can be seasonal or episodic [11]. Application of conventional disinfectants/oxidants (chlorine, chlorine dioxide, potassium permanganate) is generally not effective in removing MIB and GSM, due to the resistance of tertiary alcohols to degradation [17].

The above limitations and the ever-increasing demand for high-

* Corresponding author.
E-mail address: a.hiskia@inn.demokritos.gr (A. Hiskia).

https://doi.org/10.1016/j.ceja.2021.100196
Received 2 September 2021; Received in revised form 15 October 2021; Accepted 17 October 2021
Available online 18 October 2021

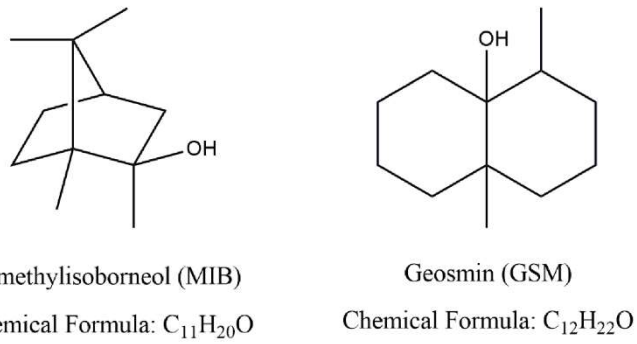

Fig. 1. Structures and chemical formulae of MIB and GSM.

quality drinking water, has led to the search for viable alternatives such as advanced oxidation processes (AOPs) [18]. AOPs are mainly driven by reactive oxygen species (ROS), i.e. hydroxyl radicals ($HO^{\bullet}$), superoxide anions ($O_2^{-\bullet}$), hydroperoxyl radicals ($HO_2^{\bullet}$), and hydrogen peroxide (H_2O_2) [19].

The removal of MIB and GSM from water with AOPs has been tested in the past with use of O_3 [20,21], O_3/H_2O_2 [22], O_3/UV [23,24], UV/H_2O_2 [25], UV/VUV photolysis [26], UV/persulfate [27,28], UV/chlorine or ClO_2 [29,30], photocatalysis with UV/Vis/TiO_2 or UV/polyoxometallates [31–34], sonolysis [14] and coupled photocatalysis/biodegradation [35], however the role of individual ROS generated by various AOPs has not been thoroughly investigated. For example, MIB and GSM are effectively degraded using TiO_2 or polyoxometallates/UV photocatalysis, which produce mainly $HO^{\bullet}$ [32], while their degradation is not efficient with doped TiO_2/visible light [36], possibly due to predominance of other ROS [31]. Shedding light onto ROS-driven degradation mechanisms is essential to select the most efficient AOPs for specific applications and to fine-tune the processes.

Water radiolysis, i.e. irradiation of water with high-energy gamma rays or electron beams, produces instantaneous transformation of water molecules, through energy transfer to the orbital electrons, resulting in the breakage of interatomic bonds and the formation of highly reactive products [37]. The products of the process include various ROS ($HO^{\bullet}$, $O_2^{-\bullet}$), and other reactive species (RS), such as hydrogen atoms, $H^{\bullet}$, and hydrated electrons, e_{aq}^- [38,39]. Among them, $HO^{\bullet}$ is the predominant oxidative species, by virtue of its high yield as well as of its high oxidation potential [40]. Radical reactions are presented in Supplementary Material, page 2.

Water treatment by radiolysis has been studied in the past [41] with various target pollutants, including pharmaceuticals [42–45], pesticides [46–48], phenolic compounds [49–51] and cyanobacterial toxins [52–54]. Apart from its potential to degrade a wide range of pollutants, water radiolysis can also be applied to study the effects of individual RS on pollutants, since the system can be manipulated to generate single RS [55], which are common to those produced during AOPs. Furthermore, the same RS could also be found in natural aquatic systems and play an important role in environmental processes [56]. Therefore, understanding the role of individual RS on degradation processes of target compounds could also provide information on their fate in natural water systems.

To the best of the authors' knowledge, this is the first study regarding the degradation of MIB and GSM using water radiolysis. Although in the past, the degradation of these compounds has been studied using various AOPs which produce several RS, nevertheless, the role of individual RS in the degradation process has not been elucidated. This knowledge could cover important gaps in the fundamental understanding of RS-driven redox processes that are common in AOPs for water treatment and enable the optimization and fine-tuning of AOPs targeted at the removal of MIB and GSM from water. Water radiolysis is an experimental tool able to obtain this knowledge, since is can be used to produce individual RS at a known and reproducible yield, which is helpful to understand the role of each RS in the degradation mechanism of MIB and GSM, as well as several organic pollutants with similar structure.

Based on the above, the main aims of this study were to evaluate the degradation of MIB and GSM using water radiolysis and to elucidate the roles of individual RS on the degradation pathways of MIB and GSM. The objectives were (a) to evaluate and compare the degradation kinetics of MIB and GSM by various RS ($HO^{\bullet}$, $O_2^{-\bullet}$, $HO_2^{\bullet}$, $H^{\bullet}$, e_{aq}^-) and (b) to identify the transformation products (TPs) and clarify the degradation pathways.

Materials and methods

Chemicals and reagents

Standards of GSM (98% purity) and MIB (99.8% purity) were purchased from Wako Pure Chemical Industries Ltd, tertiary butyl alcohol (TBA) (≥99.0%) and dichloromethane (DCM) of analytical grade from Sigma Aldrich, formic acid (HCOOH) (>98%) and perchloric acid (>98%) from Riedel-de Haën. High purity water (18.2 MΩ) was produced on-site, using a Temak TSDW10 system. High-purity oxygen, nitrous oxide and nitrogen were obtained from Linde Corporate Hellas.

Radiolysis experiments

Water radiolysis was carried out in a ^{60}Co 6500 Ci Gamma Chamber (model 4000A, Isotope Group, Bhaba Atomic Research centre, Trombay, India). The dose rate was 0.064 Gy s^{-1}, (1 Gy equals 1 J kg^{-1} or 1 J L^{-1}) and was determined by the Fricke dosimeter, which is based on the oxidation of ferrous (Fe^{2+}) to ferric (Fe^{3+}) ions and the subsequent measurement of Fe^{3+} absorbance at 304 nm [57] in a PE Lambda 19 spectrophotometer (Perkin Elmer).

In a typical degradation experiment, aqueous solutions (10 mL) of MIB or GSM at initial concentration of 1 mg L^{-1} (6 μM and 5.5 μM, respectively) were placed in borosilicate 12 mL glass vials and closed with serum caps. The vials were placed in specified positions in the irradiation chamber and each one was irradiated for a specified period of time (0–60 min) in order to achieve the desired absorbed dose, up to 230.4 Gy. Experiments for identification of TPs were carried out at initial concentrations of MIB and GSM, at 10 mg L^{-1} (60 and 55 μM, respectively) after 30 min of irradiation (115.2 Gy). Degradation experiments were performed in triplicate and the error bars on figures represent the mean ± SD of the replicates.

The following RS are produced during aerated water radiolysis, originating from water molecules: e^-_{aq} (0.28), $H^{\bullet}$ (0.06), $HO^{\bullet}$ (0.28), $O_2^{-\bullet}$ /$HO_2^{\bullet}$ (0.0027). H_2O_2 (0.07), H_2 (0.05) and H^+ (0.27) are also produced via secondary reactions, as shown in Supplementary Material, page 2. The values in brackets are the well known radiation-chemical yields of the produced species, which are expressed as G-values, i.e. number of μmol of RS produced per Joule of absorbed energy (G-values, μmol J^{-1}), as shown in Table 1 (column "aerated") [55].

In order to study the effects of single RS, controlled experimental

Table 1
Selected experimental conditions for the production of specific RS along with the radiation-chemical yield (G value) of their production [55,58] given in μmol of RS formed per J of absorbed energy. Predominant RS are given in bold italics.

Prominent RS	G (RS) value (μmol of RS J^{-1}) Experimental Conditions aerated	N_2O	Deaerated/ TBA	Deaerated/ TBA pH 1	O_2	O_2/ HCOOH
e_{aq}^-	***0.28***	0	***0.28***	0	0	0
$H^{\bullet}$	0.06	0.06	0.06	***0.34***	0	0
$HO^{\bullet}$	***0.28***	***0.56***	0	0	***0.28***	0
$O_2^{-\bullet}$ / $HO_2^{\bullet}$	0.0027	0	0	0	***0.34***	***0.62***

conditions with use of selective scavengers were applied, as shown in Table 1 [55,58]. For this purpose, the system can be manipulated to produce solely $HO^{\bullet}$ by the use of nitrous oxide (N_2O), which quantitatively converts the e_{aq}^- to $HO^{\bullet}$ [58], as shown in detail in Supplementary Material, page 2. The predominant formation of e_{aq}^- is achieved by irradiation of deaerated aqueous solutions, in the presence of TBA (initial concentration 2×10^{-2} M), which acts as a $HO^{\bullet}$ scavenger. $H^{\bullet}$ is produced by irradiation of dearerated water solution, in the presence of TBA (initial concentration 2×10^{-2} M) with adjustment to acidic pH to 1, using prechloric acid. Radicals $O_2^{-\bullet}$ / $HO_2^{\bullet}$ are predominantly generated by irradiation in saturated water solutions with oxygen, in the presence of HCOOH (initial concentration 2×10^{-2} M).

Calculation of rate constants and yields

Observed degradation rate constants were calculated by fitting the plots (concentrations vs absorbed dose) to a first-order kinetic model, as described by Eqs. (1) and (2) [44]:

$$Rate = -\frac{d[C]}{dD} = k_{obs}[C] \tag{1}$$

$$-ln\left(\frac{C}{C_0}\right) = k_{obs}D \tag{2}$$

where:

- C (μmol L^{-1}) is the concentration of MIB or GSM
- D (Gy) is the absorbed radiation dose
- k_{obs} (Gy^{-1}) is the observed reaction rate constant based on absorbed dose

The radiation-chemical yield (G value, μmole J^{-1}) of MIB or GSM degradation, defined as the amount of MIB or GSM transformed (ΔC, μmol L^{-1}) per unit of absorbed dose (D, Gy), was calculated using Eq. (3) [43,59].

$$G\ (MIB\ or\ GSM) = \frac{(\Delta C)}{(D)} \tag{3}$$

An indicator of the efficiency of each RS to degrade MIB or GSM is ratio Y, which is given in Eq. (4).

$$Y(MIB\ or\ GSM) = \frac{G\ (RS)}{G(MIB\ or\ GSM)} \tag{4}$$

Y indicates the μmoles of RS which are necessary to degrade one μmole of MIB or GSM under the selected experimental conditions.

Chemical analysis

Monitoring of MIB and GSM was carried out by headspace solid-phase microextraction (HS-SPME) followed by gas chromatography – mass spectrometry (GC–MS) [32,60]. More specifically, samples of 2 mL were placed in 4 mL screw-capped headspace vials with PTFE-lined silicone septa. A magnetic stir bar and sodium chloride (750 mg) were added to the vials. A fiber coated with polydimethylsiloxane (PDMS), 100 μm coating thickness (Supelco) was inserted in the headspace of the sample and the vial was extracted at 70 °C for 30 min while stirring. Samples were analyzed in an Agilent 6890 Series GC–MS system, equipped with an Agilent HP-5 ms capillary column (30 m × 0.25 mm × 0.25 μm) coupled to an Agilent 5973 mass selective detector. The GC oven temperature gradient program started from 50 °C (held for 1 min) and ended at 230 °C (held for 6 min), with a ramp (12 °C min^{-1}) under constant helium flow (0.8 mL min^{-1}). Desorption was carried out in splitless mode at 250 °C. Detection was performed in selected ion monitoring (SIM) mode at *m/z*: 95 (MIB) and 112 (GSM). Data acquisition and instrument control were performed using the Agilent MSD Chem-Station software.

Detection and identification of TPs was carried out using a Bruker 456-TQ GC–MS/MS (triple quadrupole mass spectrometer), equipped with a Rxi-5 MS column, 30 m x 0.25 mm x 0.25 μm (Restek). Samples (10 ml) were extracted with DCM and then injected (2 μl) into the GC system in splitless mode. A GC oven temperature gradient program from 35 °C to 250 °C at 10 °C min^{-1} and at constant helium flow (1 mL min^{-1}) was used. MS was performed in full-scan mode, with a *m/z* range from 50 to 500 amu. Identification of new TPs was based on the NIST MS library. In addition, the chromatographic system was calibrated for determination of Linear Retention Indices (LRI) of eluting compounds, using the standardized n-alkane method [61]. LRIs of suspect compounds were compared to LRIs reported for the same column in NIST webbook or publications. The Bruker MSWS software was used for data acquisition and instrument control.

Results and discussion

Water radiolysis experiments were conducted under various experimental conditions to study the effect of single RS on the degradation of MIB and GSM in aqueous solutions. Plots of MIB and GSM ratios of residual concentration (C) to initial concentration (C_0) versus absorbed dose (derived from irradiation time and dosimetry) are presented in Fig. 2a,b, respectively. Degradation data show a good fit (coefficient of determination values $R^2 > 0.95$) to a first-order reaction model, as presented in Figs. S1 and S2. Tables 2 and 3 present the kinetic parameters calculated from these data, i.e. k_{obs}, R^2, initial degradation rates, as well as the efficiency of each RS to degrade target compounds (Y), G-values of RS and doses required for 50% ($D_{0.5}$) and 90% ($D_{0.9}$) degradation, respectively).

Radiolytic degradation of MIB and GSM

As shown in Fig. 2a, MIB is generally degraded by water radiolysis under various experimental conditions, where different RS dominate the radiolytic-chemical system. Observed degradation rate constants (k_{obs}) differ among experimental conditions / dominant RS and follow the order: $HO^{\bullet} > H^{\bullet} > HO^{\bullet}$ / $O_2^{-\bullet}$ / $HO_2^{\bullet} > e_{aq}^- > O_2^{-\bullet}$ / $HO_2^{\bullet}$, ranging from maximum 0.083 Gy^{-1} ($HO^{\bullet}$) to minimum 0.002 Gy^{-1} ($O_2^{-\bullet}$ / $HO_2^{\bullet}$) as shown in Table 2. The dose required to remove 50% ($D_{0.5}$) of the initial MIB followed the same trend ranging from 8.35 Gy ($HO^{\bullet}$) to 289 Gy ($O_2^{-\bullet}$ / $HO_2^{\bullet}$).

The degradation rates of GSM (Fig. 2b) were also dependent on experimental conditions and dominant RS. The observed degradation rate constants, k_{obs} (Table 3) followed the same order as in MIB, ranging from maximum 0.068 Gy^{-1} ($HO^{\bullet}$) to minimum 0.006 Gy^{-1} ($O_2^{-\bullet}$ / $HO_2^{\bullet}$). Fig. 2b depicts the degradation profile of GSM, under different experimental conditions. The dose required to remove 50% of the initial GSM ($D_{0.5}$) followed the same trend and ranged from 10.1 Gy ($HO^{\bullet}$) to 124 Gy ($O_2^{-\bullet}$ / $HO_2^{\bullet}$).

Efficiency of RS in degrading MIB and GSM

Among the various experimental conditions applied, the highest degradation rates of MIB and GSM were observed with the addition of N_2O, where $HO^{\bullet}$ was the dominant RS. In this case, the total amount of radiolytically produced e_{aq}^- is quantitatively converted to $HO^{\bullet}$ ($G_{HO\bullet}$ = 0.56 μmol J^{-1}, Table 1, supplementary material, page 2), which accounts for the increase in degradation rate.

The ratio Y (Tables 2 and 3) was 1.14 for MIB and 1.49 for GSM, indicating that for each degraded μmole of MIB and GSM, 1.14 and 1.49 μmoles of $HO^{\bullet}$ were consumed, respectively. Since the experimental conditions were identical, this difference implies the varying reactivity of hydroxyl radicals towards MIB or GSM, which could be attributed to differences in their chemical structures. This indicator is critical in AOPs for water treatment that proceed via $HO^{\bullet}$, since it is directly related to

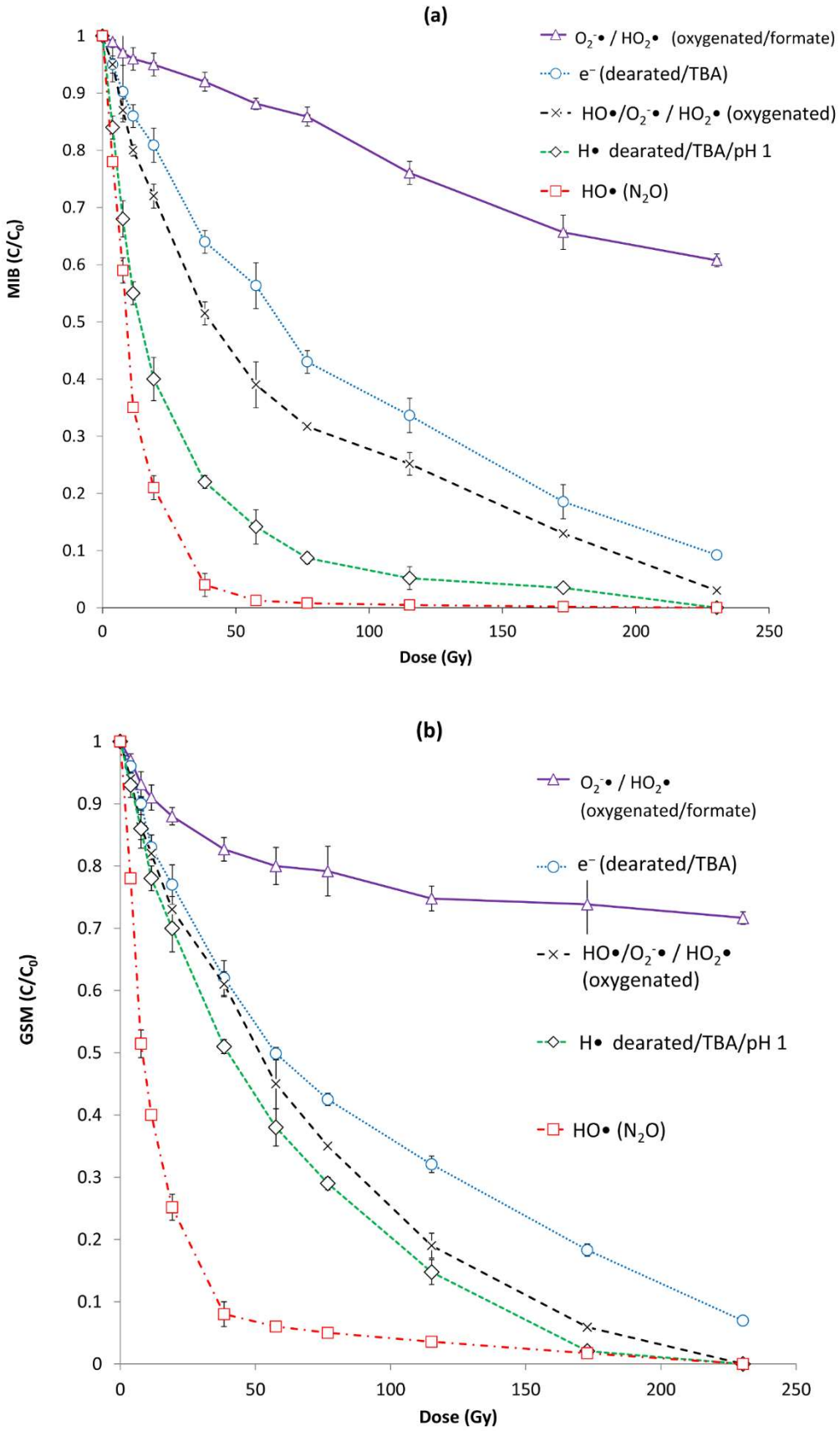

Fig. 2. Degradation of a) MIB and b) GSM, under regulated experimental conditions, producing specific reactive species (RS).

Table 2
Parameters extracted from the assessment of the first order kinetic reaction model for the degradation of MIB.

Experimental Conditions	Prominent RS	k_{obs} (Gy^{-1})	R^2	Initial rate (μmol J^{-1})	Y (MIB)	G (RS) (μmol J^{-1})	$D_{0.5}$ (Gy)	$D_{0.9}$ (Gy)
N_2O	$HO^{\bullet}$	0.083	0.996	0.49	1.14	$HO^{\bullet}$ (0.56)	8.35	27.7
Deaerated / TBA	e_{aq}^-	0.012	0.995	0.07	4.03	e_{aq}^- (0.28)	59.2	197
Deaerated / TBA /pH 1	$H^{\bullet}$	0.042	0.974	0.25	1.36	$H^{\bullet}$ (0.34)	16.5	54.7
O_2	$HO^{\bullet}$ / $O_2^{-\bullet}$ / $HO_2^{\bullet}$	0.017	0.997	0.10	5.92	$HO^{\bullet}$ (0.28) $O_2^{-\bullet}$/$HO_2^{\bullet}$ (0.33)	39.8	132
O_2/HCOOH	$O_2^{-\bullet}$ / $HO_2^{\bullet}$	0.002	0.960	0.01	43.48	$O_2^{-\bullet}$/$HO_2^{\bullet}$ (0.62)	289	959

Table 3
Parameters extracted from the assessment of the first order kinetic model for the degradation of GSM.

Experimental Conditions	Prominent RS	k_{obs} (Gy^{-1})	R^2	Initial rate (μmol J^{-1})	Y (GSM)	G (RS) (μmol J^{-1})	$D_{0.5}$ (Gy)	$D_{0.9}$ (Gy)
N_2O	$HO^{\bullet}$	0.068	0.988	0.38	1.49	$HO^{\bullet}$ (0.56)	10.1	33.7
Deaerated / TBA	e_{aq}^-	0.013	0.997	0.07	4.02	e_{aq}^- (0.28)	54.6	181
Deaerated / TBA / pH 1	$H^{\bullet}$	0.018	0.922	0.10	3.42	$H^{\bullet}$ (0.34)	38.3	127
O_2	$HO^{\bullet}$ / $O_2^{-\bullet}$ / $HO_2^{\bullet}$	0.014	0.956	0.08	7.94	$HO^{\bullet}$ (0.28) $O_2^{-\bullet}$/$HO_2^{\bullet}$ (0.33)	49.6	164
O_2/HCOOH	$O_2^{-\bullet}$ / $HO_2^{\bullet}$	0.006	0.880	0.03	20.0	$O_2^{-\bullet}$/$HO_2^{\bullet}$ (0.62)	124	411

the efficiency of the processes.

Similarly, in the presence of $H^{\bullet}$ (deaerated solutions, TBA, pH 1), the ratio Y was 1.36 for MIB and 3.42 for GSM, while for other RS the values were higher (Tables 2 and 3). These results prove the increased reactivity and efficiency of $HO^{\bullet}$ in degrading MIB and GSM. However, they also point out the importance of $H^{\bullet}$, rendering AOPs that produce $H^{\bullet}$, such as ultrasonication [62], capable for efficient degradation of target compounds. $H^{\bullet}$ can act as reducing or oxidizing agents and in the case of saturated compounds such as MIB and GSM can induce degradation mostly via hydrogen abstraction [63]. Results also indicate the possible role of reductive degradation pathways (e^-_{aq}), while the efficiency of $O_2^{-\bullet}$ / $HO_2^{\bullet}$ in degrading compounds such as MIB and GSM is considerably lower.

Summarizing the results shown in Tables 2 and 3, it was found that degradation of MIB was generally faster than GSM while the yields of degradation with single RS followed the order: ($HO^{\bullet}$ saturated with N_2O) > ($H^{\bullet}$ deaerated / TBA /pH 1) > (e_{aq}^- deaerated /TBA) > > ($O_2^{-\bullet}$ / $HO_2^{\bullet}$ oxygenated with formic acid).

Transformation products of MIB

Fig. S3 depicts the Total Ion Count (TIC) chromatograms of TPs from MIB in the presence of different RS at the experimental conditions described in Section 2.2 and Table 1. The tentative structures of the TPs generated from MIB radiolysis, are given in Table S1, along with their molecular ions (M^+), their characteristic fragment ions, the match of their mass spectrum against the NIST mass spectral database (indicated as relative score), as well as their theoretical (based on LRIs) and experimental retention times. The experimental mass spectrum of each proposed TP is presented in Table S3, in comparison to the one proposed by the NIST mass spectral.

In general, degradation of MIB by $HO^{\bullet}$ and $H^{\bullet}$ resulted in the highest number of detected TPs (Table S1) and in the highest degradation rates (Table 2). The radiolysis of MIB in the selective presence of $O_2^{-\bullet}$ / $HO_2^{\bullet}$ resulted in the lowest number of TPs (Table S1), which is in accordance with the low rate of MIB degradation (Table 2). Reductive degradation by e_{aq}^- produced several TPs that were structurally different than those produced by oxidative pathways (Table S1).

Fig. 3 presents a TIC chromatogram of MIB at initial concentration of 10 mg L^{-1} (60 μM), overlayed by a chromatogram of the TPs produced by MIB after 30 min of water radiolysis (irradiation dose 115.2 Gy), in the presence of $HO^{\bullet}$ upon saturation with N_2O. The radiolytically produced TPs are presented in Fig. 4 in groups, with reference to the specific transformations occurred during the degradation process. Under these conditions, the TPs are generated, mainly via hydroxylation, oxidation, cleavage of cyclic structure and rearrangement (Fig. 4). Initially, oxidation leads to ketone-derivatives via β-scission reaction (A1:Camphor and A5:Exo-ketoborneol) as well as dihydroxylated products A2 and A9, following hydroxylation, demethylation, oxidation of hydroxyl group and rearrangement reactions. This is in agreement with previous studies, where hydroxylation, demethylation and

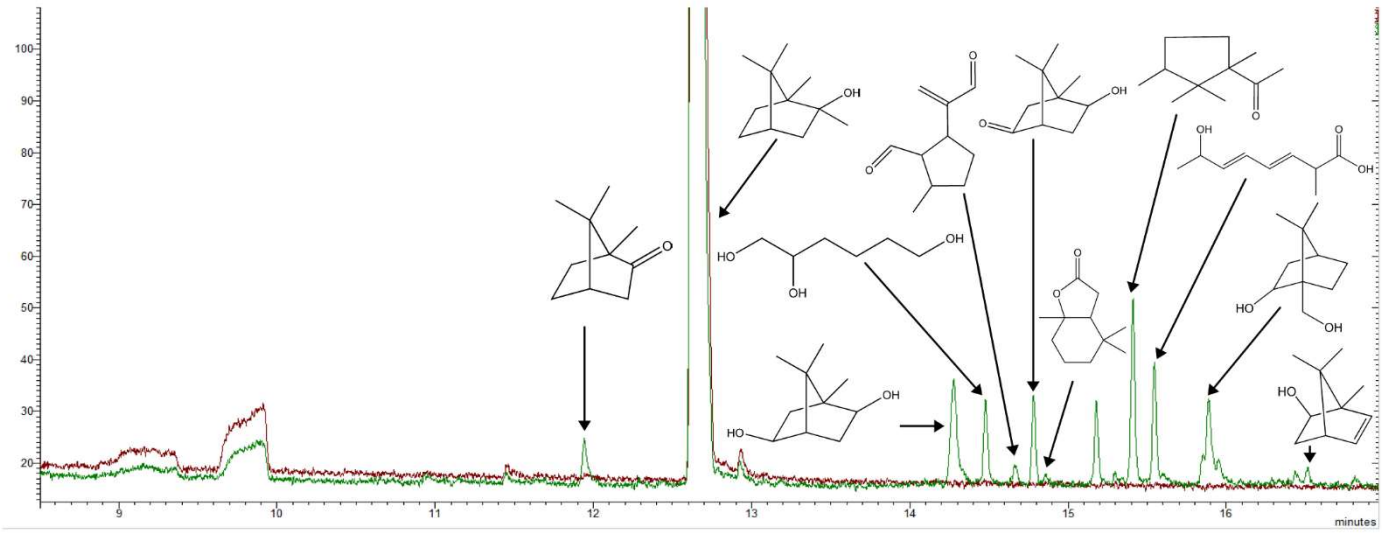

Fig. 3. Representative GC-MS chromatogram of TPs, radiolytically produced from MIB, in the selective presence of $HO^{\bullet}$, overlayed on a chromatogram of a non-irradiated MIB aquatic solution (10 mg L^{-1}).

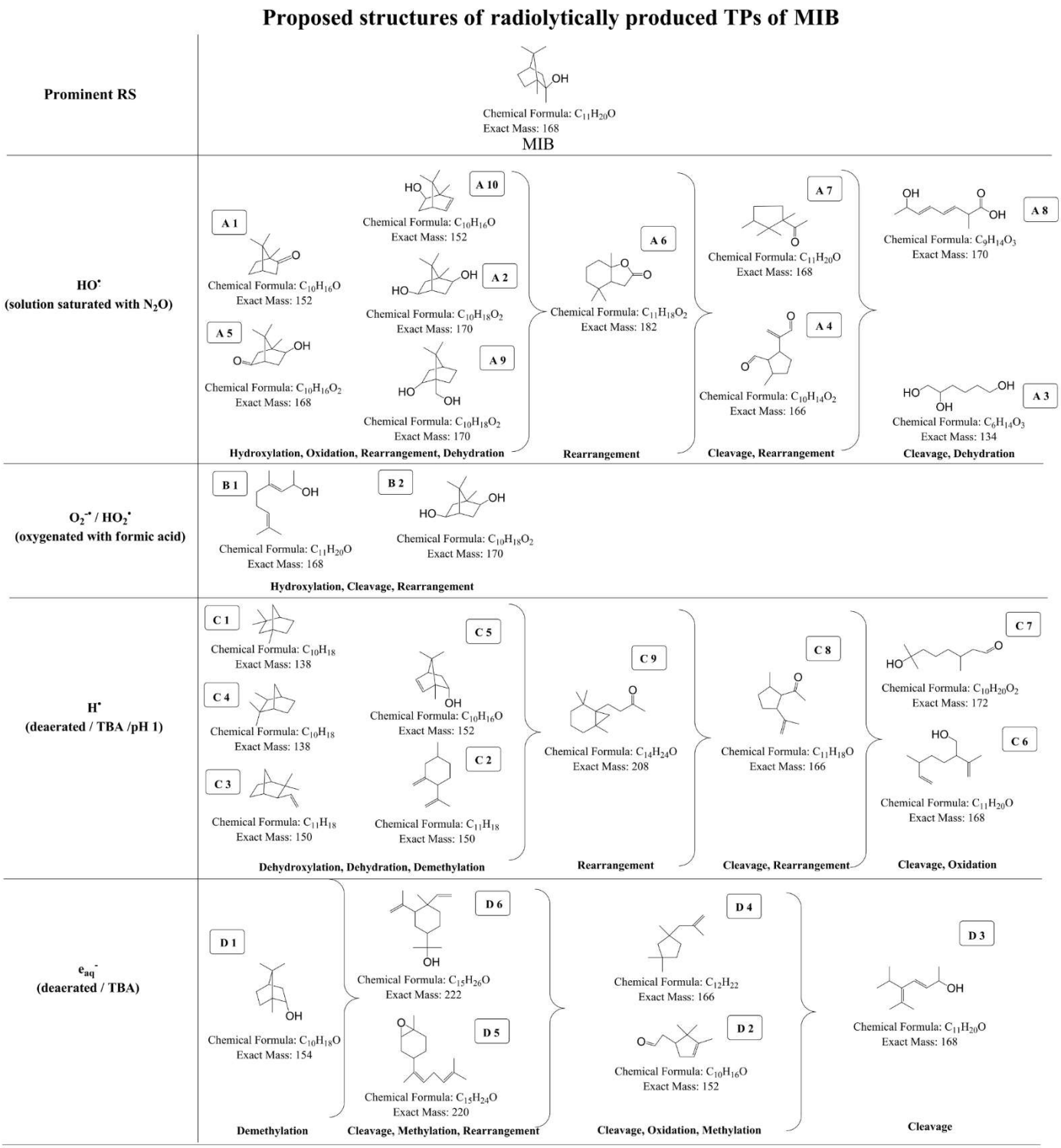

Fig. 4. The influence of various RS to the transformation products of MIB.

rearrangement reactions have been proposed for the degradation of organic pollutants with cyclic structures during water radiolysis [43,52,53,64]. The degradation of MIB also produces A10, which is a product of demethylation, hydroxylation and subsequent dehydration, producing a C = C bond [65]. A1 and A10 have also been detected during the degradation of MIB using AOPs such as ultrasonication, UV/TiO_2 photocatalysis and polyoxometalate photocatalysis, which mainly produce HO• [14,32]. Further degradation leads to the formation of ketone-products and rearrangement towards bicyclic product A6 (4,4,7a-trimethylhexahydrobenzofuran-2(3H)-one). Consequent cleavage of cyclohexane group and demethylation, produces oxidated cyclopente products, such as aldehyde A4 (2-methyl-5-(3-oxoprop-1-en-2-yl)cyclopentanecarbaldehyde) and ketone A7 (1-(1,2,2,3-tetramethylcyclopentyl)ethanone). Next steps include the consecutive dehydration and cleavage of cyclopentane group, with production of open-chain aliphatic products, i.e. trihydroxylated alcohol A3 (hexane-1,2,6-triol) and carboxylic acid A8 (hydroxy-2-methylocta-3,5-dienoic acid) similarly to the ones reported during photocatalysis with UV/TiO_2 and polyoxometalate photocatalysis, which mainly produce HO• [32].

Only two TPs of MIB in the presence of $O_2^{-\bullet}$ / $HO_2^{\bullet}$ (under O_2/ HCOOH) were identified, a dihydroxylated product (B2) and a product of ring cleavage (B1) (Table S1 and Fig. 4). These TPs gave small chromatographic peaks, indicating lower concentrations, in accordance to the low degradation rates of MIB by $O_2^{-\bullet}$ / $HO_2^{\bullet}$.

Degradation of MIB by $H^{\bullet}$ was efficient, showing increased reaction rates and generation of numerous TPs (Fig. 4). Nevertheless, under these conditions (deaeration/TBA/pH 1), degradation seems to follow different reaction pathways than the ones with ROS [66]. Initially, dehydroxylated and dehydrated TPs with the simultaneous loss of one methyl group, were produced (C1- C5). In addition, a derivative based on cyclopentane moiety was also detected, including a methylallyl (probably from the tert-butyl radical produced under these conditions, the addition and subsequent dehydration of the moiety) and a ketone moiety (C8). Other products detected included a non-linear aldehyde (C7) and a non-linear diene (C6). This may be attributed to the tert-butyl radical and its self-recombination products, which are present in the solution under these conditions, its addition (isopropanol moiety) and

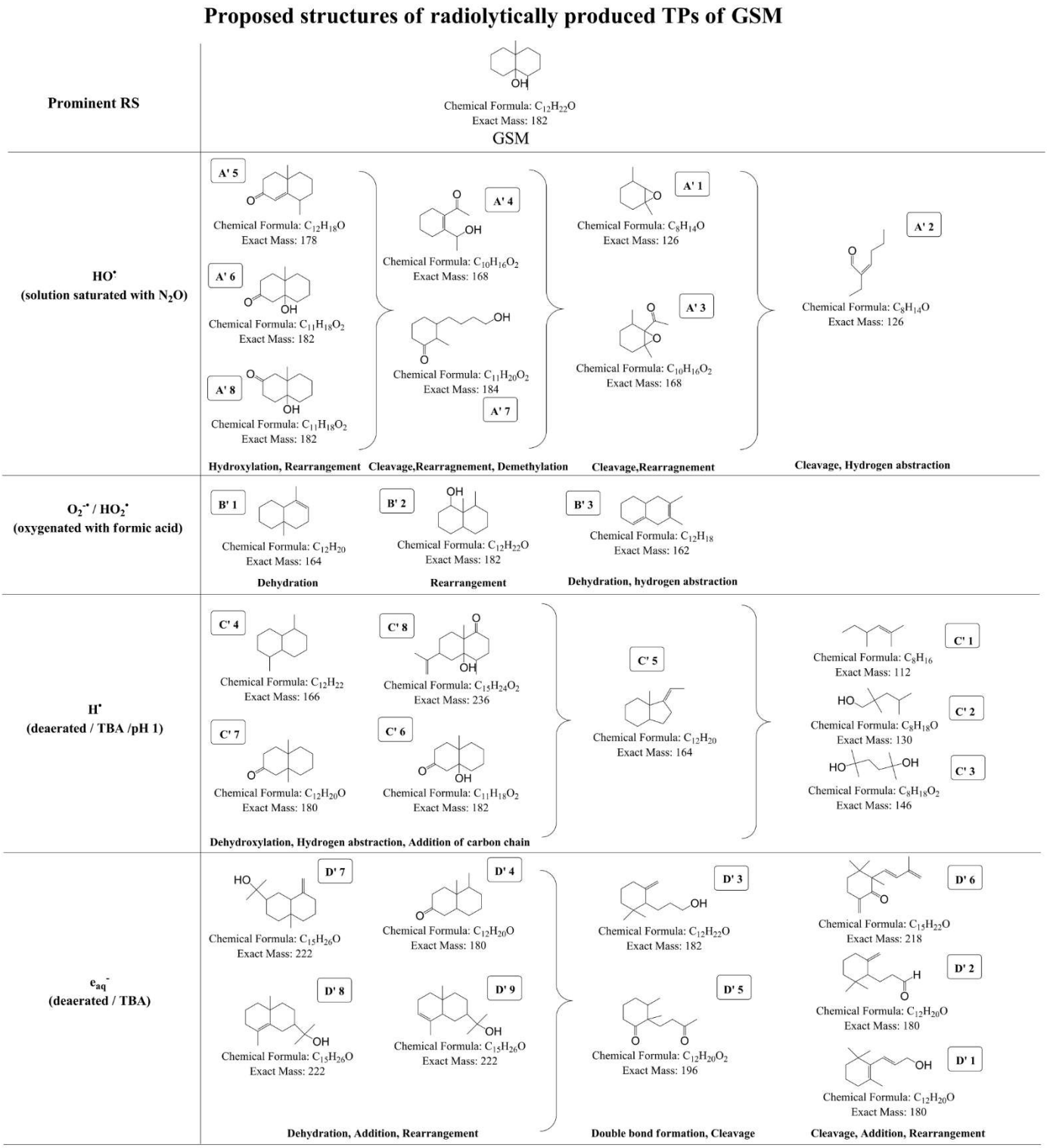

Fig. 5. The influence of various RS to the transformation products of GSM.

subsequent dehydration of the group, leading to the formation of methylallyl- moiety [67]. Past studies have shown that charge transfer and structural rearrangement play important roles in the degradation processes under similar conditions [68].

TPs identified from MIB degradation by e_{aq}^- (under deaeration/TBA), included the initial formation of a demethylated derivative (D1) and further formation of TPs. These included the oxabicyclostructure D5 ($C_{15}H_{24}O$). The formation of these TPs follow the cleavage of the cyclopentane structure of MIB, the consequent addition of non-linear carbon chains and rearrangement to produce final TPs [65]. Furthermore, some of the proposed TPs could be attributed to the tert-butyl radical which is present in the solution under these experimental conditions and its consequent recombination products, as described in the previous paragraph [67]. Therefore, derivatives including a structure (D4) possibly produced due to the addition of tert-butyl radical and subsequently its dehydration, with a further oxidation form of acetaldehyde moiety (D2). Also product D6, was possibly generated with initial addition of isopropanol-moiety (D6) and further dehydration. Formation of the above TPs is probably due to the fact that the hydrated electron, being a good nucleophile, can reduce a solute to produce the solute radical anion [69]. Further cleavage leads to the formation of an isopropyl-dienol (D3) created by cleavage of the cyclic structure, abstraction of hydrogen and formation of a diene structure.

Summarizing, the reaction of $HO^\bullet$ with MIB, seems to lead to formation of hydroxylated TPs, oxidized ketone and aldehyde products and further production of smaller cyclopentane derivatives and linear oxidized carbon chains. $O_2^{-\bullet}$ / $HO_2^\bullet$ generate far less TPs, mainly via hydroxylation. MIB is effectively degraded by $H^\bullet$, with numerous TPs, including dehydroxylated and demethylated products, as well as products of carbon chain addition and hydrogen abstraction to form alkene or aldehyde structures.

Transformation products of GSM

Table S2 presents the tentative structure of the TPs that were detected during radiolytic degradation of aqueous GSM solutions under various conditions, along with their molecular ion M^+, their characteristic fragment ions, the match of their mass spectrum against the NIST mass spectral database (indicated as relative score), and their theoretical (based on LRIs) and experimental retention times. The experimental mass spectrum of each proposed TP is presented in Table S4, in comparison to the one proposed by the NIST mass spectral.

The proposed TPs are also graphically presented in Fig. 5, in groups with reference to the specific transformations occurred during the degradation process. Fig. S4 depicts the obtained TIC chromatograms of TPs from GSM in the presence of different RS.

The mass spectrum of each proposed TP and the match against the NIST mass spectral database is presented in Table S4. In accordance with MIB, degradation of GSM by $HO^\bullet$ produced a large number of TPs and also presented the highest degradation rates (Fig. 2b). Similarly to MIB, $O_2^{-\bullet}$ / $HO_2^\bullet$ produced the lowest number of TPs (Fig. 2b and Table 3). Degradation by $H^\bullet$ was carried out through oxidation hydrogen abstraction, rearrangement reactions and the breakage of bicyclic formation (Fig. S4). Degradation in the presence of e_{aq}^- resulted in a large number of detected TPs, mainly via dehydration, rearrangement and the scission of the bicyclic group (Fig. S4).

In the presence of $HO^\bullet$, the initial formation of oxidated ketone and hydroxyketone structures was observed (A'5, A'6 and A'8), similar to compounds detected in previous studies [32]. Further degradation leads to breakage of the bicyclic structure and the formation of an oxidated hydroxyl-ketone structure (A'4) also observed in a previous study [32] and a cyclohexanone structure with a linear alkane derivative via opening of the second cyclohexane moiety (A'7). Similar dehydration and rearrangement reactions have also observed in the past during the ultrasonic degradation of GSM, which also produces $HO^\bullet$ [70].

Degradation of GSM by $O_2^{-\bullet}$ / $HO_2^\bullet$ (Table S2 and Fig. 5) exhibited low reaction rates and very few detected TPs, mainly produced via dehydration and rearrangement.

A number of TPs were identified from degradation of GSM by $H^\bullet$ (Fig. 5 and Table S2). Initially, dehydroxylation, methyl-group rearrangement (C'4) and oxidation (C'6 and C'7) lead to formation of bicyclic products with the same number of carbon atoms. Additionally, a product with an additional methylallyl- chain (C'8) was detected, due to the addition and subsequent dehydration of the isopropyly radical (propably derived from the self-recombination reactions of tert-butyl radical present under these conditions, similarly to the TP produced from MIB/$H^\bullet$) [67]. Further rearrangement leads to production of an indene bicyclic structure (C'5). Finally, smaller hexene (C'1) pentanol (C'2) and hexanodiol (C'3) structures were detected.

Degradation by e_{aq}^- also produced several TPs. Initially, dehydration, hydrogen abstraction and methyl-group rearragnement was observed. In some cases the addition of isopropyl moiety lead to formation of D'7, D'8 and D'9. These TPs are possibly produced due to the presence of TBA and the subsequent formation of TBA radicals, as already described above.

Next steps included the production of TPs with an opened bicycle ring structure and several additions leading to the formation of higher molecular weight compounds. The formation of smaller linear fragments was not observed under these conditions.

Summarizing, degradation of GSM by $HO^\bullet$, gave rise to hydroxylated TPs, oxidated ketone products and further ring opening of the bicyclic structure, with final formation of smaller linear aldehyde chain products. $O_2^{-\bullet}$ / $HO_2^\bullet$ generated far less TPs, mainly via hydroxylation. $H^\bullet$ led to numerous TPs via dehydroxylation and hydrogen abstraction, producing ketones with double bonds, leading to alkenes or smaller oxidized carbon chains. Reductive degradation by e_{aq}^-, yielded dehydrated and rearranged TPs with more carbon atoms via addition of isopropyl or other carbon chains as well as products via ring opening and subsequent formation of double bonds. In view of these findings, results emphasize the need to further study reductive pathways in water treatment processes (Advanced Reduction Processes-ARPs) [71], related to species such as $H^\bullet$ and e_{aq}^-.

Conclusions

Overall results prove that water radiolysis, apart from its potential application in water treatment, can also be a useful tool to study the roles of various RS -common to AOPs/ARPs for water treatment - on the degradation of emerging pollutants offering knowledge for the optimization and fine-tuning of the processes. The study showed that water radiolysis is effective in degrading MIB and GSM in water. However, degradation rates and pathways strongly depend on the operating experimental conditions and the selective presence of RS.

Degradation kinetic parameters and yields were calculated for each set of experimental conditions/single RS. It was found that MIB and GSM degradation under different experimental conditions/dominant RS generally fitted to first-order kinetics with observed rate constants following the order: $HO^\bullet > H^\bullet >> e_{aq}^- > (O_2^{-\bullet} / HO_2^\bullet)$ being generally faster in MIB than in GSM.

Degradation by $HO^\bullet$, which is a common ROS in AOPs, was very efficient, requiring 1.14 and 1.49 μmoles of $HO^\bullet$ for each degraded μmole of MIB and GSM, respectively. Besides $HO^\bullet$, results prove that there are other important degradation pathways via $H^\bullet$ and e_{aq}^-, while $O_2^{-\bullet}$ / $HO_2^\bullet$, although common in many AOPs for water treatment, are not effective in degrading saturated organic compounds such as MIB and GSM. On the contrary, ARP pathaways, related on species such as $H^\bullet$ and e_{aq}^-, should be further studied in water treatment, due to their high efficiency.

Analysis of TPs showed that different degradation pathways are followed depending on the dominant RS. Degradation of MIB and GSM by $HO^\bullet$ lead to formation of hydroxylated TPs, such as oxidized ketones and aldehydes, ending up to smaller open-ring products. Degradation by

$O_2^{-\bullet}$ / $HO_2^{\bullet}$ was much slower and a few TPs were only detected, produced mainly through hydroxylation. On the other hand, $H^{\bullet}$, a species that can have an oxidative or reductive role, lead to numerous TPs, via dehydroxylation, dehydration and ring opening. Degradation in the presence of e_{aq}^{-}, produced dehydrated, demethylated and rearranged TPs via ring opening as well as TPs with double bonds.

Declaration of Competing Interest

The authors declare that they have no known competing financial interests or personal relationships that could have appeared to influence the work reported in this paper.

Acknowledgments

This Publication is supported by the "Industrial Scholarships Program Stavros Niarchos", which was co-funded by Stavros Niarchos Foundation and EYDAP S.A. C. Christophoridis acknowledges Dr Phani Miskaki and Dr Nikolaos Deftereos (EYDAP S.A) for their support. The authors acknowledge COST Action ES 1105 "CYANOCOST – Cyanobacterial blooms and toxins in water resources: Occurrence impacts and management" and COST action CA18225 "WATERTOP - Taste and Odor in early diagnosis of source and drinking Water Problems" for adding value to this study through networking and knowledge sharing with European experts in the field.

Carlos J. Pestana acknowledges COST Action ES 1105 for funding a Short Term Scientific Mission to the Laboratory of Photo-Catalytic Processes and Environmental Chemistry, NCSR "Demokritos", to conduct a portion of the practical work for this publication.

Supplementary materials

Supplementary material associated with this article can be found, in the online version, at doi:10.1016/j.ceja.2021.100196.

References

[1] Guidelines for Drinking-Water Quality: Fourth Edition Incorporating the First Addendum. Geneva: World Health Organization; 2017. 10, Acceptability aspects: Taste, odour and appearance. Available from: https://www.ncbi.nlm.nih.gov/books/NBK442378/.
[2] W.F. Young, H. Horth, R. Crane, T. Ogden, M. Arnott, Taste and odour threshold concentrations of potential potable water contaminants, Water Res. 30 (1996) 331–340.
[3] S.B. Watson, Aquatic taste and odor: a primary signal of drinking-water integrity, J. Toxicol. Environ. Health Part A 67 (2004) 1779–1795.
[4] T. Kaloudis, T.M. Triantis, A. Hiskia, J. Meriluoto, L. Spoof, G.A. Codd, Taste and odour compounds produced by cyanobacteria. Handbook of Cyanobacterial Monitoring and Cyanotoxin Analysis, John Wiley & Sons, Ltd, West Sussex, UK, 2017.
[5] B. Zaitlin, S.B. Watson, Actinomycetes in relation to taste and odour in drinking water: myths, tenets and truths, Water Res. 40 (2006) 1741–1753.
[6] D. Bruce, P. Westerhoff, A. Brawley-Chesworth, Removal of 2-methylisoborneol and geosmin in surface water treatment plants in Arizona, J. Water Supply Res. Technol. AQUA 51 (2002) 183–197.
[7] J. Ridal, B. Brownlee, G. McKenna, N. Levac, Removal of taste and odour compounds by conventional granular activated carbon filtration, Water Qual. Res. J. Can. 36 (2001) 43–54.
[8] J.R. Rangel-Mendez, F.S. Cannon, Improved activated carbon by thermal treatment in methane and steam: physicochemical influences on MIB sorption capacity, Carbon 43 (2005) 467–479.
[9] D. Cook, G. Newcombe, P. Sztajnbok, The application of powdered activated carbon for mib and geosmin removal: predicting pac doses in four raw waters, Water Res. 35 (2001) 1325–1333.
[10] G. Newcombe, J. Morrison, C. Hepplewhite, Simultaneous adsorption of MIB and NOM onto activated carbon. I. Characterisation of the system and NOM adsorption, Carbon 40 (2002) 2135–2146.
[11] R. Srinivasan, G.A. Sorial, Treatment of taste and odor causing compounds 2-methyl isoborneol and geosmin in drinking water: a critical review, J. Environ. Sci. 23 (2011) 1–13.
[12] L. Ho, G. Newcombe, Effect of NOM, turbidity and floc size on the PAC adsorption of MIB during alum coagulation, Water Res. 39 (2005) 3668–3674.
[13] P. Ömür-Özbek, A.M. Dietrich, Determination of temperature-dependent henry's law constants of odorous contaminants and their application to human perception, Environ. Sci. Technol. 39 (2005) 3957–3963.
[14] W. Song, K.E. O'Shea, Ultrasonically induced degradation of 2-methylisoborneol and geosmin, Water Res. 41 (2007) 2672–2678.
[15] L. Ho, D. Hoefel, F. Bock, C.P. Saint, G. Newcombe, Biodegradation rates of 2-methylisoborneol (MIB) and geosmin through sand filters and in bioreactors, Chemosphere 66 (2007) 2210–2218.
[16] S.L.N. Elhadi, P.M. Huck, R.M. Slawson, Removal of geosmin and 2-methylisoborneol by biological filtration, Water Sci. Technol. (2004) 273–280.
[17] S. Lalezary, M. Pirbazari, M.J. McGuire, Oxidation of five earthy-musty taste and odor compounds, J. Am. Water Works Assoc. 78 (1986) 62–69.
[18] M. Antonopoulou, E. Evgenidou, D. Lambropoulou, I. Konstantinou, A review on advanced oxidation processes for the removal of taste and odor compounds from aqueous media, Water Res. 53 (2014) 215–234.
[19] Y. Nosaka, A.Y. Nosaka, Chapter 1. Identification and roles of the active species generated on various photocatalystsP. Pichat (Ed.), in: Photocatalysis and Water Purification. From Fundamentals to Recent Applications, Wiley-VCH, France, 2013, pp. 1–24.
[20] A. Peter, U. Von Gunten, Oxidation kinetics of selected taste and odor compounds during ozonation of drinking water, Environ. Sci. Technol. 41 (2007) 626–631.
[21] M.M.G. Berlt, R.D.C.D.S. Schneider, Ê.L. Machado, L.T. Kist, Comparative assessment of the degradation of 2-methylisoborneol and geosmin in freshwater using advanced oxidation processes, Environ. Technol. 42 (2021) 3832–3839.
[22] T. Mizuno, S. Ohara, F. Nishimura, H. Tsuno, O_3/H_2O_2 process for both removal of odorous algal-derived compounds and control of bromate ion formation, Ozone: Sci. Eng. 33 (2011) 121–135.
[23] L. Meunier, S. Canonica, U. von Gunten, Implications of sequential use of UV and ozone for drinking water quality, Water Res. 40 (2006) 1864–1876.
[24] K. Zoschke, N. Dietrich, H. Börnick, E. Worch, UV-based advanced oxidation processes for the treatment of odour compounds: efficiency and by-product formation, Water Res. 46 (2012) 5365–5373.
[25] E.J. Rosenfeldt, B. Melcher, K.G. Linden, UV and UV/H_2O_2 treatment of methylisoborneol (MIB) and geosmin in water, J. Water Supply Res. Technol. AQUA 54 (2005) 423–434.
[26] F. Visentin, S. Bhartia, M. Mohseni, S. Dorner, B. Barbeau, Performance of vacuum UV (VUV) for the degradation of MC-LR, geosmin, and MIB from cyanobacteria-impacted waters, Environ. Sci. Water Res. Technol. 5 (2019) 2048–2058.
[27] P. Xie, J. Ma, W. Liu, J. Zou, S. Yue, X. Li, M.R. Wiesner, J. Fang, Removal of 2-MIB and geosmin using UV/persulfate: contributions of hydroxyl and sulfate radicals, Water Res. 69 (2015) 223–233.
[28] L. Li, W. Zhang, Y. Zhang, S. Kuppers, L. Jin, Y. Zhang, N. Gao, D. Zhang, Sulfate radical-based technology for the removal of 2-methylisoborneol and 2-methylisoborneol-producing algae in drinking water sources, Chem. Eng. J. 356 (2019) 43–52.
[29] T.-.K. Kim, B.-.R. Moon, T. Kim, M.-.K. Kim, K.-.D. Zoh, Degradation mechanisms of geosmin and 2-MIB during UV photolysis and UV/chlorine reactions, Chemosphere 162 (2016) 157–164.
[30] M. Bai, Y. Yu, J. Cheng, Z. Ji, J. Li, [rad]OH degraded 2-Methylisoborneol during the removal of algae-laden water in a drinking water treatment system: comparison with ClO_2, Chemosphere 236 (124342) (2019).
[31] T. Fotiou, T.M. Triantis, T. Kaloudis, K.E. O'Shea, D.D. Dionysiou, A. Hiskia, Assessment of the roles of reactive oxygen species in the UV and visible light photocatalytic degradation of cyanotoxins and water taste and odor compounds using C-TiO_2, Water Res. 90 (2016) 52–61.
[32] T. Fotiou, T.M. Triantis, T. Kaloudis, E. Papaconstantinou, A. Hiskia, Photocatalytic degradation of water taste and odour compounds in the presence of polyoxometalates and TiO_2: intermediates and degradation pathways, J. Photochem. Photobiol. A 286 (2014) 1–9.
[33] T. Fotiou, T.M. Triantis, T. Kaloudis, L.M. Pastrana-Martínez, V. Likodimos, P. Falaras, A.M.T. Silva, A. Hiskia, Photocatalytic degradation of microcystin-LR and off-odor compounds in water under UV-A and solar light with a nanostructured photocatalyst based on reduced graphene oxide-TiO_2 composite. Identification of intermediate products, Ind. Eng. Chem. Res. 52 (2013) 13991–14000.
[34] L.A. Lawton, P.K.J. Robertson, R.F. Robertson, F.G. Bruce, The destruction of 2-methylisoborneol and geosmin using titanium dioxide photocatalysis, Appl. Catal. B 44 (2003) 9–13.
[35] S. Fu, X. Zhao, Z. Zhou, M. Li, L. Zhu, Effective removal of odor substances using intimately coupled photocatalysis and biodegradation system prepared with the silane coupling agent (SCA)-enhanced TiO_2 coating method, Water Res. 188 (2021), 116569.
[36] T. Fotiou, T.M. Triantis, T. Kaloudis, A. Hiskia, Evaluation of the photocatalytic activity of TiO_2 based catalysts for the degradation and mineralization of cyanobacterial toxins and water off-odor compounds under UV-A, solar and visible light, Chem. Eng. J. 261 (2015) 17–26.
[37] I.G. DraganiĆ, Z.D. DraganiĆ, Chapter 2 - Interaction of Ionizing Radiation with Water and the Origin of Short-Lived Species That Cause Chemical Changes in Irradiated Water, in: I.G. DraganiĆ, Z.D. DraganiĆ (Eds.), Physical Chemistry The Radiation Chemistry of Water, Elsevier, 1971, pp. 23–46.
[38] J.A. LaVerne, OH radicals and oxidizing products in the gamma radiolysis of water, Radiat. Res. 153 (2000) 196–200.
[39] A.H. Samuel, J.L. Magee, Theory of radiation chemistry. II. Track effects in radiolysis of water, J. Chem. Phys. 21 (1953) 1080–1087.
[40] G.V. Buxton, C.L. Greenstock, W.P. Helman, A.B. Ross, Critical Review of rate constants for reactions of hydrated electrons, hydrogen atoms and hydroxyl radicals (·OH/·O^-) in Aqueous Solution, J. Phys. Chem. Ref. Data 17 (1988) 513–886.
[41] N. Getoff, Radiation chemistry and the environment, Radiat. Phys. Chem. 54 (1999) 377–384.

[42] R. Ocampo-Pérez, J. Rivera-Utrilla, M. Sánchez-Polo, J.J. López-Peñalver, R. Leyva-Ramos, Degradation of antineoplastic cytarabine in aqueous solution by gamma radiation, Chem. Eng. J. 174 (2011) 1–8.
[43] B.G. Zheng, Z. Zheng, J.B. Zhang, X.Z. Luo, J.Q. Wang, Q. Liu, L.H. Wang, Degradation of the emerging contaminant ibuprofen in aqueous solution by gamma irradiation, Desalination 276 (2011) 379–385.
[44] Y. Liu, J. Wang, Degradation of sulfamethazine by gamma irradiation in the presence of hydrogen peroxide, J. Hazard. Mater. (2013) 99–105, 250-251.
[45] S. Wang, J. Wang, Carbamazepine degradation by gamma irradiation coupled to biological treatment, J. Hazard. Mater. 321 (2017) 639–646.
[46] J. Wang, J. Zhang, M. Yan, B. Zheng, Y.Zhao Zheng, Degradation of atrazine in water by gamma-ray irradiation, Fresenius Environ. Bull. 21 (2012) 2778–2784.
[47] M.S. Hossain, A.N.M. Fakhruddin, M.A.Z. Chowdhury, M.K. Alam, Degradation of chlorpyrifos, an organophosphorus insecticide in aqueous solution with gamma irradiation and natural sunlight, J. Environ. Chem. Eng. 1 (2013) 270–274.
[48] S.Y. Yu, H.Q. Zhang, X.D. Hu, X.H. Zhang, W. Zhang, Study on degradation mechanism of carbendazim by γ-irradiation,Atomic Energy, Science and Technology 51 (2017) 256–261.
[49] S.Y. Liu, Y.P. Chen, H.Q. Yu, Q.R. Li, Degradation of p-chlorophenol by γ-radiolysis: radiolytic intermediates and theoretical calculations, Chem. Lett. 34 (2005) 488–489.
[50] J. Biswal, J. Paul, D.B. Naik, S.K. Sarkar, S. Sabharwal, Radiolytic degradation of 4-nitrophenol in aqueous solutions: pulse and steady state radiolysis study, Radiat. Phys. Chem. 85 (2013) 161–166.
[51] Y.N. Yin, J. Hu, J.L. Wang, Degradation kinetics of 2,4-dichlorophenol by gamma ray irradiation in the presence of ozone, Nucl. Sci. Tech. 27 (64) (2016).
[52] W. Song, T. Xu, W.J. Cooper, D.D. Dionysiou, A.A.d.l. Cruz, K.E. O'Shea, Radiolysis studies on the destruction of microcystin-LR in aqueous solution by hydroxyl radicals, Environ. Sci. Technol. 43 (2009) 1487–1492.
[53] W. Song, S. Yan, W.J. Cooper, D.D. Dionysiou, K.E. O'Shea, Hydroxyl radical oxidation of cylindrospermopsin (Cyanobacterial Toxin) and its role in the photochemical transformation, Environ. Sci. Technol. 46 (2012) 12608–12615.
[54] J.B. Zhang, Z. Zheng, G.J. Yang, Y.F. Zhao, Degradation of microcystin by gamma irradiation, Nucl. Instrum. Methods Phys. Res. Sect. A Accel. Spectrom. Detect. Assoc. Equip. 580 (2007) 687–689.
[55] H.W. Richter, Radiation chemistry: principles and applications. Photochemistry and Radiation Chemistry, American Chemical Society 1998, 2021, pp. 5–33.
[56] N.V. Blough, R.G. Zepp, C.S. Foote, J.S. Valentine, A. Greenberg, J.F. Liebman, Reactive oxygen species in natural waters. Active Oxygen in Chemistry, Springer, Netherlands, Dordrecht, 1995, pp. 280–333.
[57] A. Olszanski, N. V. Klassen, C.K. Ross, K.R. Shortt, (2002) The IRS fricke dosimetry system. Ionizing Radiation Standards, Institute for National Measurement Standards, National Research Council Canada (NRC), publications archive / archives des publications du CNRC. Identifier PIRS-0815, NRC-INMS-315. Record identifier / Identificateur de l'enregistrement: 3e38a08d-312a-4f14-82a9-9f6a4634a90c, August 2002.
[58] J.W.T. Spinks, R.J. Woods, Chapter 7. Water and inorganic aqueous systems. An Introduction to Radiation Chemistry, 3rd, John Wiley and Sons, Inc., New York, 1990, p. 243.
[59] A. Kimura, M. Osawa, M. Taguchi, Decomposition of persistent pharmaceuticals in wastewater by ionizing radiation, An Introduction to Radiation Chemistry, Radiat. Phys. Chem. 81 (2012) 1508–1512.
[60] T. Kaloudis, T.M. Triantis, A. Hiskia, J. Meriluoto, L. Spoof, G.A. Codd, Standard operating procedure - determination of geosmin and 2-methylisoborneol in water by hs-spme-gc/MS. Handbook of Cyanobacterial Monitoring and Cyanotoxin Analysis, John Wiley & Sons, Ltd, 2017, pp. 469–474.
[61] B.d.A. Zellner, C. Bicchi, P. Dugo, P. Rubiolo, G. Dugo, L. Mondello, Linear retention indices in gas chromatographic analysis: a review, Flavour Fragr J. 23 (2008) 297–314.
[62] R.A. Torres-Palma, E.A. Serna-Galvis, S.C. Ameta, R. Ameta, Chapter 7 - sonolysis. Advanced Oxidation Processes For Waste Water Treatment, Academic Press, 2018, pp. 177–213.
[63] J. Wang, S. Wang, Reactive species in advanced oxidation processes: formation, identification and reaction mechanism, Chem. Eng. J. 401 (2020), 126158.
[64] Z. Zhang, Q. Yang, J. Wang, Degradation of trimethoprim by gamma irradiation in the presence of persulfate, Radiat. Phys. Chem. 127 (2016) 85–91.
[65] C. Lamouroux, N. Aychet, A. Lelièvre, C.K. Jankowski, C. Moulin, High-performance liquid chromatography with electrospray ionisation mass spectrometry and diode array detection in the identification and quantification of the degradation products of calix[4]arene crown-6 under radiolysis, Rapid Commun. Mass Spectrom. 18 (2004) 1493–1503.
[66] R. Li, X. Cao, H. Zhao, C. Liu, Z. Li, J. Wang, L. Zhang, Q. Li, Radiolysis products and degradation mechanism studies on di-1-methyl heptyl methyl phosphonate, J. Radioanal. Nucl. Chem. 314 (2017) 1715–1725.
[67] S.P. Mezyk, K.P. Madden, Self-recombination rate constants for 2-propanol and tert-Butyl alcohol radicals in Water, J. Phys. Chem. A 103 (1999) 235–242.
[68] D. Cao, X. Zhang, S. Zhao, Y. Guan, H. Zhang, Appropriate dose for degradation of levofloxacin lactate: gamma radiolysis and assessment of degradation product activity and cytotoxicity, Environ. Eng. Sci. 28 (2011) 183–189.
[69] M.H. Wu, N. Liu, G. Xu, J. Ma, L. Tang, L. Wang, H.Y. Fu, Kinetics and mechanisms studies on dimethyl phthalate degradation in aqueous solutions by pulse radiolysis and electron beam radiolysis, Radiat. Phys. Chem. 80 (2011) 420–425.
[70] W. Song, K.E. O'Shea, Ultrasonically induced degradation of 2-methylisoborneol and geosmin, Water Res. 41 (2007) 2672–2678.
[71] A.G. Capodaglio, Critical perspective on advanced treatment processes for water and wastewater: aOPs, ARPs, and AORPs, Appl. Sci. 10 (2020).

SUPPLEMENTARY MATERIAL

Radiolytic degradation of 2-methylisoborneol and geosmin in water: reactive radical species and transformation pathways

Christophoridis C.[1], Pestana C.J.[2], Kaloudis T.[1,3], Lawton L.A.[2], Triantis, T.M.[1], Hiskia A.[1*]

[1] Laboratory of Photo-Catalytic Processes and Environmental Chemistry, Institute of Nanoscience & Nanotechnology, NCSR "Demokritos", Patr. Gregoriou E & 27 Neapoleos Str, 15341 Agia Paraskevi, Athens, Greece

[2] School of Pharmacy and Life Sciences, Robert Gordon University, Aberdeen, UK

[3] Water Quality Control Department, Athens Water Supply and Sewerage Company (EYDAP SA), Athens, Greece

*corresponding author: e-mail: a.hiskia@inn.demokritos.gr

Radical reactions in water radiolysis

Radiolysis of aerated water mainly generates hydrated electrons (e_{aq}^-) and $HO^\bullet$. Secondary RS are superoxide anion ($O_2^{-\bullet}$) and hydrogen radicals ($H^\bullet$). Water radiolysis also produces H_2O_2, H_2 and H^+. Overall, the products of aerated water radiation are given below with their G values in brackets [1, 2].

e_{aq}^- (0.28), $H^\bullet$ (0.06), HO• (0.28), $O_2^{\bullet-}$ /$HO_2^\bullet$ (0.0027), H_2 (0.05) and H^+ (0.27)

The effect of $HO^\bullet$ on the target compounds was studied in aquatic solutions of MIB and GSM pre-saturated with nitrous oxide (N_2O), which quantitatively converts the e_{aq}^- to $HO^\bullet$ [2], as shown in Eq. (1).

$$e_{aq}^- + N_2O \rightarrow N_2O^- \xrightarrow{H_2O} N_2 + HO^- + HO^\bullet \quad (1)$$

Under these conditions, the overall G value of $HO^\bullet$ is expected to be 0.56 μmol J^{-1}, since all the e_{aq}^- are converted to $OH^\bullet$ (Table 1).

Moreover, e_{aq}^- is predominantly formed by irradiation of degassed aqueous solutions, in the presence of TBA, which acts as a $HO^\bullet$ scavenger, as shown in Eq. (2).

$$HO^\bullet + (CH_3)_3C\text{-}OH \rightarrow H_2O + (CH_2^\bullet)(CH_3)_2C\text{-}OH \quad (2)$$

In this system the overall G value of e_{aq}^- is equal to 0.28 (Table 1) since all the $HO^\bullet$ have been scavenged.

.

H•, is produced by irradiation of degassed solution, in the presence of TBA with adjustment to acidic pH, as shown in Eq. (3).

$$e_{aq}^- + H^+_{aq} \rightarrow H^\bullet \quad (3)$$

In this case, all e_{aq}^- is converted to $H^\bullet$ with an overall G value of $H^\bullet$ equal to G value of e_{aq}^- converted to $H^\bullet$ + initial G value of $H^\bullet$=0.28+0.06=0.34 (Table 1).

The $O_2^{-\bullet}$ / $HO_2^\bullet$ radicals will be generated by irradiation in saturated with oxygen solution in the presence of formic acid, as shown in Eq. (4-8) [1, 3].

$$e_{aq}^- + O_2 \rightarrow O_2^{-\bullet} \quad (4)$$
$$H^\bullet + O_2 \rightarrow HO_2^\bullet \quad (5)$$
$$HO_2^\bullet \rightleftarrows O_2^{-\bullet} + H^+ \quad (6)$$
$$HO^\bullet + HCOO^- \rightarrow H_2O + COO^{\bullet-} \quad (7)$$
$$COO^{\bullet-} + O_2 \rightarrow CO_2 + O_2^{-\bullet} \quad (8)$$

Therefore in this manipulated system, the overall G value of $O_2^{-\bullet}$ / $HO_2^\bullet$ is expected to be equal to (G value of e_{aq}^- converted to $O_2^{-\bullet}$) + (initial G value of $H^\bullet$ converted to $HO_2^\bullet$) + (G value of $HO^\bullet$ converted to $O_2^{-\bullet}$) =0.28+0.06+0.34=0.62 (Table 1) since all the e_{aq}^-, $H^\bullet$ and $HO^\bullet$ have been converted to $O_2^{-\bullet}$.

Further reactions include Eq (9-11)

$$HO_2^{\bullet} + O_2^{-\bullet} \rightarrow H_2O_2 + O_2 \text{ (at pH<7)} \quad (9)$$

$$HO_2^{\bullet} + HO_2^{\bullet} \rightarrow H_2O_2 + O_2 \quad (10)$$

$$H^{\bullet} + OH^{-} \rightarrow e_{aq}^{-} + H_2O \quad (11)$$

Finally, at increased adsorbed radiation doses, further reactions (radical-radical or recombination) take place as shown in Eq. (12-15)

$$e_{aq}^{-} + HO^{\bullet} \rightarrow OH^{-} \quad (12)$$

$$HO^{\bullet} + HO^{\bullet} \rightarrow H_2O_2 \quad (13)$$

$$HO^{\bullet} + H^{\bullet} \rightarrow H_2O \quad (14)$$

$$H_2O + H^{\bullet} + e_{aq}^{-} \rightarrow H_2 + OH^{-} \quad (15)$$

FIGURES

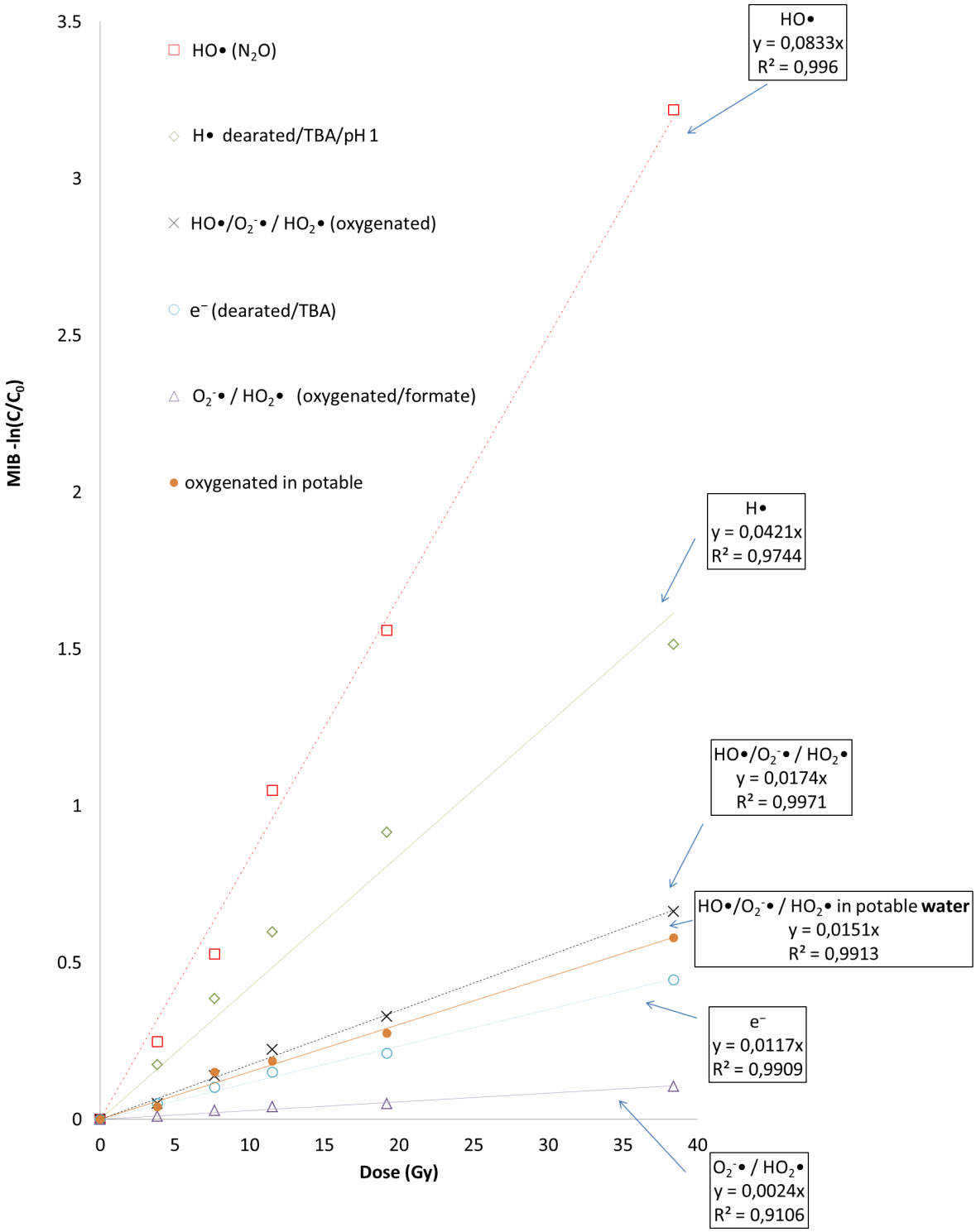
HO• (N2O)
H• dearated/TBA/pH 1
HO•/O2-• / HO2• (oxygenated)
e⁻ (dearated/TBA)
O2-• / HO2• (oxygenated/formate)
oxygenated in potable
HO•
y = 0,0833x
R² = 0,996
H•
y = 0,0421x
R² = 0,9744
HO•/O2-• / HO2•
y = 0,0174x
R² = 0,9971
HO•/O2-• / HO2• in potable water
y = 0,0151x
R² = 0,9913
e⁻
y = 0,0117x
R² = 0,9909
O2-• / HO2•
y = 0,0024x
R² = 0,9106
MIB -ln(C/C0)
Dose (Gy)
0
0.5
1
1.5
2
2.5
3
3.5
0
5
10
15
20
25
30
35
40

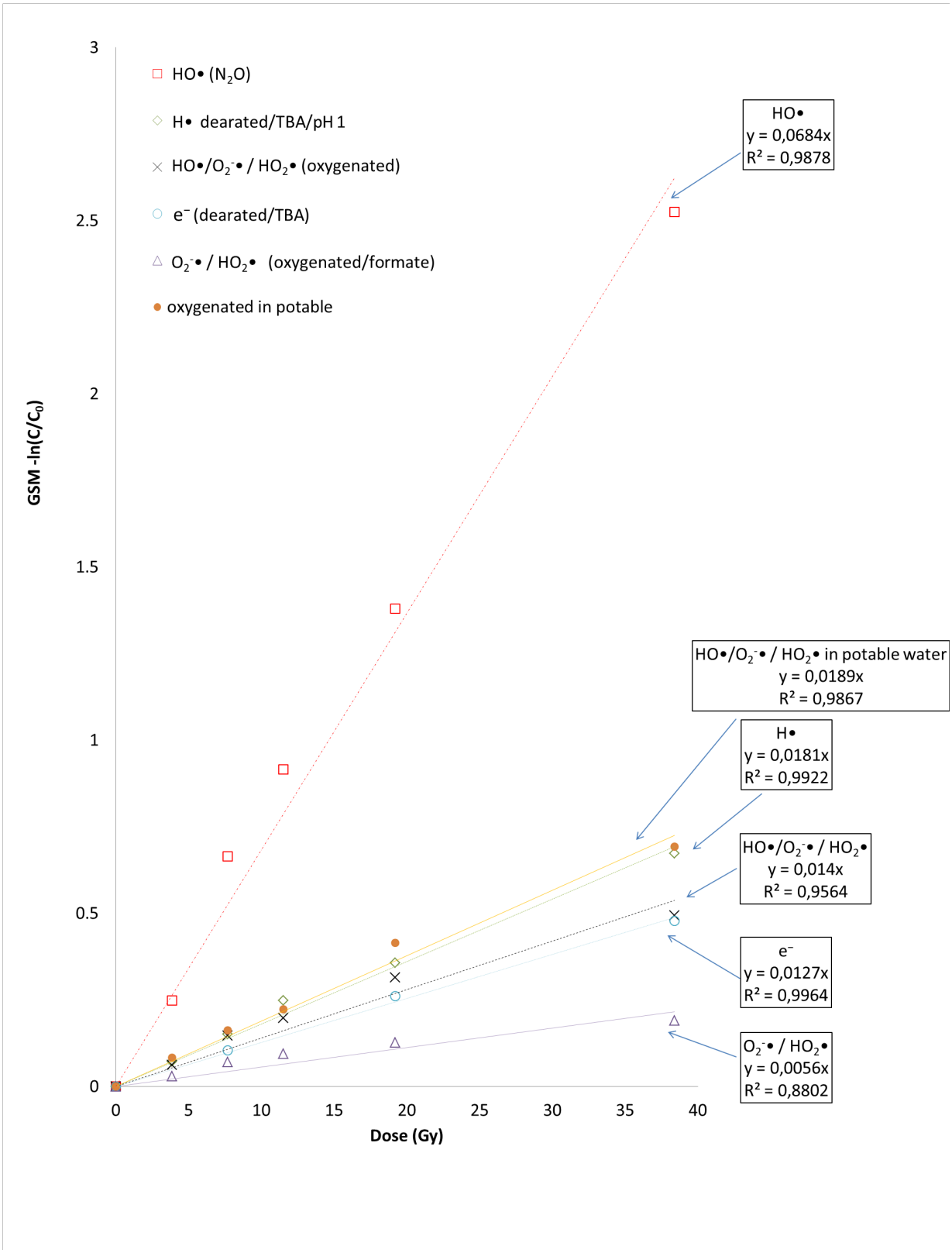

Figure S2. Fit of first order kinetic model to the degradation of GSM, under regulated experimental conditions, which produce specific RS

$HO^{\bullet}$ (solution saturated with N_2O)

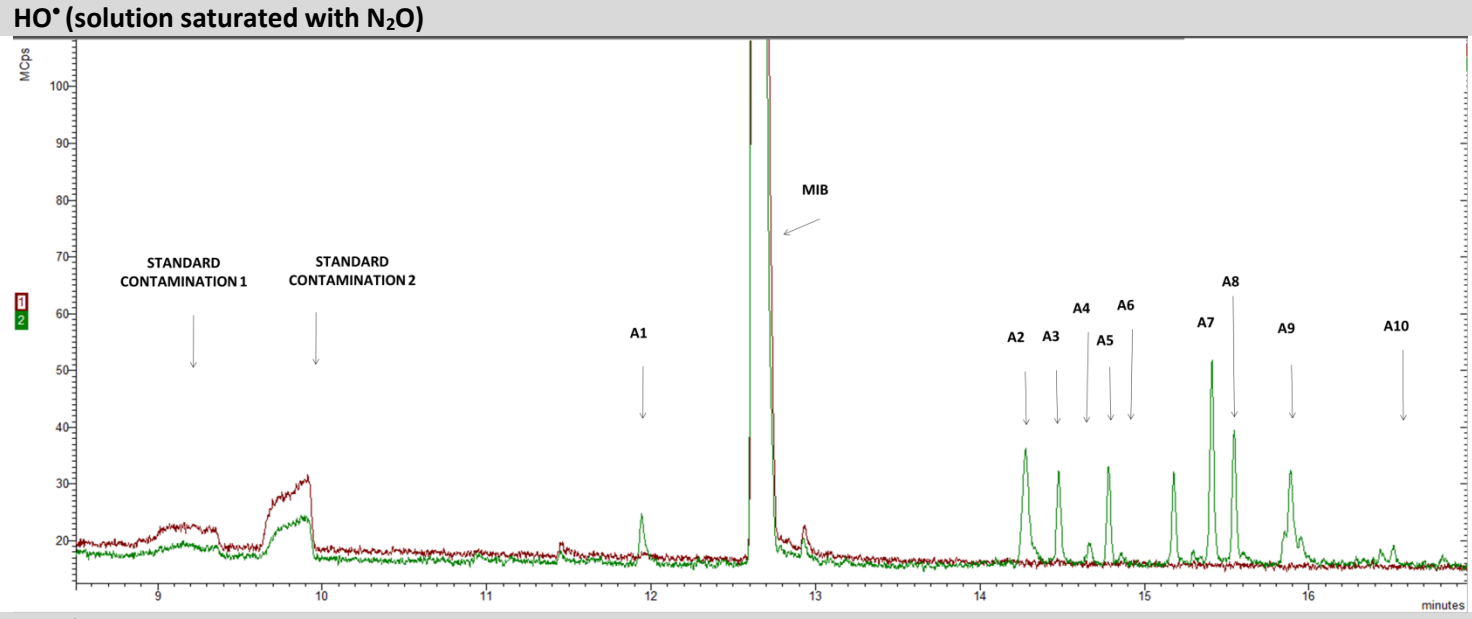

$O_2^{-\bullet}$ / $HO_2^{\bullet}$ (oxygenated with formic acid)

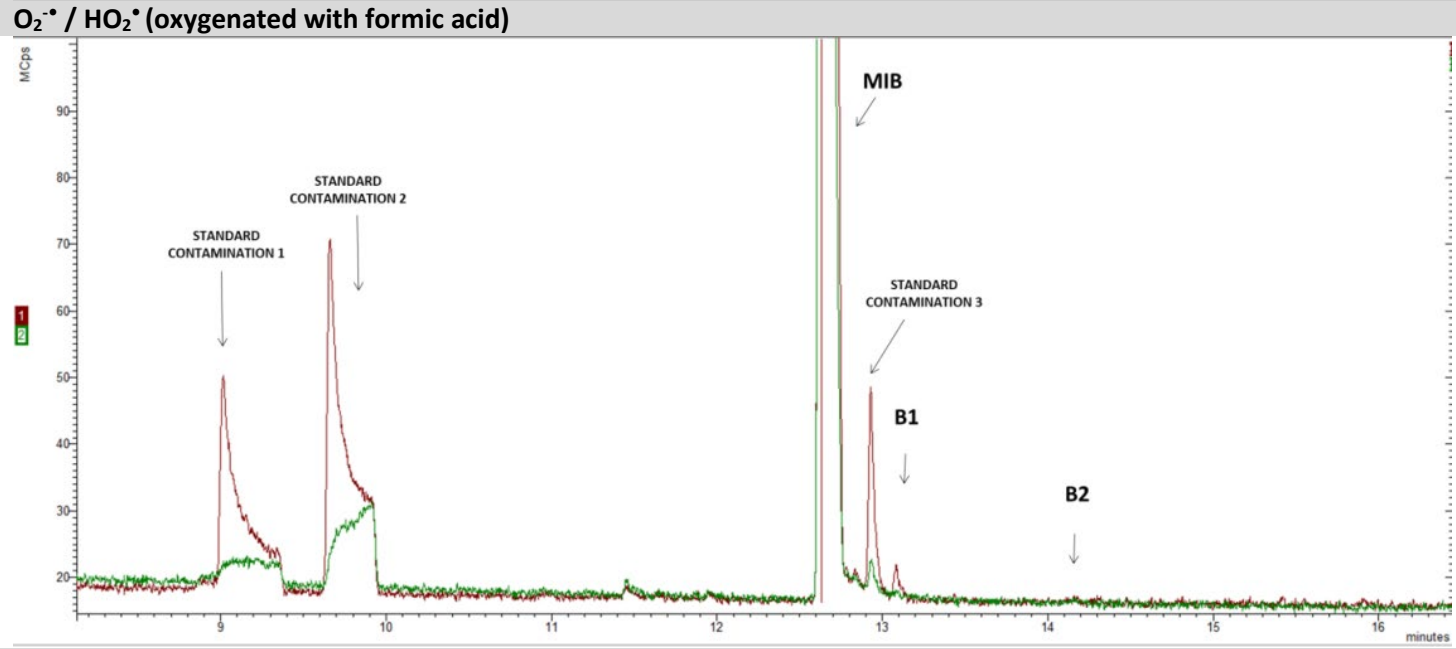

$H^{\bullet}$ (deaerated / TBA /pH 1)

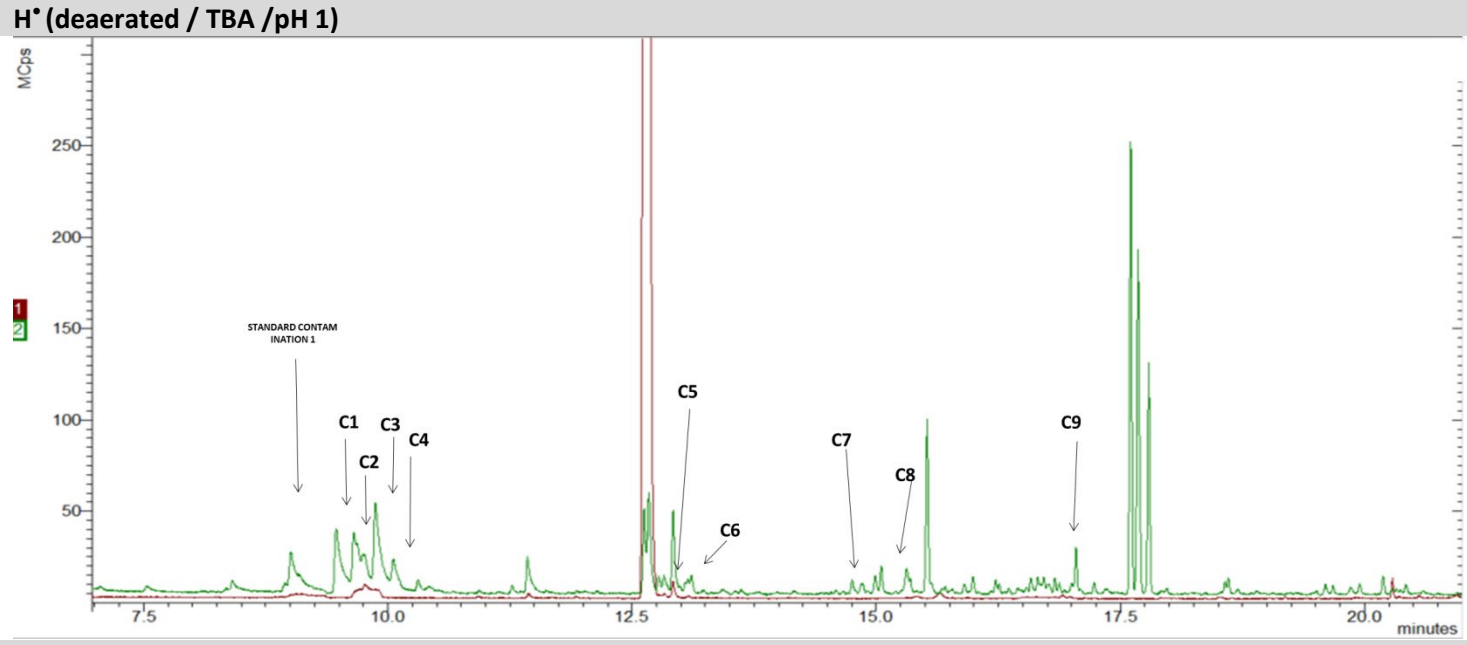

e_{aq}^{-} (deaerated / TBA)

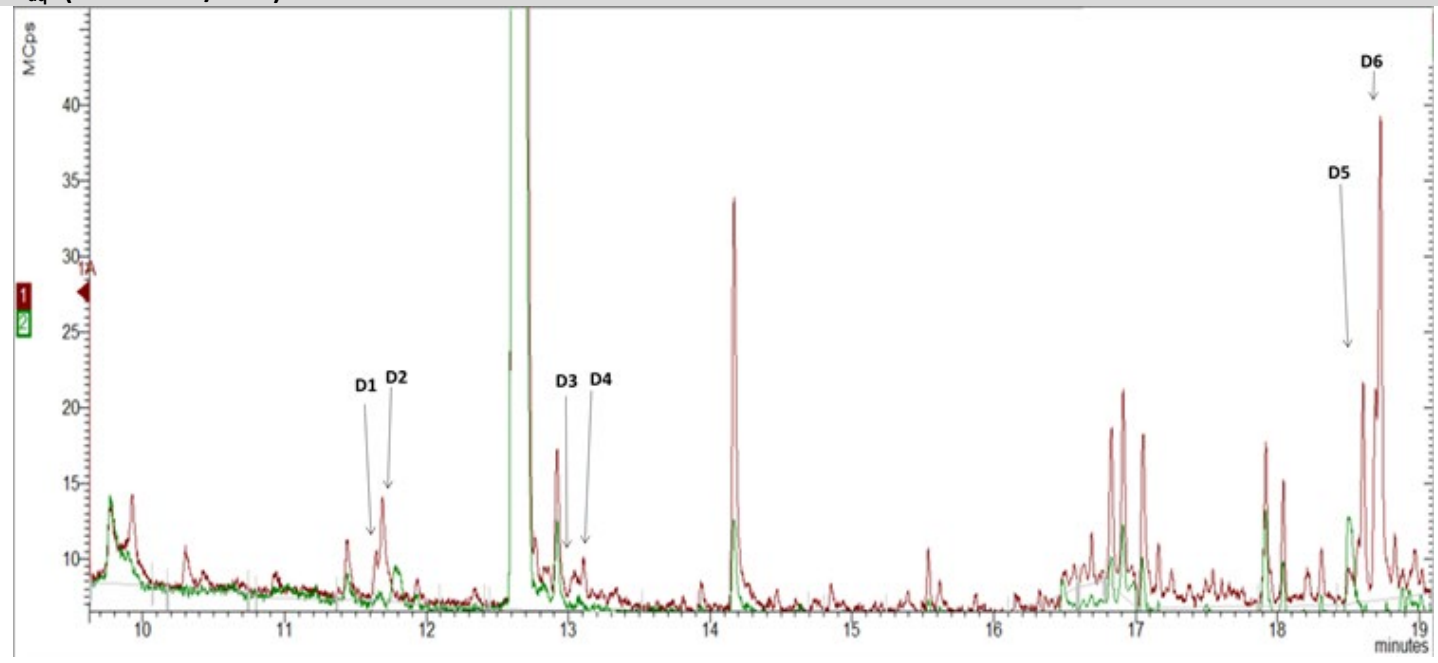

Figure S3. TIC chromatograms of TPs produced from degradation of MIB under the influence of selected RS, overlayed on a chromatogram of a non-irradiated MIB aquatic solution (10 mg L^{-1}).

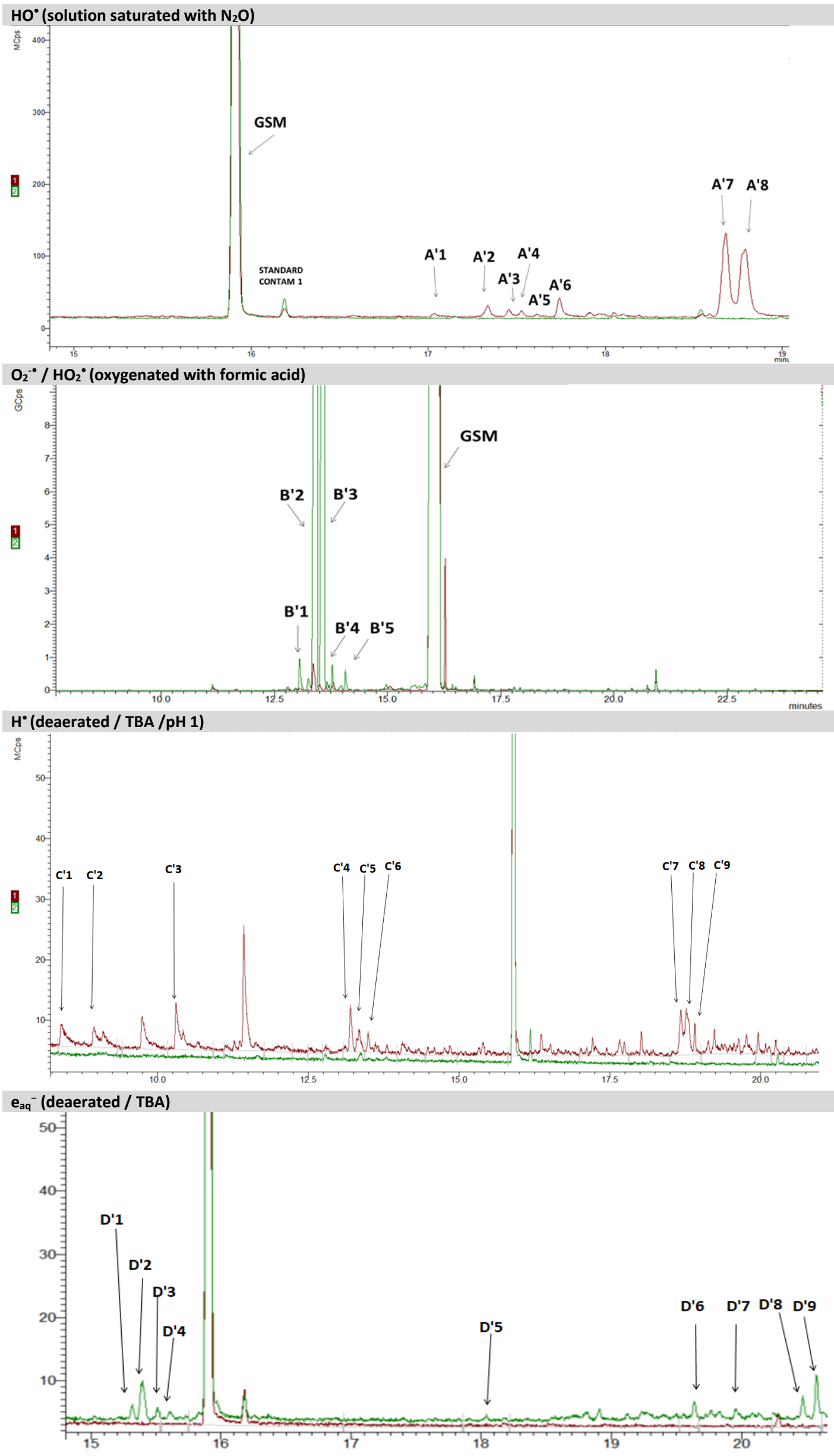

Figure S4. TIC chromatograms of TPs produced from degradation of GSM under the influence of selected RS, overlayed on a chromatogram of a non-irradiated GSM aquatic solution (10 mg L^{-1}).

TABLES

Table S1. Tentative structures of the TPs generated from MIB radiolysis

HO• (solution saturated with N_2O)								
TP	**Name**	**Formula**	**M^+ m/z**	**characteristic fragment ions**	**Relative Score**	**Structure**	**t_R (min) theoretical expected**	**t_R (min) experimental**
	2-methyl-isoborneol (MIB)	$C_{11}H_{20}O$	168		893	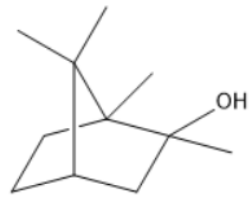		12.7
A1	Camphor	$C_{10}H_{16}O$	152	108, 95, 81, 69, 55, 41	900	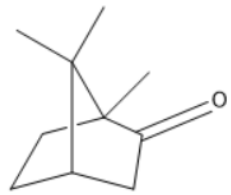	11.7	11.9
A2	(1S,4S,5S)-1,7,7-trimethylbicyclo[2.2.1]heptane-2,5-diol	$C_{10}H_{18}O_2$	170	108, 95, 43	705		14.5	14.3
A3	hexane-1,2,6-triol	$C_6H_{14}O_3$	134	85, 57, 43	700	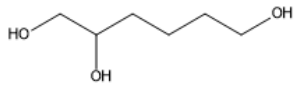	14.1	14.6
A4	2-methyl-5-(3-oxoprop-1-en-2-yl)cyclopentanecarbaldehyde	$C_{10}H_{14}O_2$	166	123, 95, 43	723	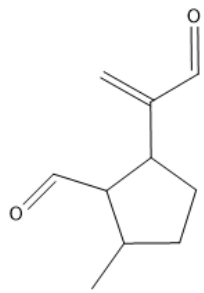	14.5	14.7
A5	Exo-ketoborneol	$C_{10}H_{16}O_2$	168	109, 70, 43	679		14.3	14.8
A6	4,4,7a-trimethylhexahydrobenzofuran-2(3H)-one	$C_{11}H_{18}O_2$	182	167, 109, 81, 69	644	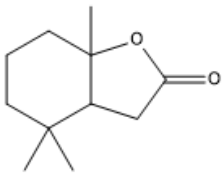	15.2	14.9

A7	1-(1,2,2,3-tetramethylcyclopentyl)ethanone	$C_{11}H_{20}O$	168	124, 109, 69, 55	688	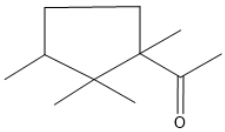	13.1	15.1
A8	(3E,5E)-7-hydroxy-2-methylocta-3,5-dienoic acid	$C_9H_{14}O_3$	170	124. 109, 55, 43	610	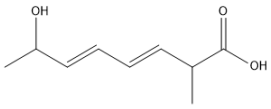	14.8	15.2
A9	(1R,4S)-1-(hydroxymethyl)-7,7-dimethylbicyclo[2.2.1]heptan-2-ol	$C_{10}H_{18}O_2$	170	152, 108, 95, 79, 67	825	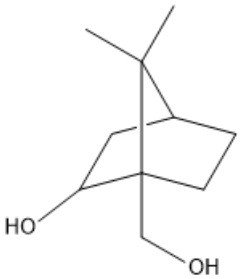	15.2	15.3
A10	(1R,2R,4S)-1,7,7-trimethylbicyclo[2.2.1]hept-5-en-2-ol	$C_{10}H_{16}O$	152	108, 93, 91,77,67	721	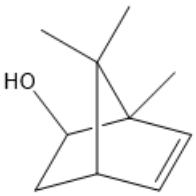	12.4	16.5
$O_2^{-\bullet}$ / $HO_2^{\bullet}$ (oxygenated with formic acid)								
TP	**Name**	**Formula**	**M^+ m/z**	**characteristic fragment ions**	**Relative Score**	**Structure**	**t_R (min) theoretical expected**	**t_R (min) experimental**
B1	(E)-4,8-dimethylnona-3,7-dien-2-ol	$C_{11}H_{20}O$	168	135, 107, 69	691	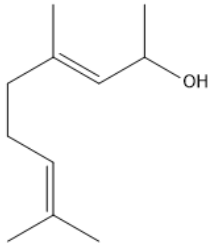	13.4	13.2
B2	(1S,4S,5S)-1,7,7-trimethylbicyclo[2.2.1]heptane-2,5-diol	$C_{10}H_{18}O_2$	170	124, 108, 95, 67	715		14.5	14.3
$H^{\bullet}$ (deaerated / TBA /pH 1)								
TP	**Name**	**Formula**	**M^+ m/z**	**characteristic**	**Relative**	**Structure**	**t_R (min) theoretical expected**	**t_R (min) experimental**

				fragment ions	Score			
C1	(1R,4R)-1,3,3-trimethylbicyclo[2.2.1]heptane	$C_{10}H_{18}$	138	123, 109, 95, 81	844		9.6	9.5
C2	p-Menth-8-ene, 3-methylene-	$C_{11}H_{18}$	150	135, 121, 107, 79	804	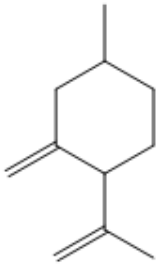	10.1	9.6
C3	2,2-Dimethyl-3-vinyl-bicyclo[2.2.1]heptane	$C_{11}H_{18}$	150	135, 107, 79, 67	688	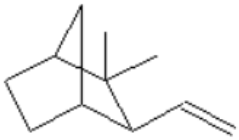	10.0	9.7
C4	(1S,3S,4R)-2,2,3-trimethylbicyclo[2.2.1]heptane	$C_{10}H_{18}$	138	123, 109, 95, 82	828	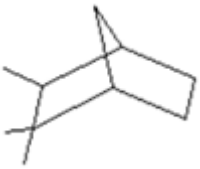	10.0	9.9
C5	1,7,7-Trimethyl bicyclo[2.2.1]hept-5-en-2-ol	$C_{10}H_{16}O$	152	108, 93, 77	791	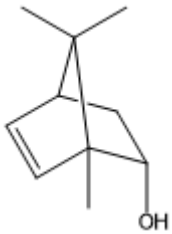	12.4	12.7
C6	2-isopropenyl-5-methyl-6-hepten-1-ol	$C_{11}H_{20}O$	168	107, 81, 69	701	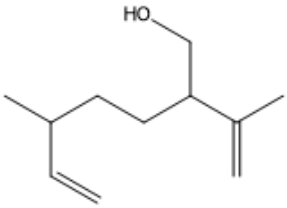	12.5	12.8
C7	Octanal, 7-hydroxy-3,7-dimethyl-	$C_{10}H_{20}O_2$	172	113, 97, 71	630	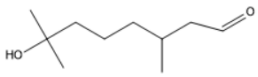	13.5	14.7

C8	Cyclopentane, 1-methyl-2-acetyl-3-(1-methylethenyl)-	$C_{11}H_{18}O$	166	151. 123, 81	711	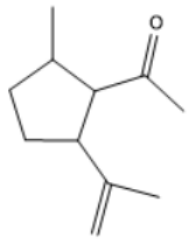	12.6	14.95
C9	4-(2,2,6-Trimethyl-bicyclo[4.1.0]hept-1-yl)-butan-2-one	$C_{14}H_{24}O$	208	150, 135, 107	813	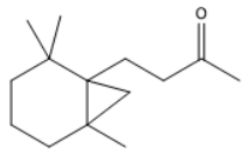	16.4	17.0

e_{aq}^{-} (deaerated / TBA)

TP	Name	Formula	M^+ m/z	characteristic fragment ions	Relative Score	Structure	t_R (min) theoretical expected	t_R (min) experimental
D1	(2S,4R)-1,7,7-trimethylbicyclo[2.2.1]heptan-2-ol	$C_{10}H_{18}O$	154	108, 93, 77	797	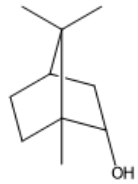	11.3	11.6
D2	2-(2,2,3-trimethylcyclopent-3-en-1-yl)acetaldehyde	$C_{10}H_{16}O$	152	108, 93, 55	746	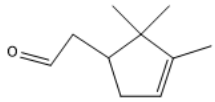	11.35	11.65
D3	(E)-5-isopropyl-6-methylhepta-3,5-dien-2-ol	$C_{11}H_{20}O$	168	111, 95, 69	704	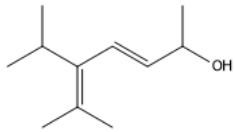	12.6	13.0
D4	1,1,3-trimethyl-3-(2-methylallyl)cyclopentane	$C_{12}H_{22}$	166	111, 95, 69	736	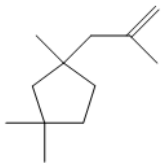	12.7	13.1

D5	Trans-Z-α-bisabolene epoxide	$C_{15}H_{24}O$	220	149, 121, 109, 93	730	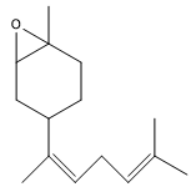	18.6	18.5
D6	Cyclohexanemethanol, 4-ethenyl-α,α,4-trimethyl-3-(1-methylethenyl)-,	$C_{15}H_{26}O$	222	189, 161, 133, 121, 108, 93	748	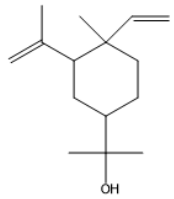	17.4	18.7

Table S2. Tentative structures of the TPs generated from GSM radiolysis

HO• (solution saturated with N_2O)								
TP	**Name**	**Formula**	**M^+ m/z**	**characteristic fragment ions**	**Relative Score**	**Structure**	**t_R (min) theoretical expected**	**t_R (min) experimental**
	Gεosmin	$C_{12}H_{22}O$	182	835	839	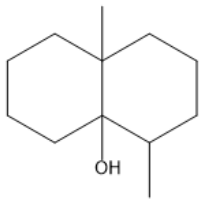		
A'1	1,5-dimethyl-7-oxabicyclo[4.1.0]heptane	C_8H_{14O}	126	770	703	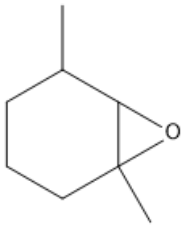		
A'2	(Z)-2-ethylhex-2-enal	$C_8H_{14}O$	126	744	769	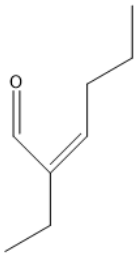		
A'3	1-(2,6-dimethyl-7-oxabicyclo[4.1.0]heptan-1-yl)ethanone	$C_{10}H_{16}O_2$	168	707	632	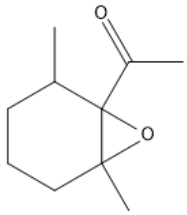		
A'4	1-(2-(1-hydroxyethyl)cyclohex-1-en-1-yl)ethanone	$C_{10}H_{16}O_2$	168	626	671	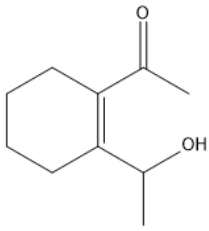	15.3	17.2
A'5	4a,8-dimethyl-4,4a,5,6,7,8-hexahydronaphthalen-2(3H)-one	$C_{12}H_{18}O$	178	732	809	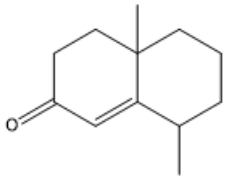	17.2	17.6

A'6	8a-hydroxy-4a-methyloctahydronaphthalen-2(1H)-one	$C_{11}H_{18}O_2$	182	672	680	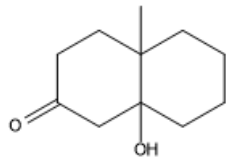	16.9	17.7
A'7	3-(4-hydroxybutyl)-2-methylcyclohexanone	$C_{11}H_{20}O_2$	184	709	737	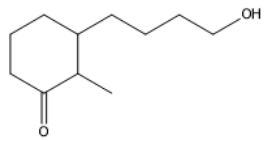	17.5	18.7
A'8	4a-hydroxy-8a-methyloctahydronaphthalen-2(1H)-one	$C_{11}H_{18}O_2$	182	774	782	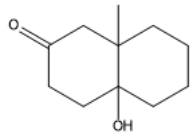	16.9	18.9
$O_2^{-\bullet}$ / $HO_2^{\bullet}$ (oxygenated with formic acid)								
TP	**Name**	**Formula**	**M^+ m/z**	**characteristic fragment ions**	**Relative Score**	**Structure**	**t_R (min) theoretical expected**	**t_R (min) experimental**
B'1	4a,8-dimethyl-1,2,3,4,4a,5,6,8a-octahydronaphthalene	$C_{12}H_{20}$	164	149, 109, 57	821	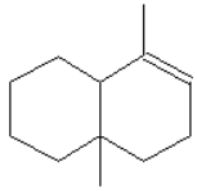		
B'2	8,8a-dimethyldecahydronapthalen-1-ol	$C_{12}H_{22}O$	182	149, 107, 93	854	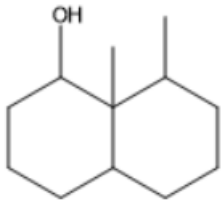		
B'3	6,7-dimethyl-1,2,3,5,8,8a-hexahydronaphthalene	$C_{12}H_{18}$	162	147, 119, 105	864	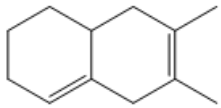		
$H^{\bullet}$ (deaerated / TBA /pH 1)								

TP	Name	Formula	M^+ m/z	characteristic fragment ions	Relative Score	Structure	t_R (min) theoretical expected	t_R (min) experimental
C'1	2-Pentene, 2,4-dimethyl-	C_7H_{14}	112	98, 83, 55	736		7.4	8.3
C'2	2,2,4-trimethylpentan-1-ol	$C_8H_{18}O$	130	99, 83, 57	745	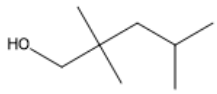	9.1	8.9
C'3	2,5-dimethylhexane-2,5-diol	$C_8H_{18}O_2$	146	113, 95, 70, 59	863	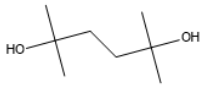	10.1	10.3
C'4	1,5-dimethyldecahydronaphthalene	$C_{12}H_{22}$	166	151, 123, 109, 95, 81	750	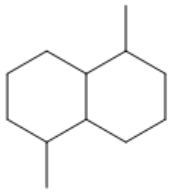	12.9	13.1
C'5	1H-Indene, 1-ethylidene octahydro-7a-methyl	$C_{12}H_{20}$	164	149, 124, 108, 93	776	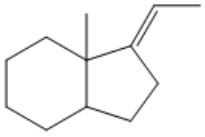	13.1	13.3
C'6	2Naphthalenone, octahydro-8a-hydroxy-4a-methyl	$C_{11}H_{18}O_2$	182	126, 112, 97, 55	744	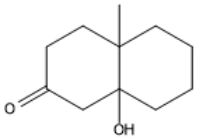	16.5	18.7
C'7	2Naphthalenone, octahydro-4a-5-dimethyl	$C_{12}H_{20}O_2$	180	95, 81, 69	694	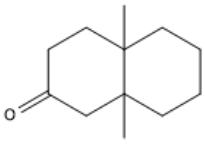	15.5	18.8
C'8	Crymbolone or 4a-hydroxy-4,8a-dimethyl-6-(prop-1-en-2-yl)octahydronaphtha	$C_{15}H_{24}O_2$	236	218, 203, 109, 95, 69	729	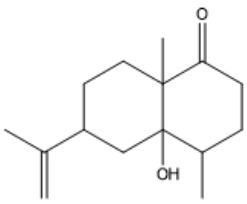	18.9	18.8

	len-1(2H)-one							
e_{aq}^- (deaerated / TBA)								
TP	**Name**	**Formula**	**M^+ m/z**	**characteristic fragment ions**	**Relative Score**	**Structure**	**t_R (min) theoretical expected**	**t_R (min) experimental**
D'1	3-(2,6,6-trimethylcyclohex-1-en-1-yl)prop-2-en-1-ol	$C_{12}H_{20}O$	180	147, 119, 105, 93	706	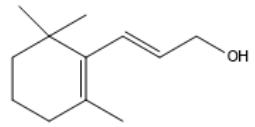	15.5	15.3
D'2	3-(2,2-dimethyl-6-methylene cyclohexyl)propanal	$C_{12}H_{20}O$	180	147, 119, 106, 91	636	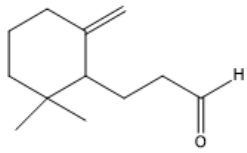	15.1	15.4
D'3	3-(2,2-dimethyl-6-methylene cyclohexyl)propan-1-ol	$C_{12}H_{22}O$	182	167, 149, 121	670	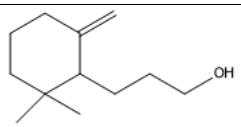	15.3	15.4
D'4	4a,5-dimethyloctahydronaphthalen-2(1H)-one	$C_{12}H_{20}O$	180	165, 109, 81, 55	633	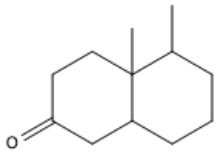	15.6	15.6
D'5	2,3-dimethyl-2-(3-oxobutyl)cyclohexanone	$C_{12}H_{20}O_2$	196	139, 126, 55	591	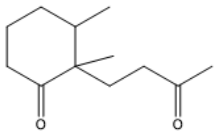	17.1	18.0
D'6	2,3,3-trimethyl-2-(3-methylbuta-1,3-dien-1-yl)-6-methylenec	$C_{15}H_{22}O$	218	203, 163, 147, 119	687	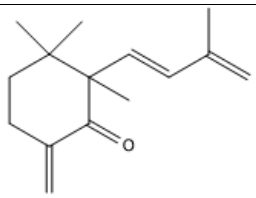	17.5	19.6

D'7 (artifact)	2-(4a-methyl-8-methylene decahydro naphthalen-2-yl)propan-2-ol	$C_{15}H_{26}O$	222	164, 149, 135, 109	639	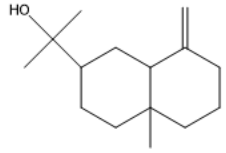	18.0	19.9
D'8 (artifact)	2-(4a,8-dimethyl-1,2,3,4,4a,5,6,7-octahydro naphthalen-2-yl)propan-2-ol	$C_{15}H_{26}O$	222	204, 189, 161, 147, 133	671	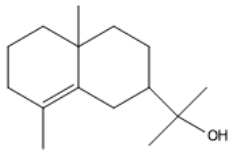	18.2	20.6
D'9 (artifact)	2-(4a,8-dimethyl-1,2,3,4,4a,5,6,8a-octahydro naphthalen-2-yl)propan-2-ol	$C_{15}H_{26}O$	222	204, 189, 161, 149, 81	742	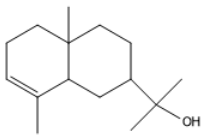	17.8	20.7

Table S3. MS spectrums of TPs produced from degradation of MIB under the influence of various RS and their match with NIST library (top (red): spectrum from NIST library, bottom (blue): experimentally obtained spectrum)

HO• (solution saturated with N_2O)		
MIB	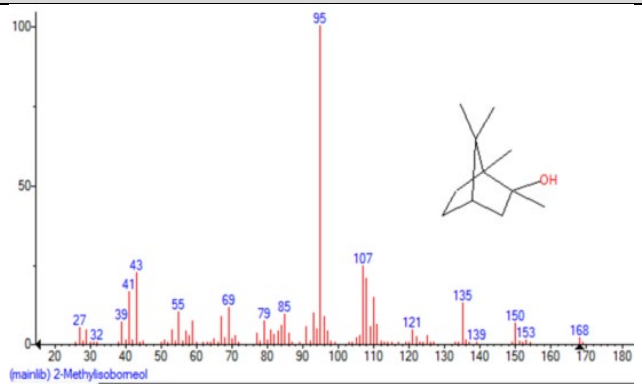	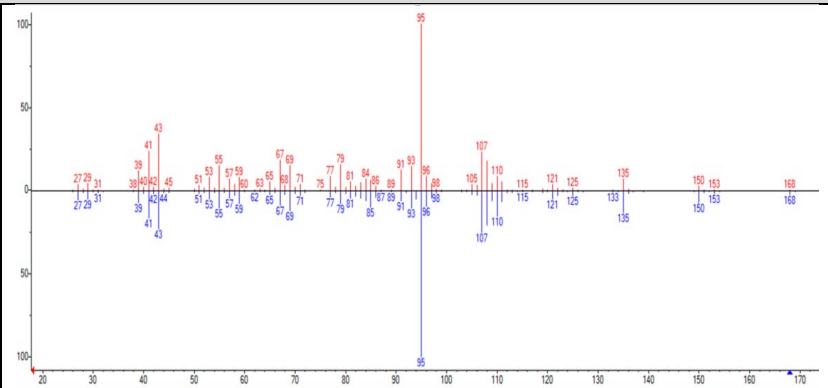
A1	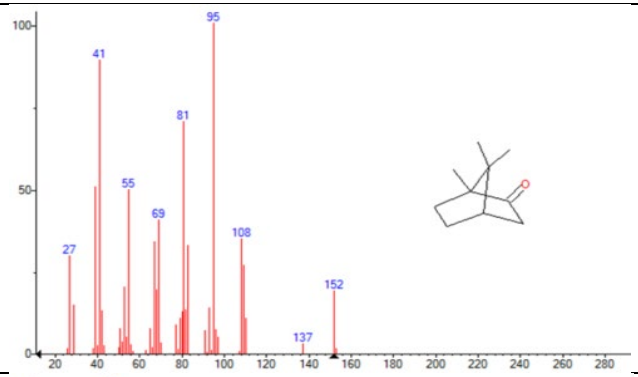	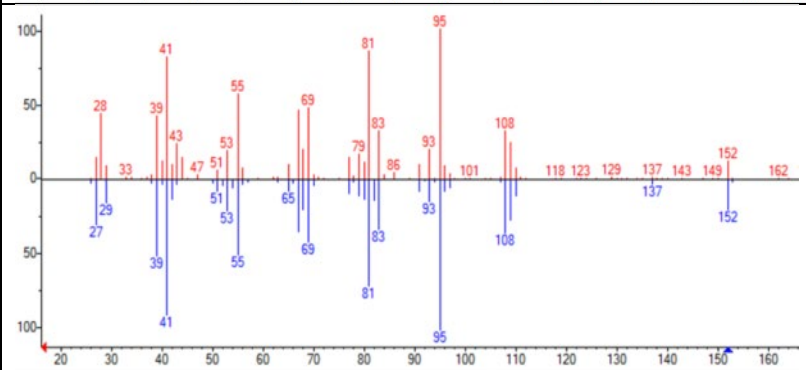
A2	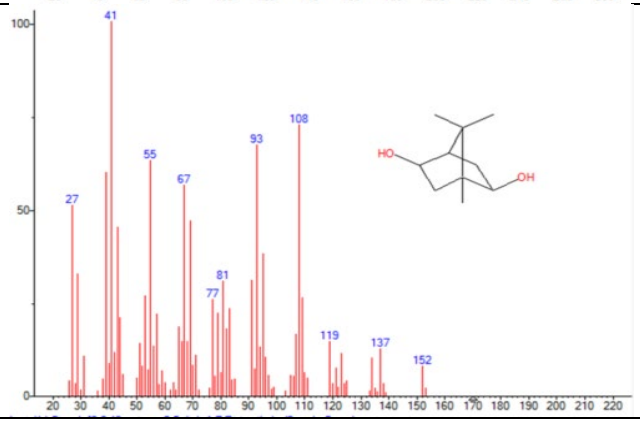	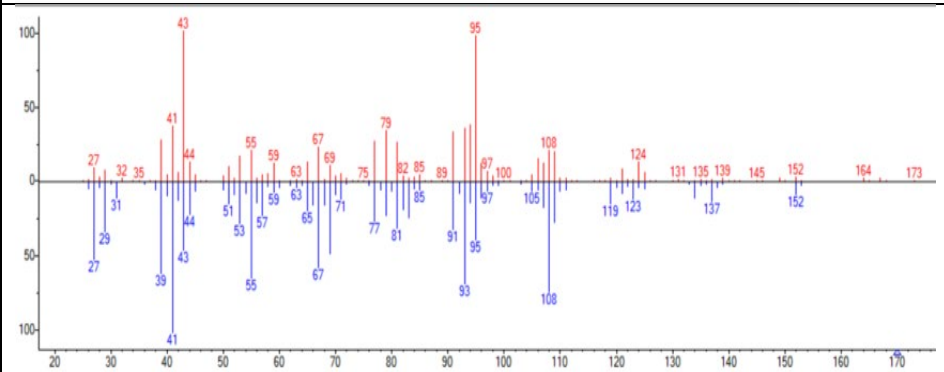

A3

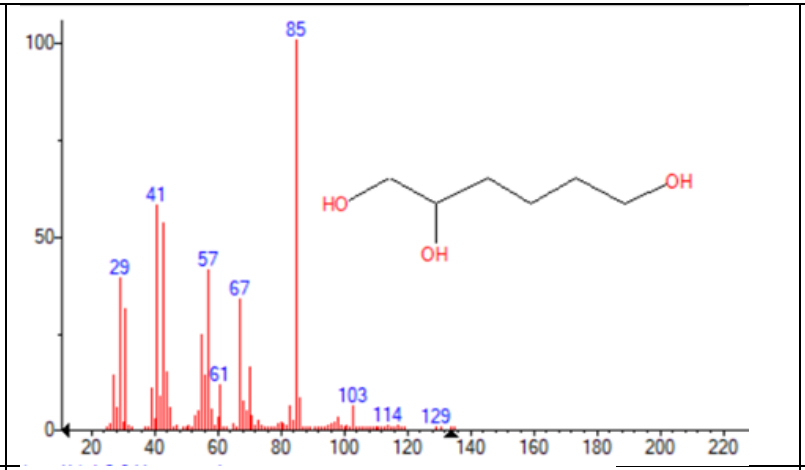

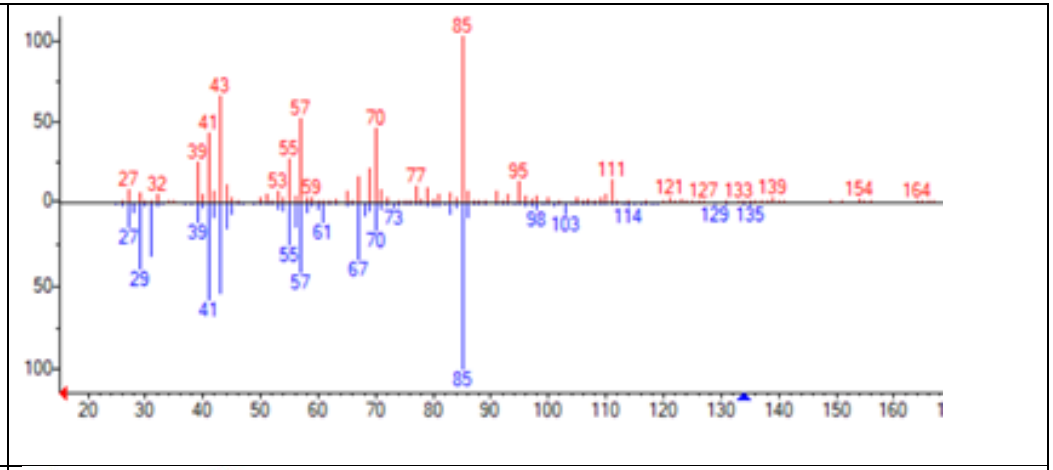

A4

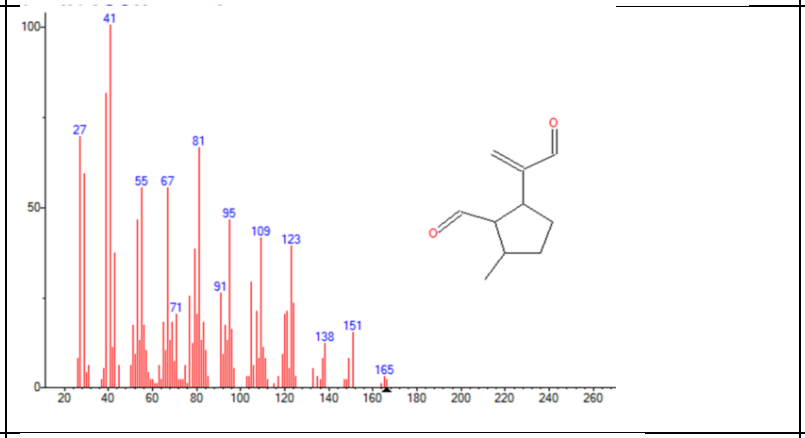

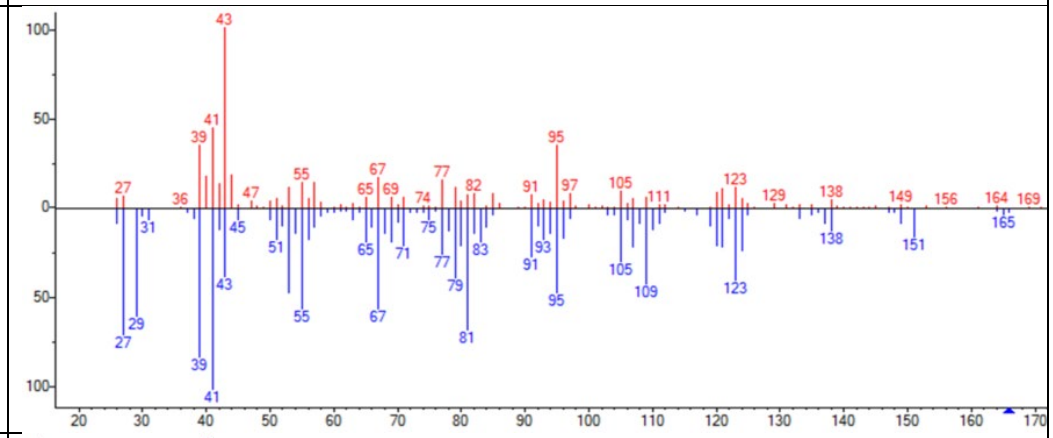

A5

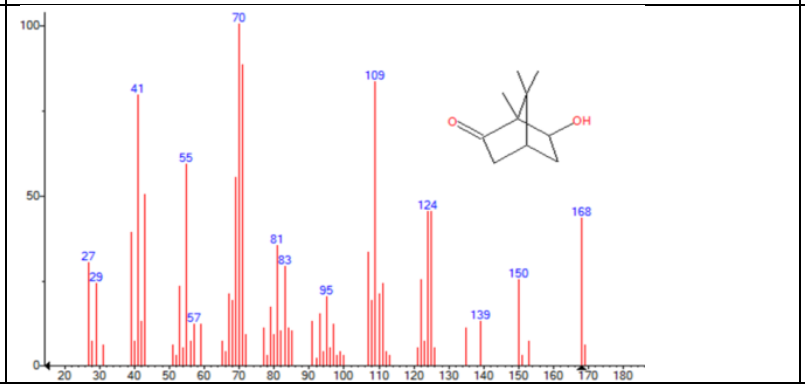

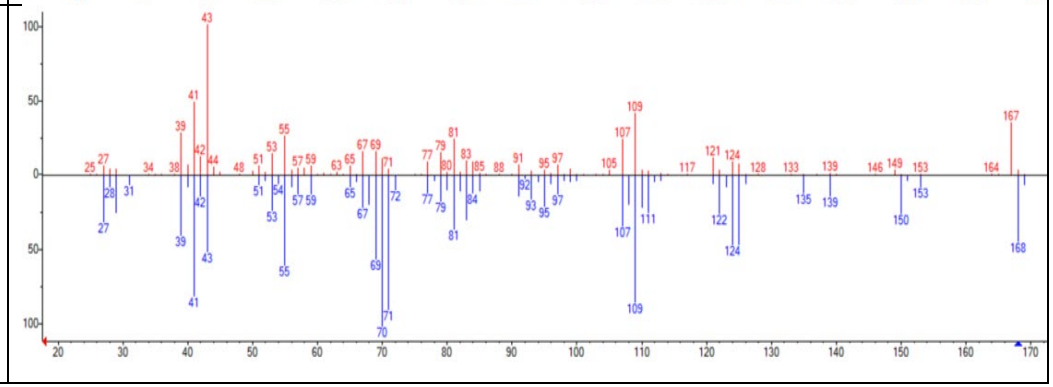

A6	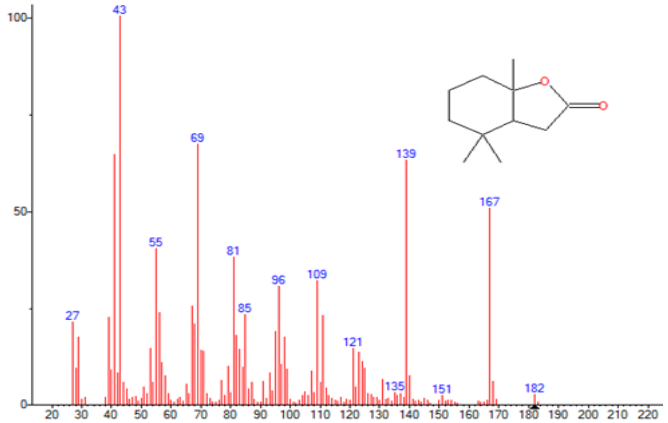	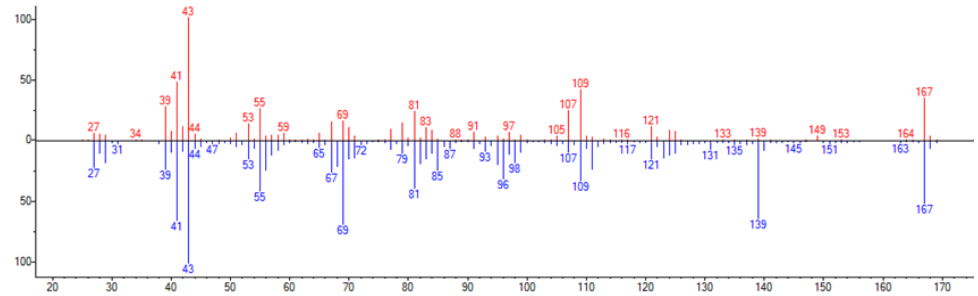
A7	unidentified	
A8	unidentified	
A9	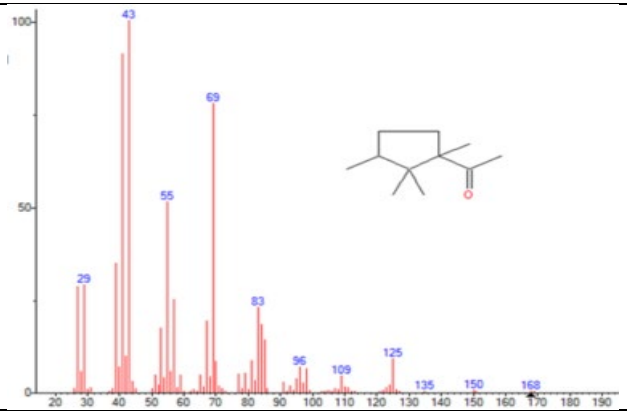	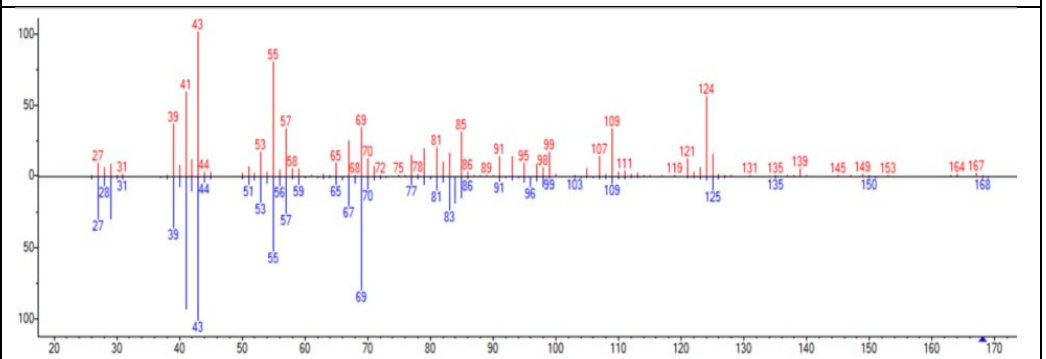
A10	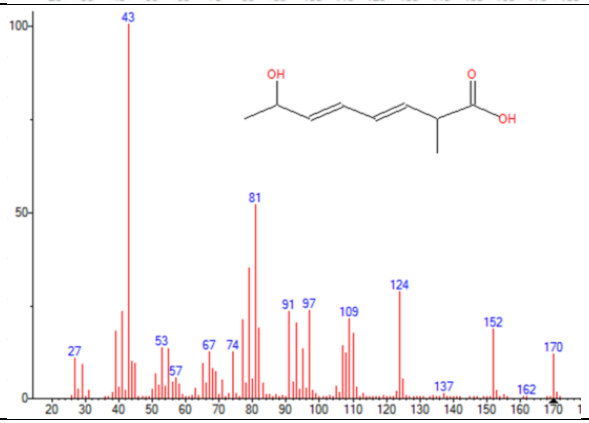	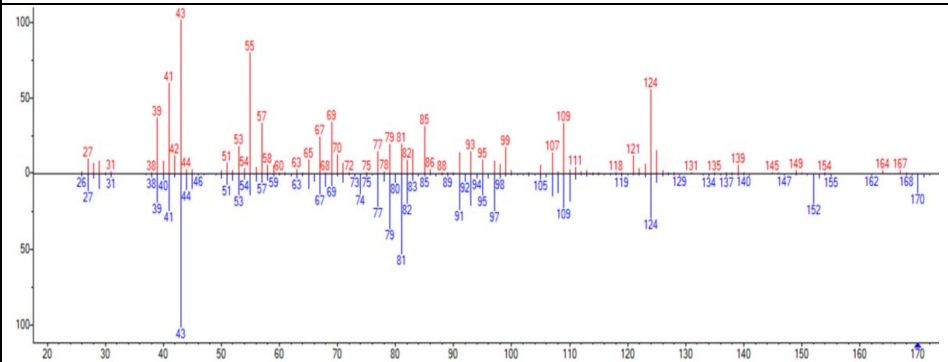

A11	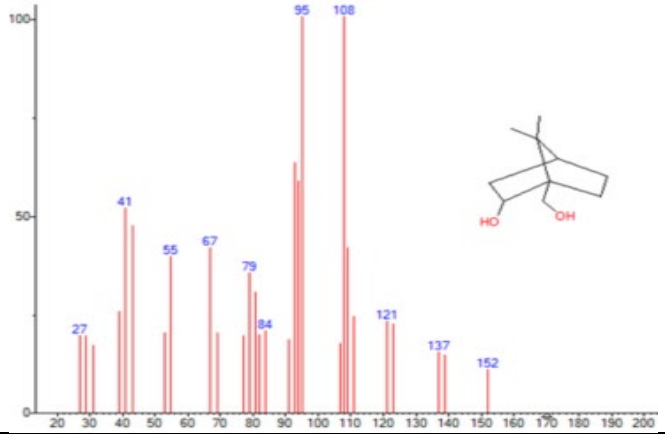	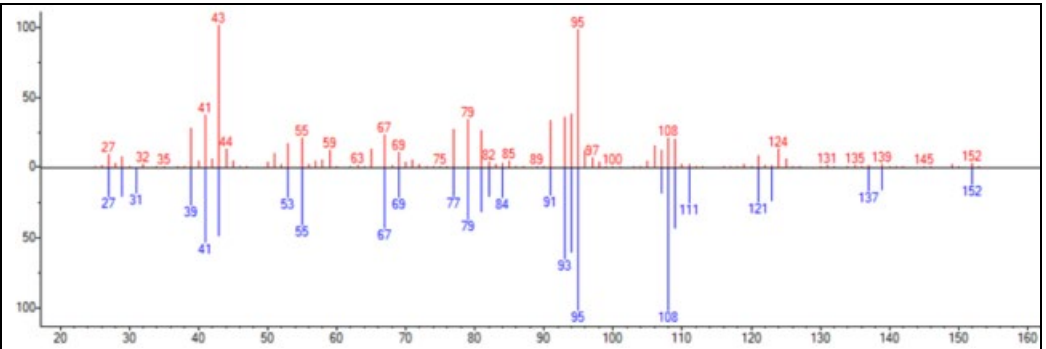
A12	unidentified	
A13	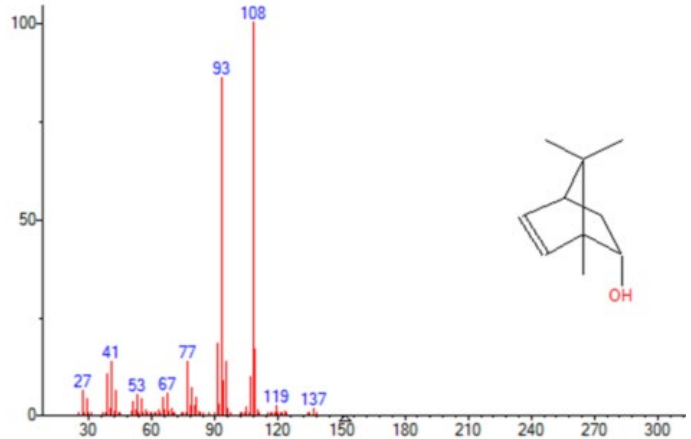	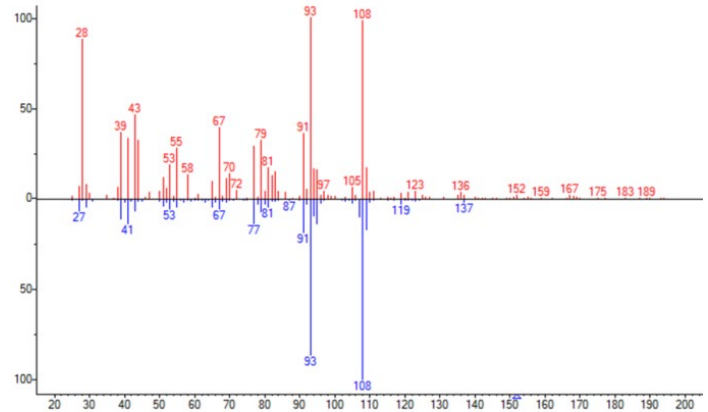

STD contaminant 1	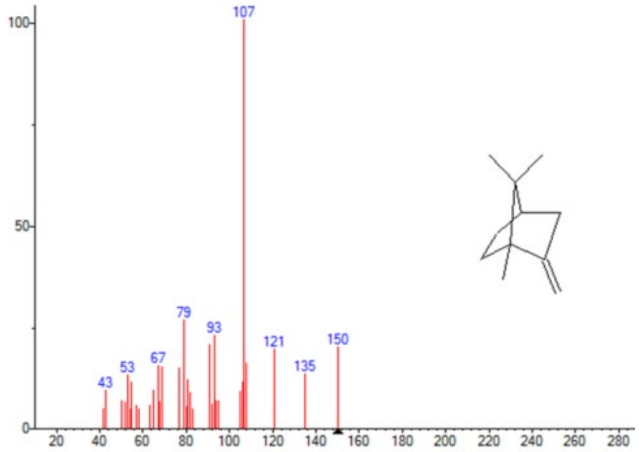	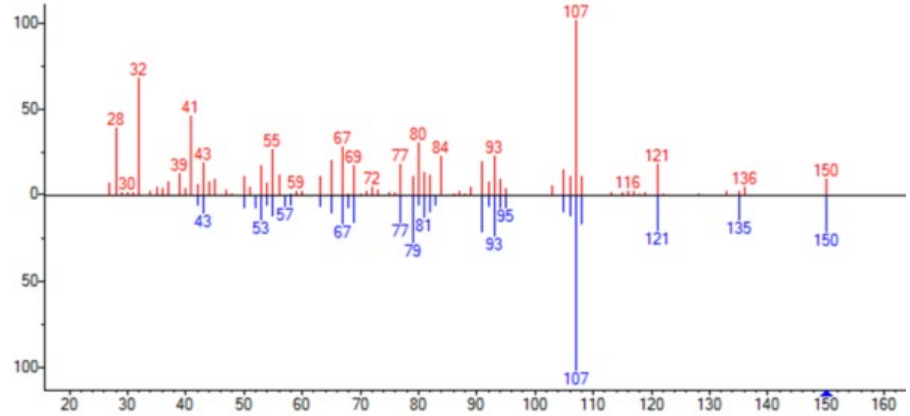
STD contaminant 2	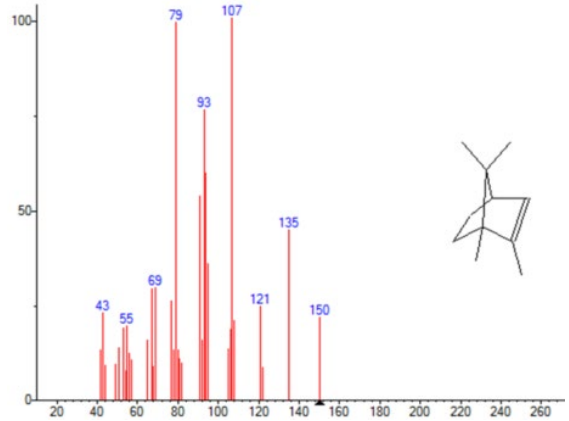	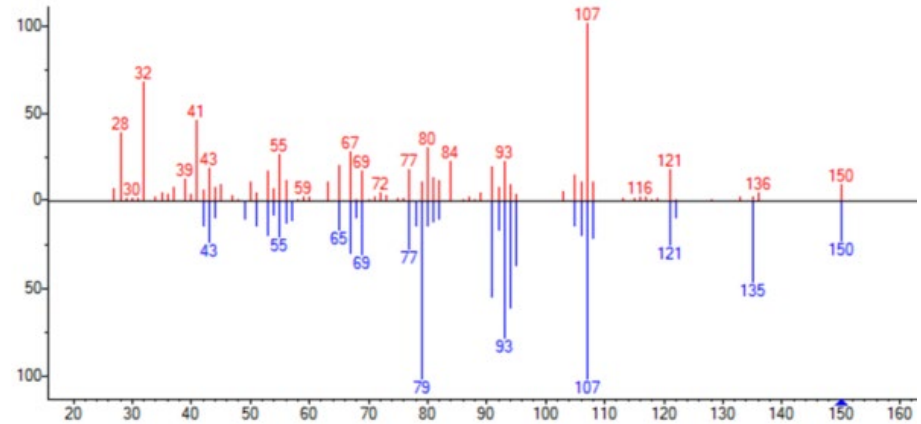
$O_2^{-\bullet}$ / $HO_2^{\bullet}$ (oxygenated)		

C1	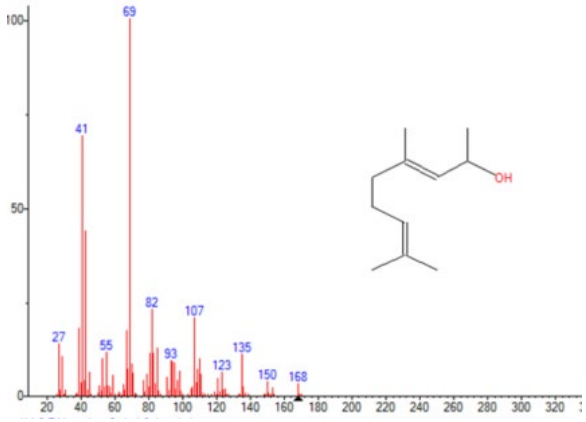	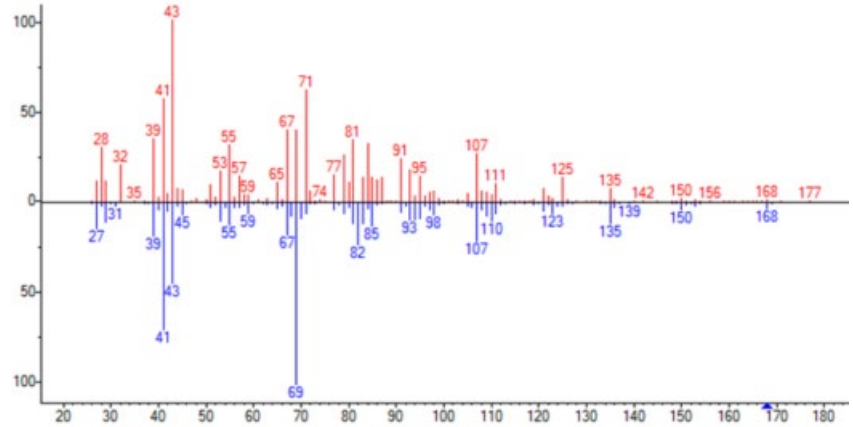
C2	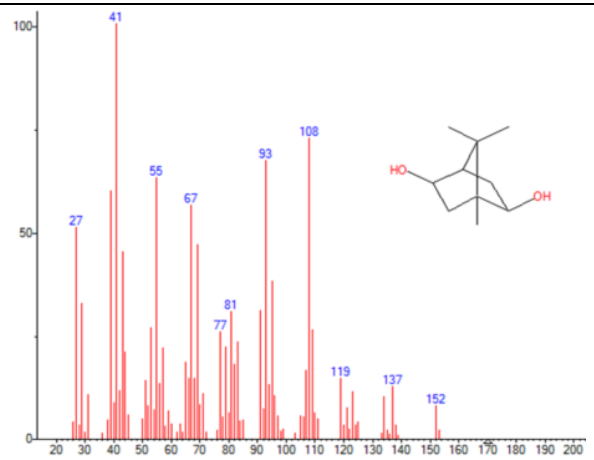	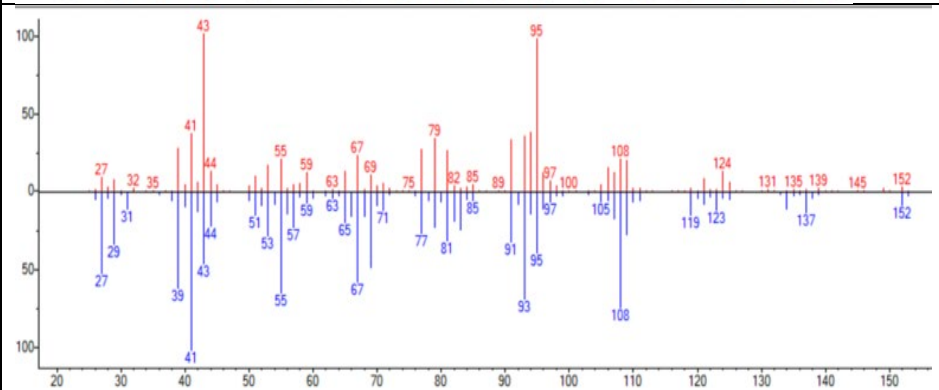
STD contamination	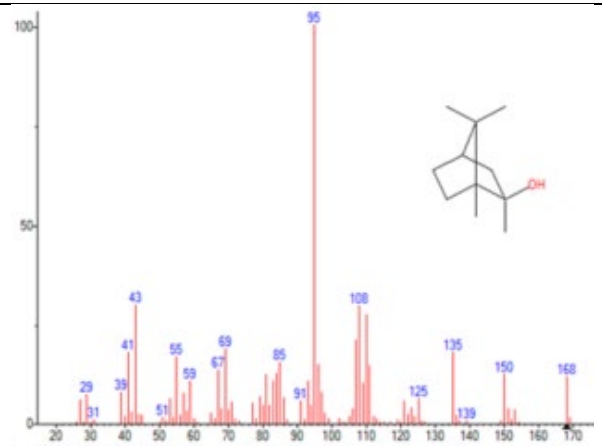	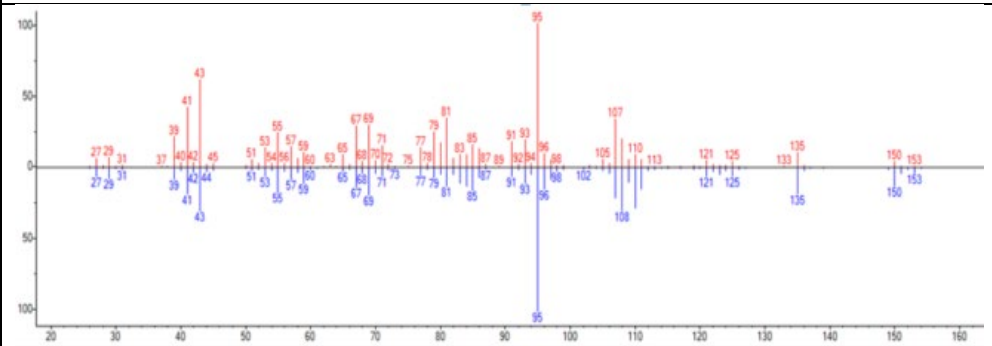

H• (deaerated / TBA /pH 1)		
C1	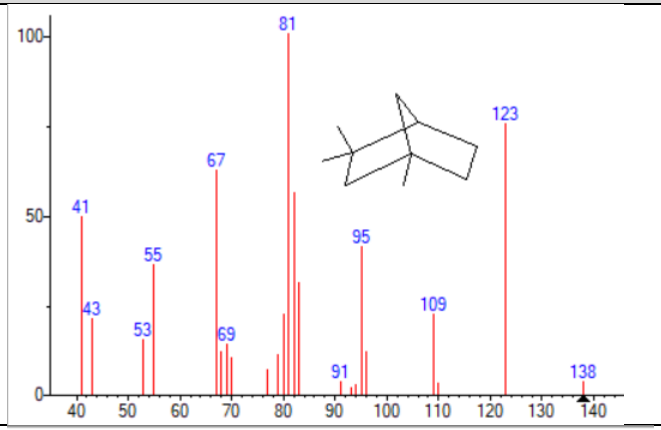	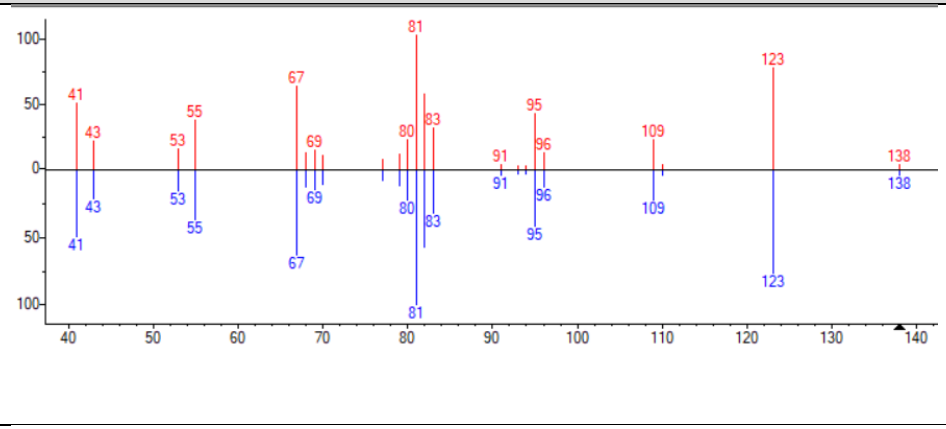
C2	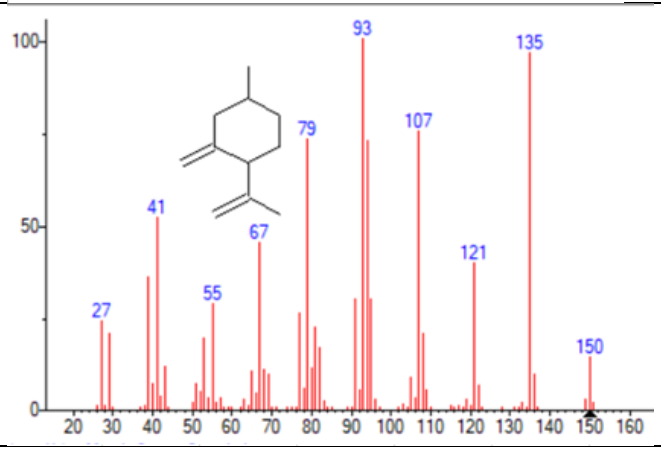	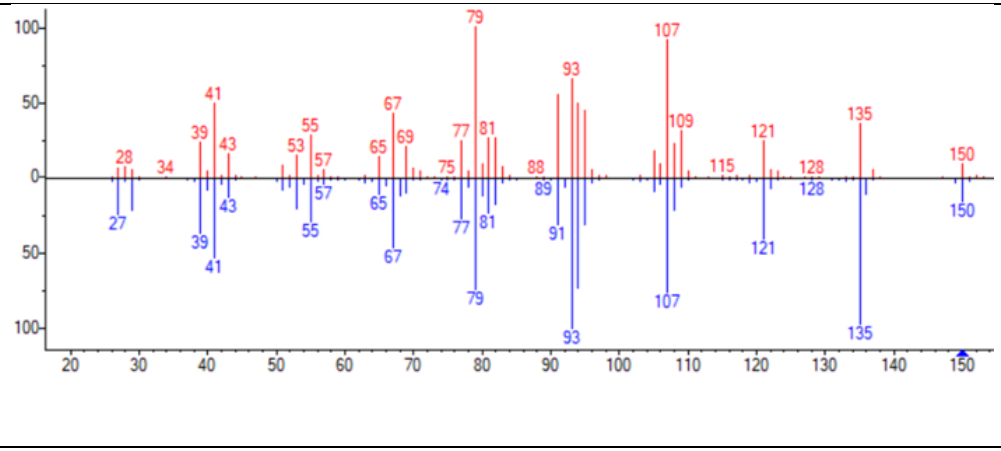

C3	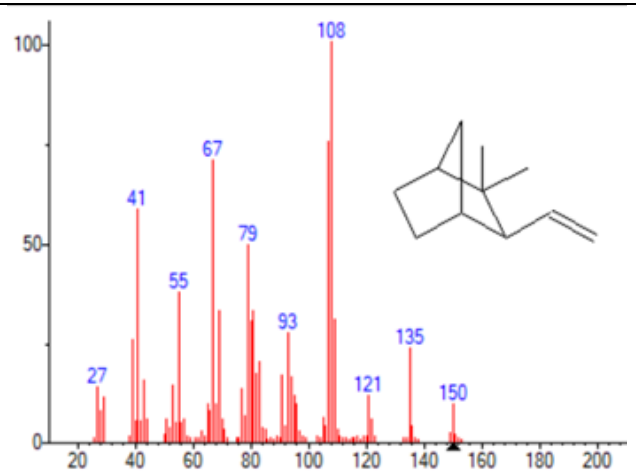	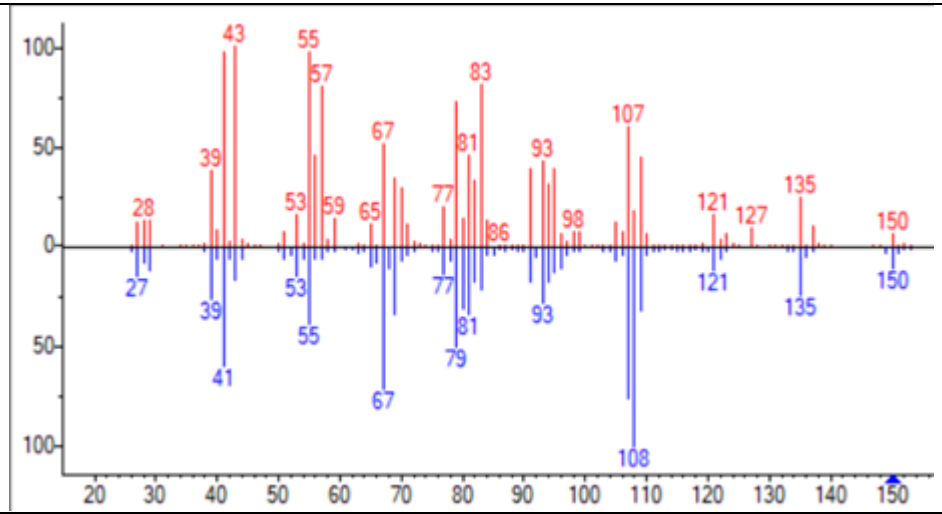
C4	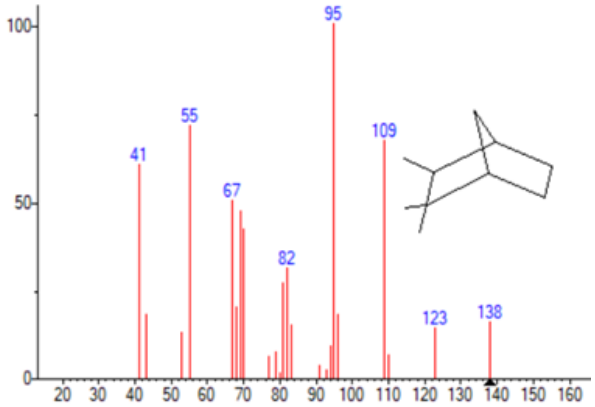	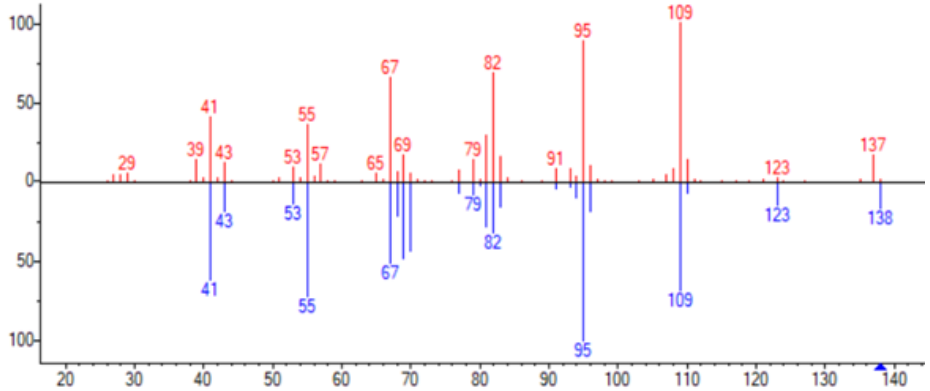

C5	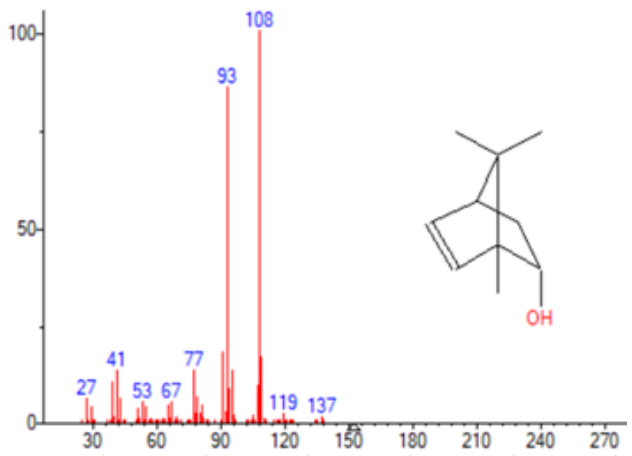 108 93 41 27 53 67 77 119 137 OH	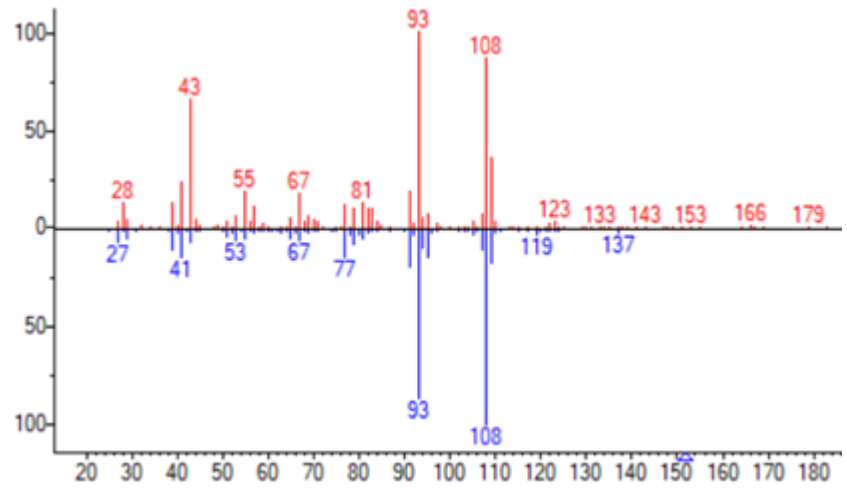 93 108 43 28 55 67 81 123 133 143 153 166 179 27 41 53 67 77 119 137 93 108
C6	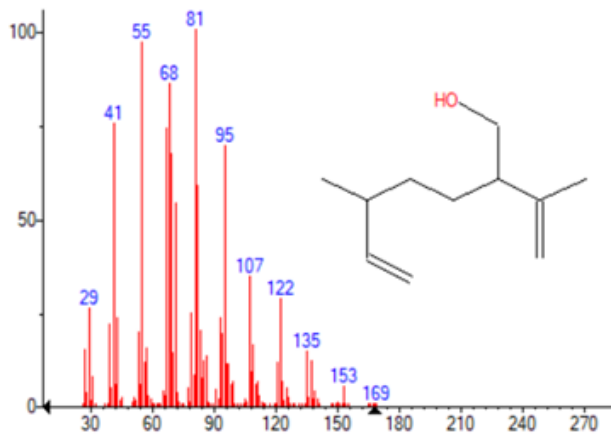 55 81 68 41 95 HO 107 122 29 135 153 169	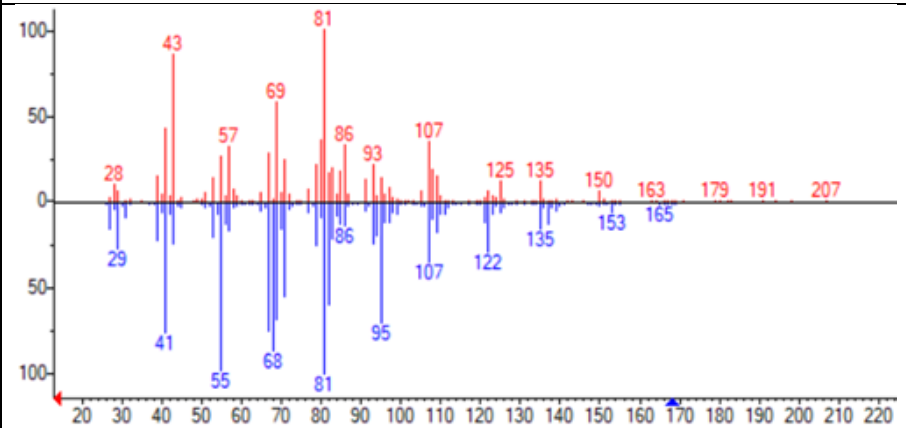 81 43 69 57 86 93 107 28 125 135 150 163 179 191 207 153 165 29 86 135 107 122 41 95 55 68 81

C7	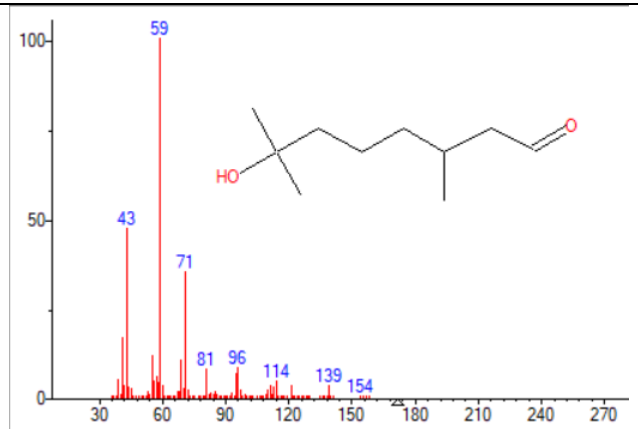	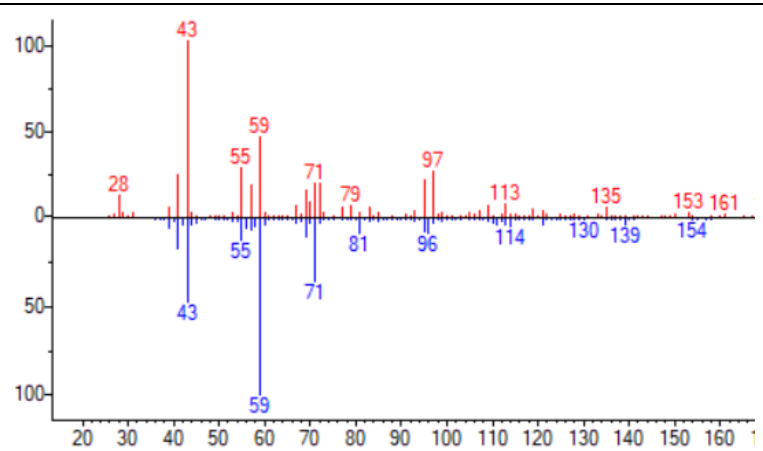
C8	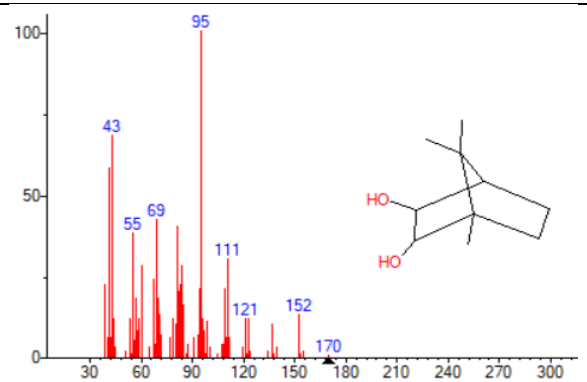	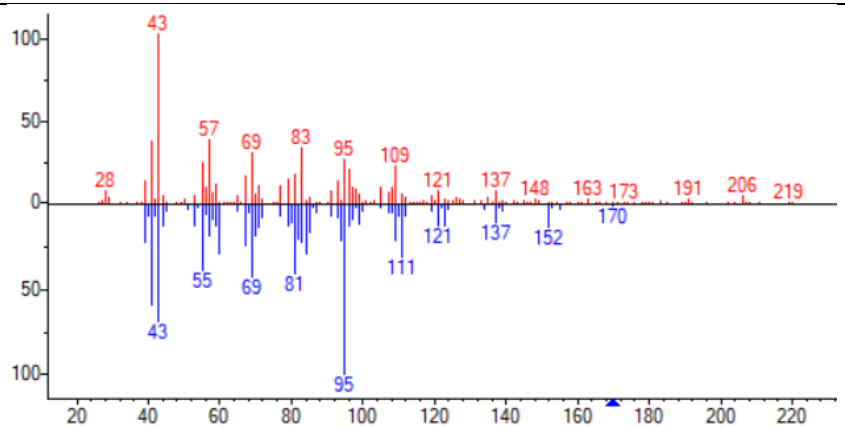
C9	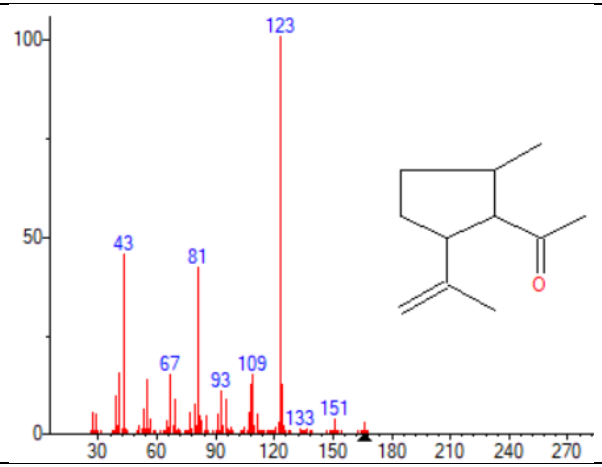	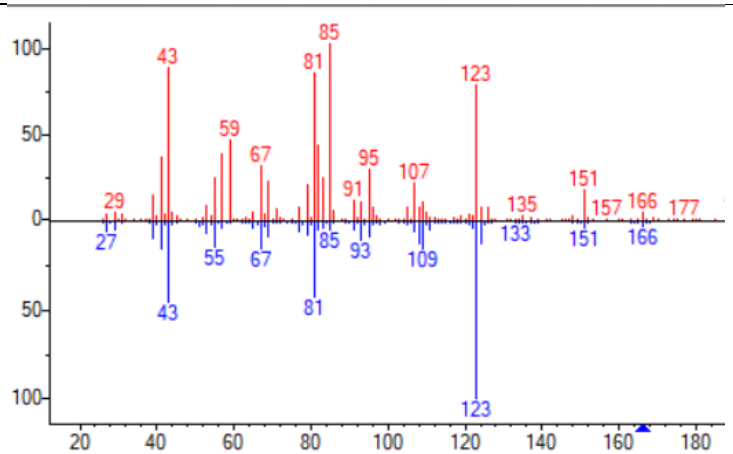

C10	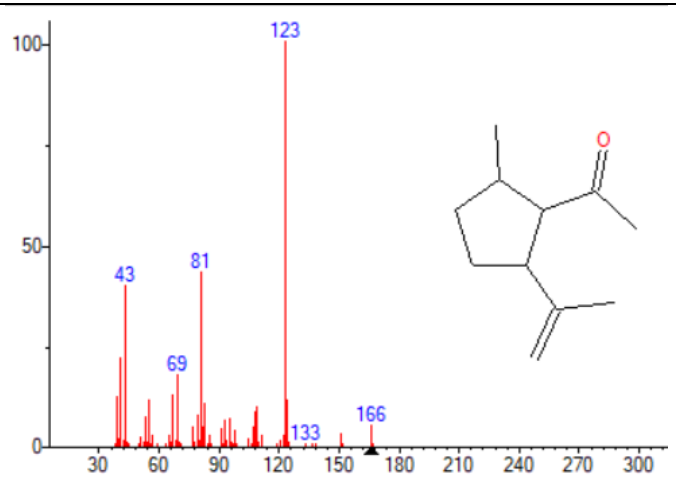 123 43 81 69 133 166 O	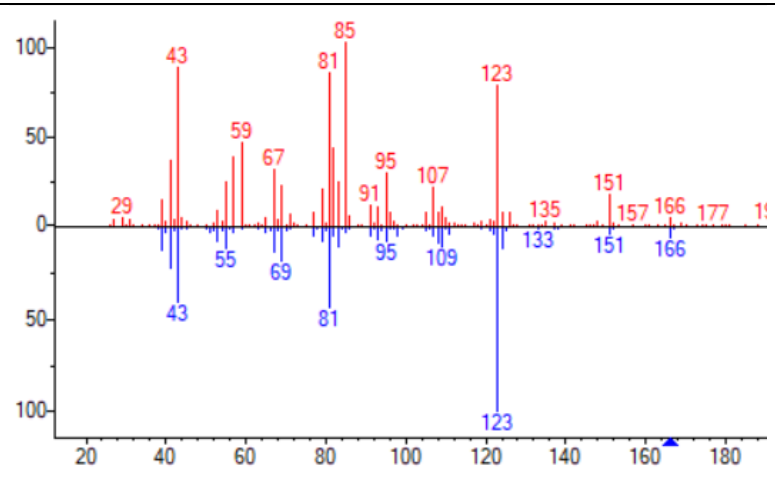 43 85 81 123 59 67 95 107 91 29 135 151 157 166 177 55 69 95 109 133 151 166 43 81 123
C11	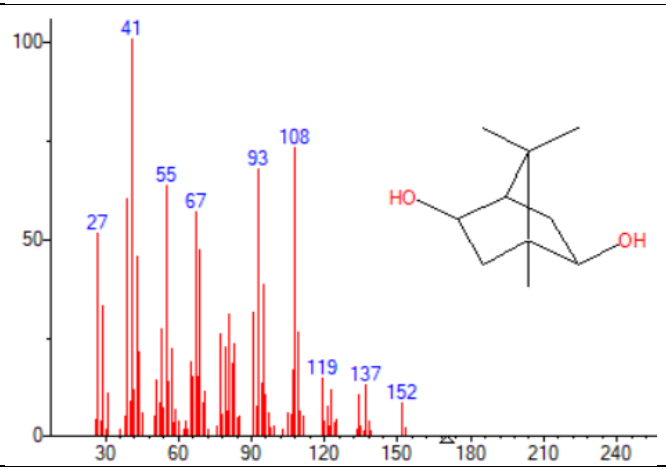 41 108 93 55 67 27 HO OH 119 137 152	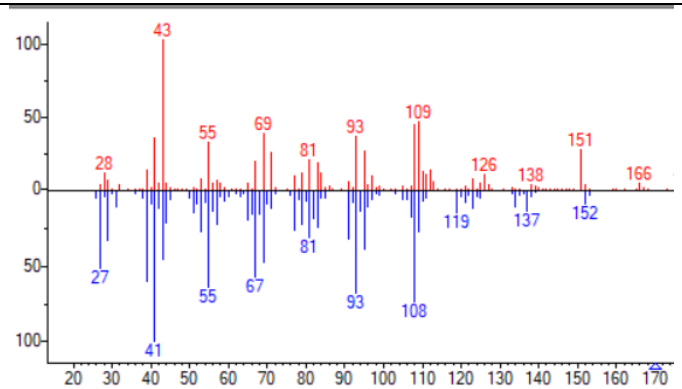 43 109 55 69 93 81 151 28 126 138 166 119 137 152 27 55 67 81 93 108 41

C12

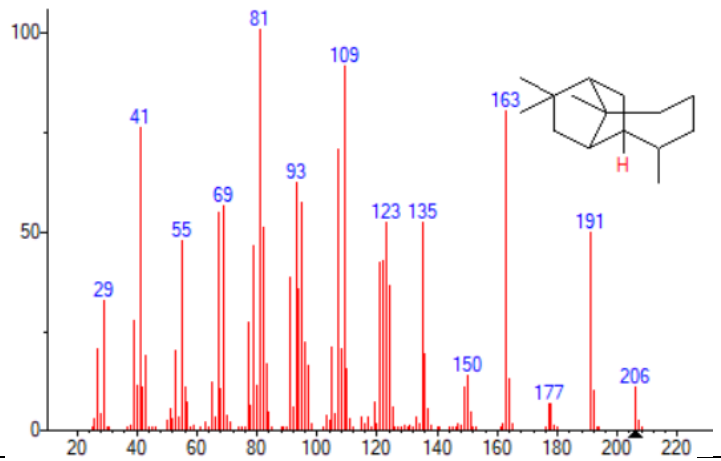
81
109
41
163
93
69
55
123 135
191
29
150
177
206
H

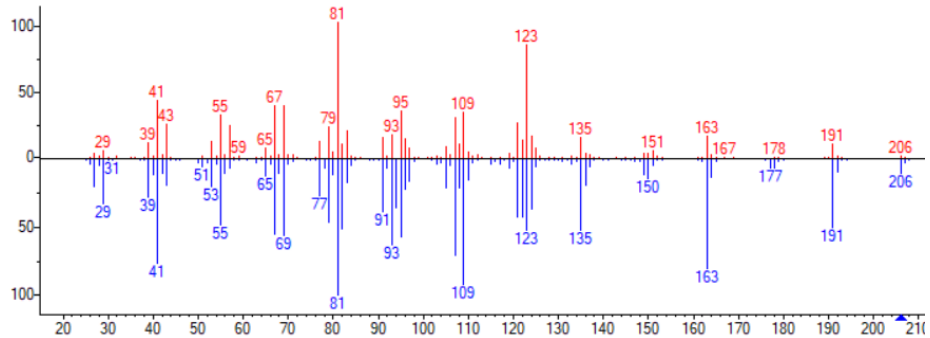
81
123
41
43
55
67
95
109
79
93
135
151
163
167
178
191
206
29
39
59
65
31
51
53
77
91
150
177
29
39
41
55
69
81
93
109
123
135
163
191
206

C13

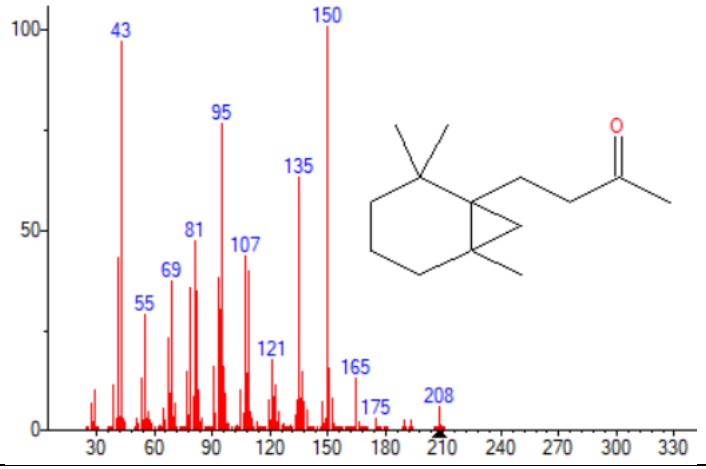
43
150
95
135
81
107
69
55
121
165
175
208
O

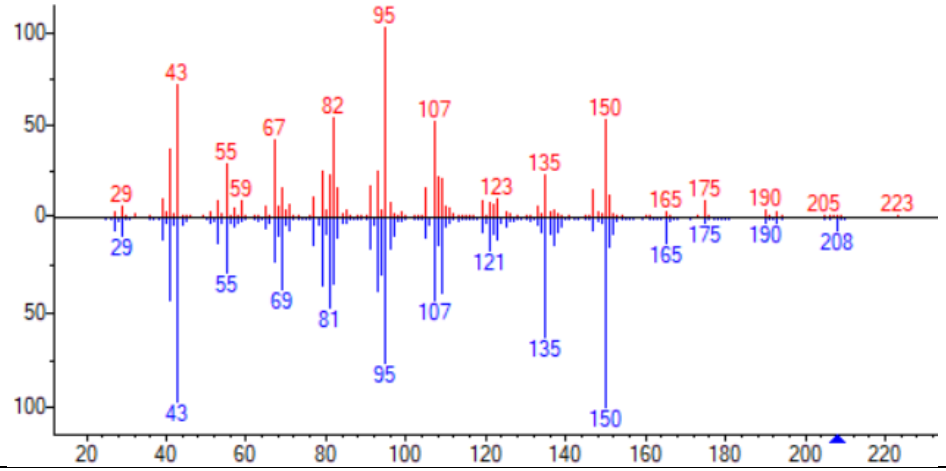
95
43
82
107
150
67
55
135
29
59
123
165
175
190
205
223
121
29
55
69
81
107
135
150
165
175
190
208
95
43

C14	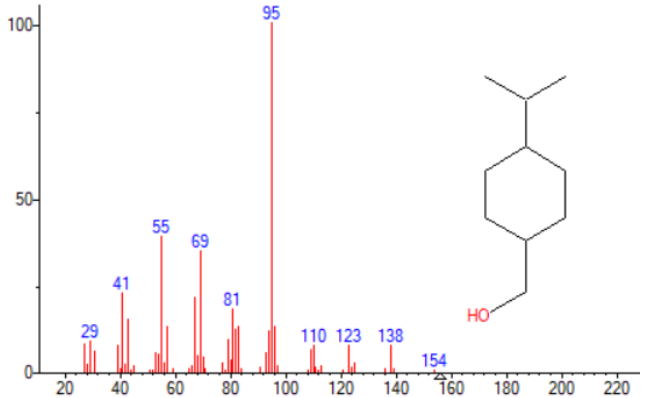	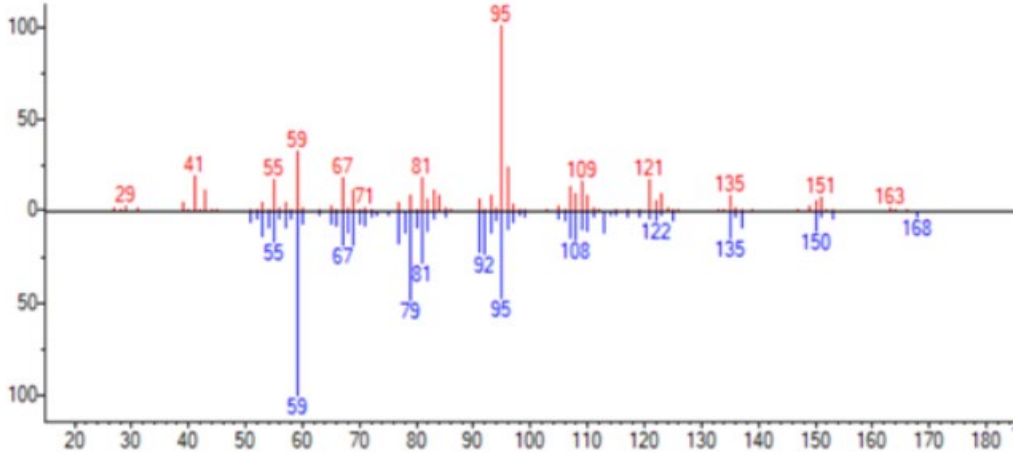
C15	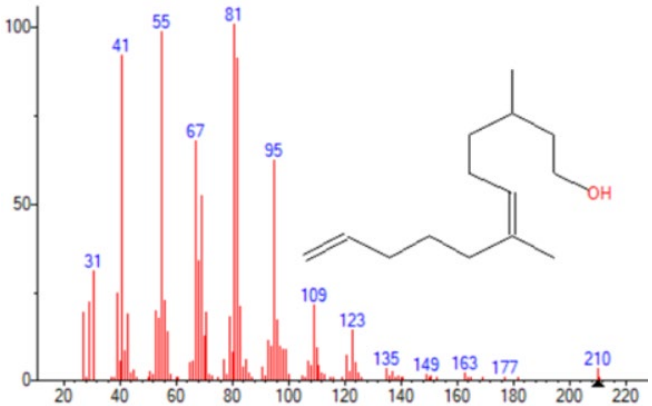	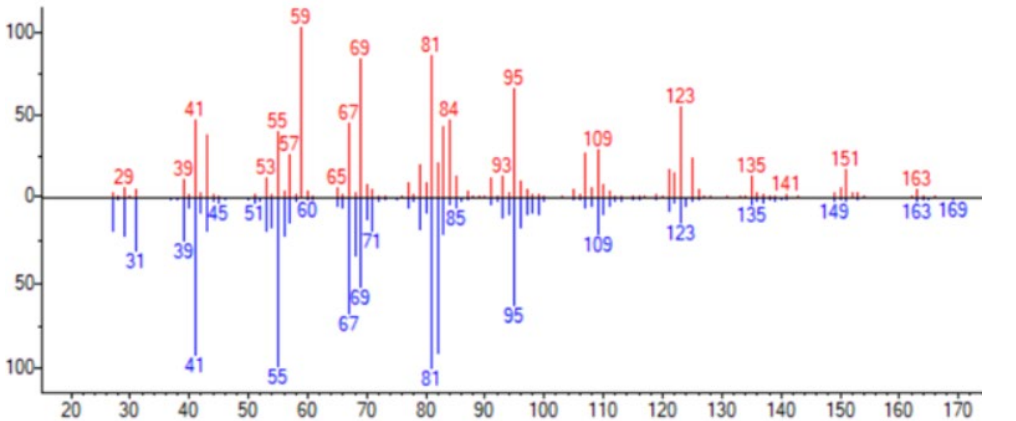
C16	Isomer of C15	
e_{aq}^- (deaerated / TBA)		

D1

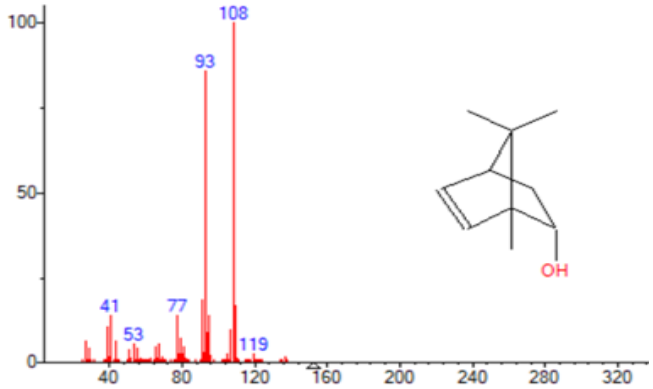
108
93
41
53
77
119
OH

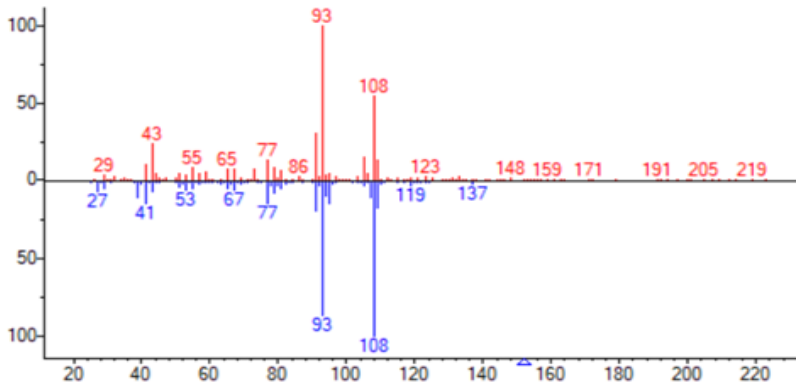
93
108
43
29
55
65
77
86
123
148
159
171
191
205
219
27
41
53
67
77
119
137
93
108

D2

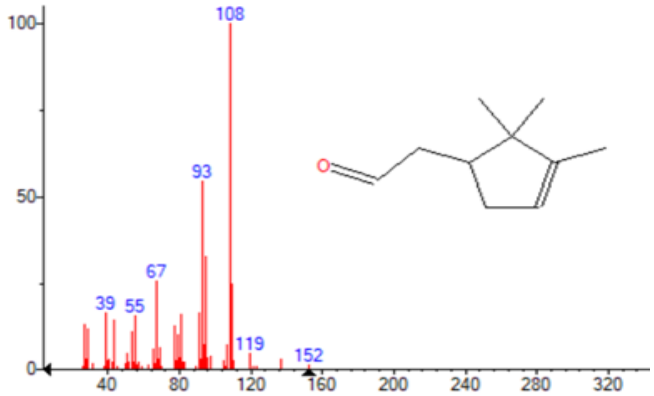
108
93
67
39
55
119
152
O

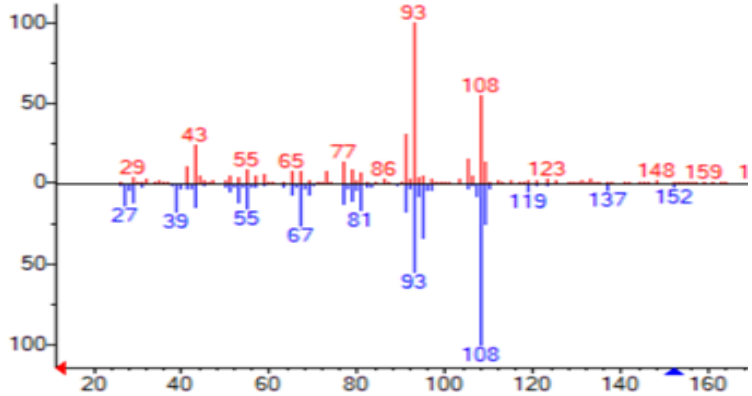
93
108
43
29
55
65
77
86
123
148
159
27
39
55
67
81
119
137
152
93
108

D3

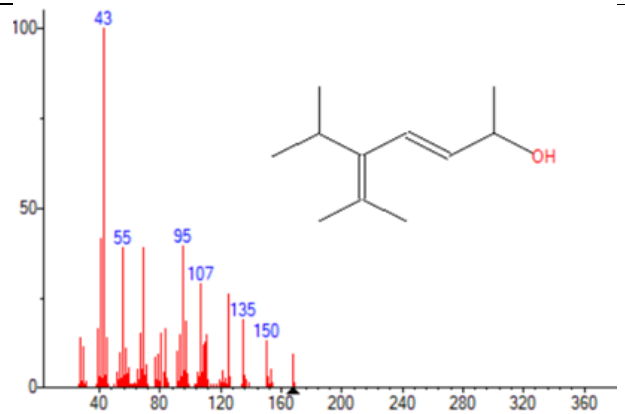
43
55
95
107
135
150
OH

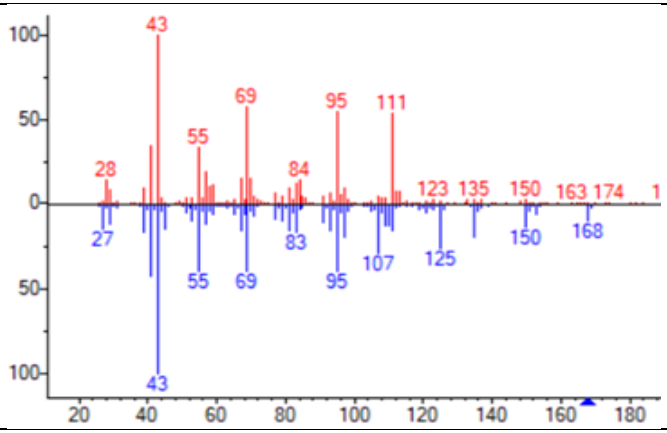
43
69
95
111
55
28
84
123
135
150
163
174
27
55
69
83
95
107
125
150
168
43

D4	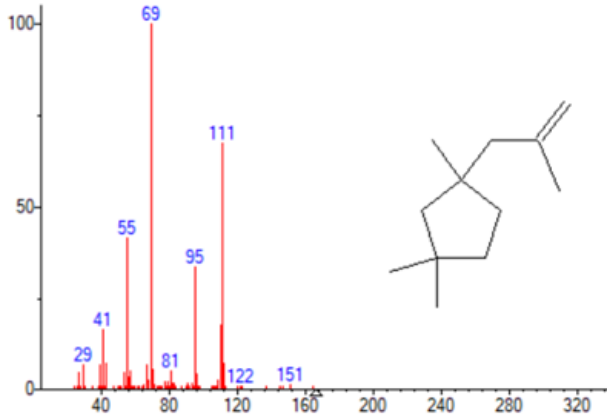	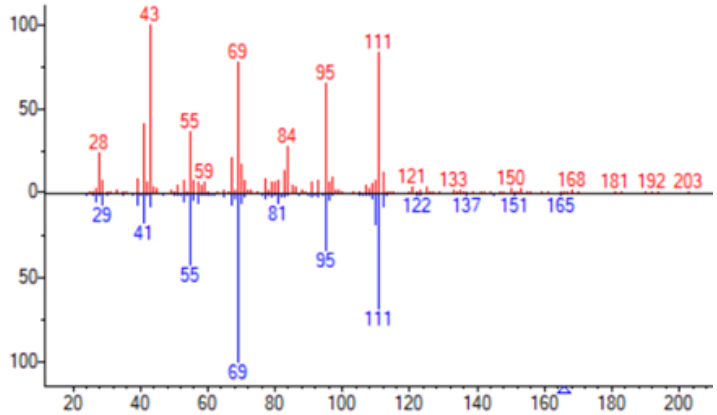
D5	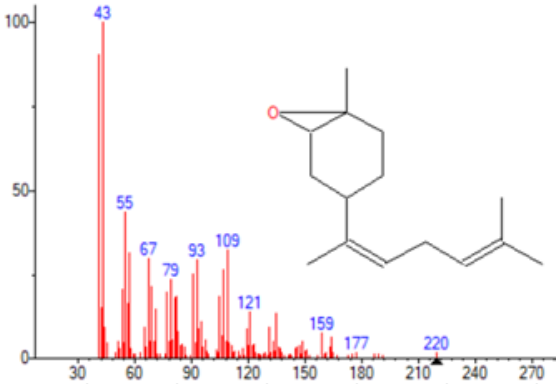	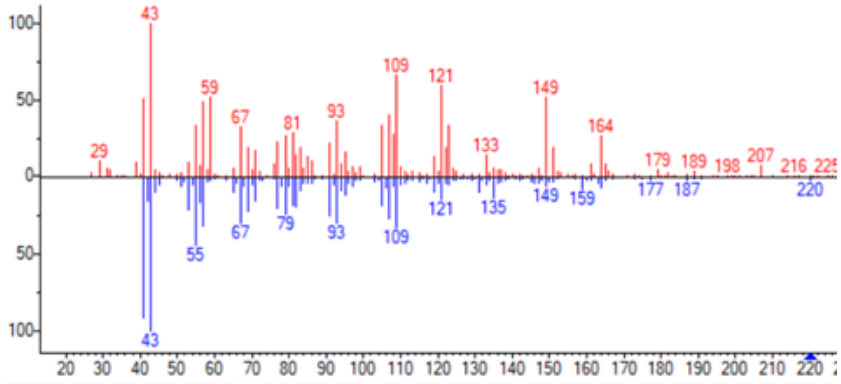
D6	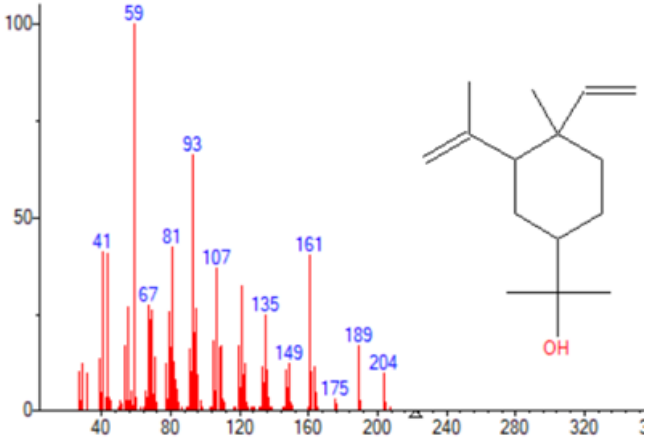	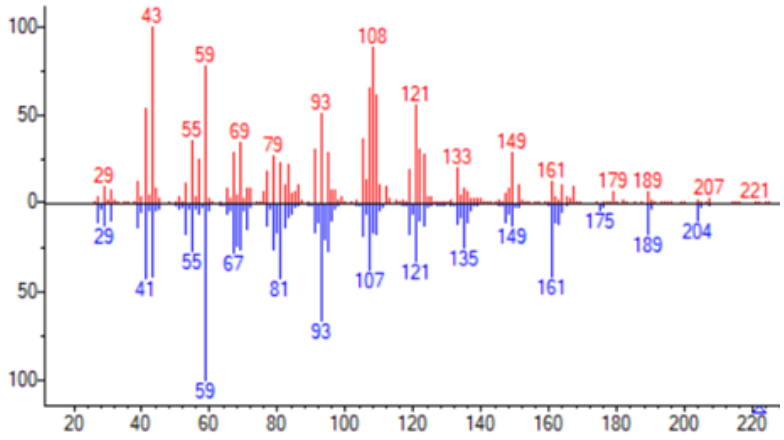

Table S4. MS spectrums of TPs produced from degradation of GSM under the influence of various RS and their match with NIST library (top (red): spectrum from NIST library, bottom (blue): experimentally obtained spectrum)

HO• (solution saturated with N_2O)		
GSM	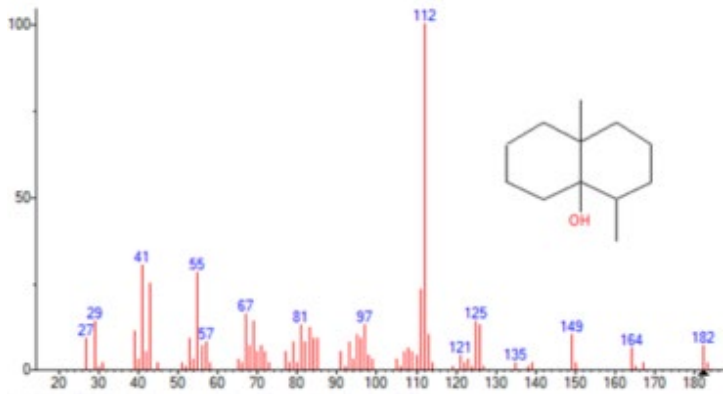	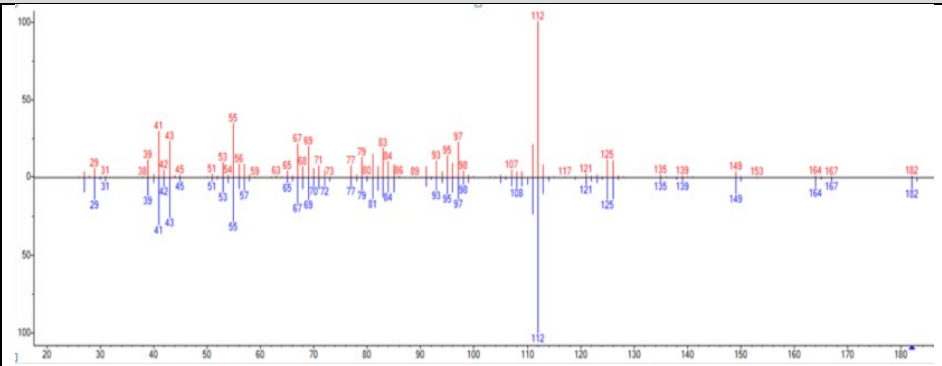
A'1	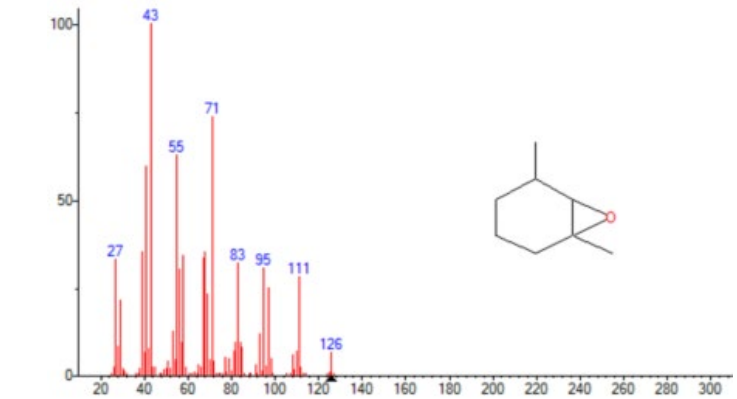	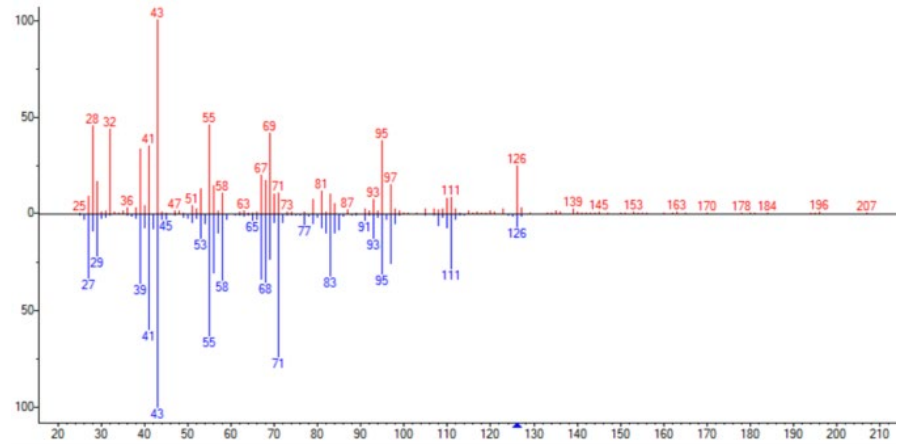

A’2	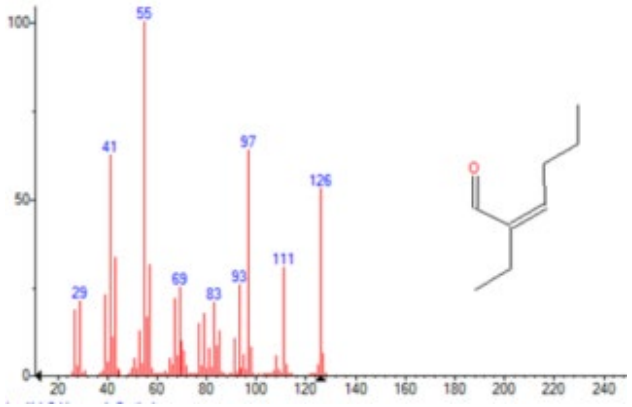	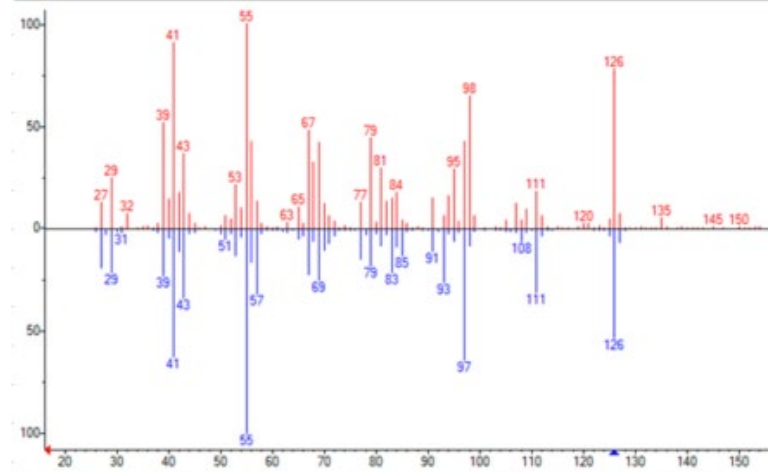
A’3	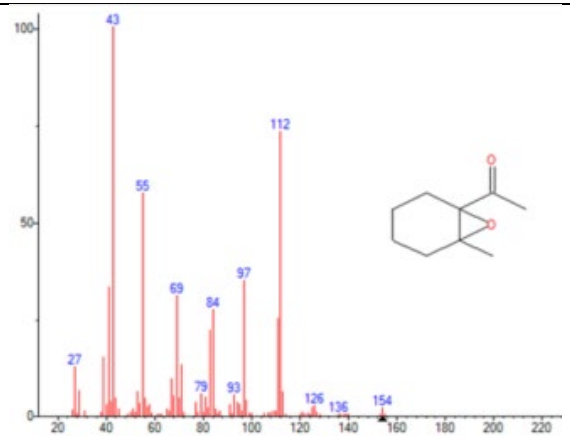	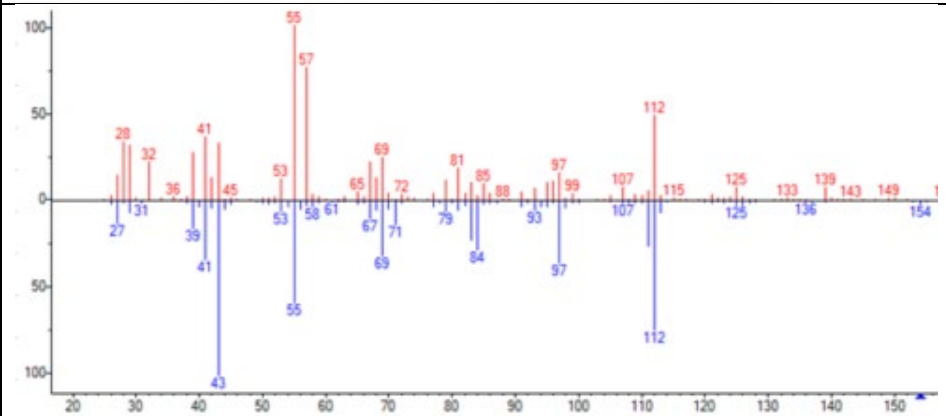

A’4	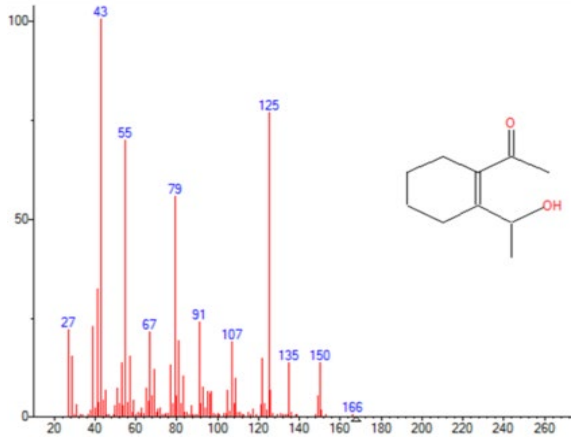	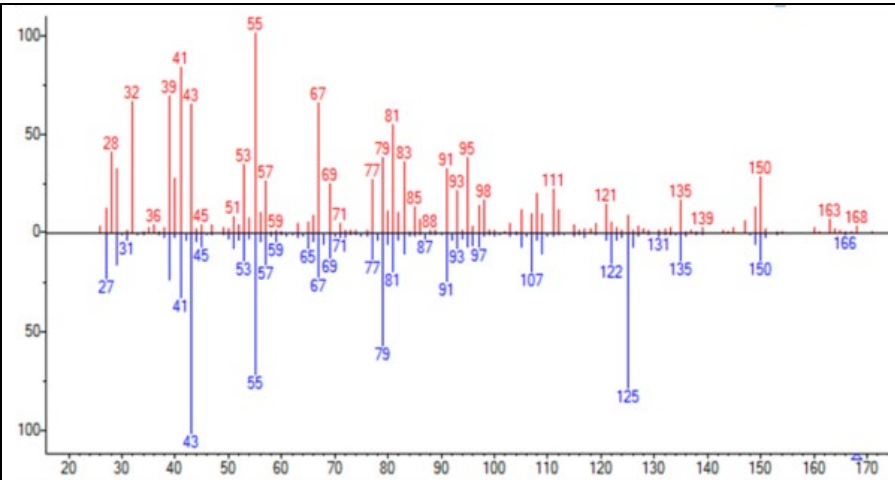
A’5	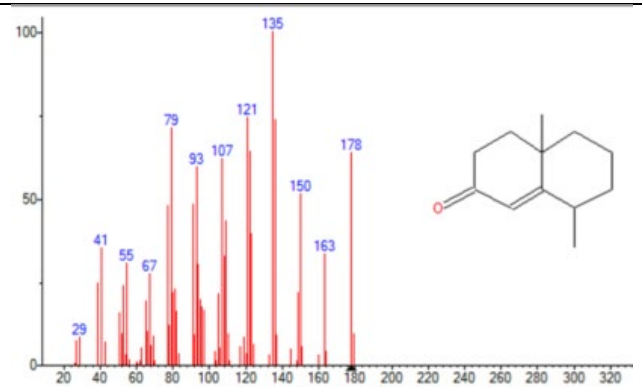	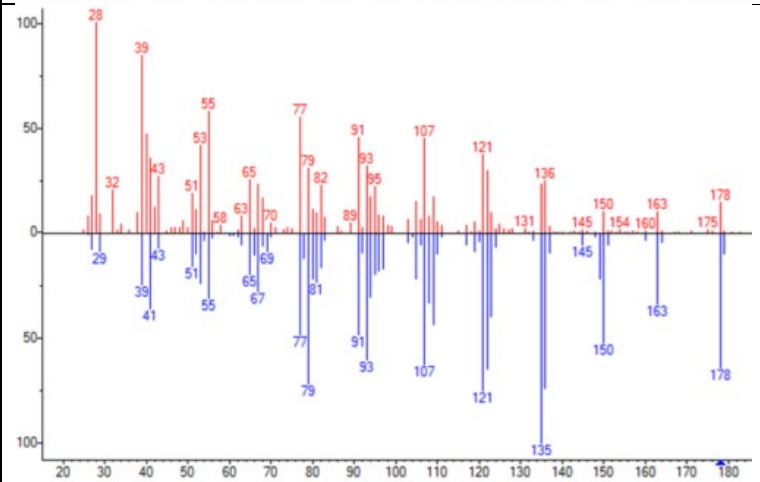

A’6	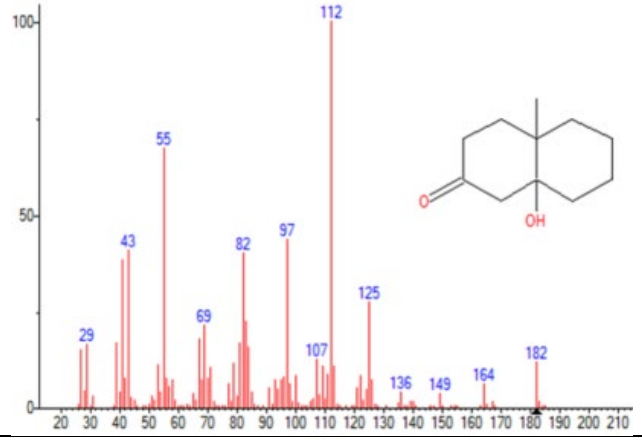	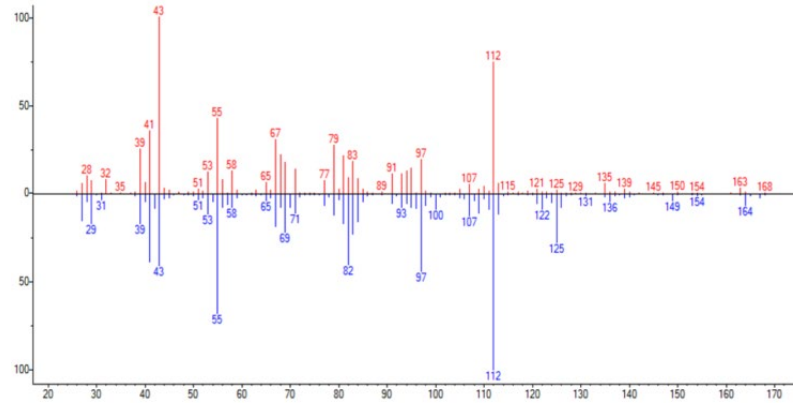
A’7	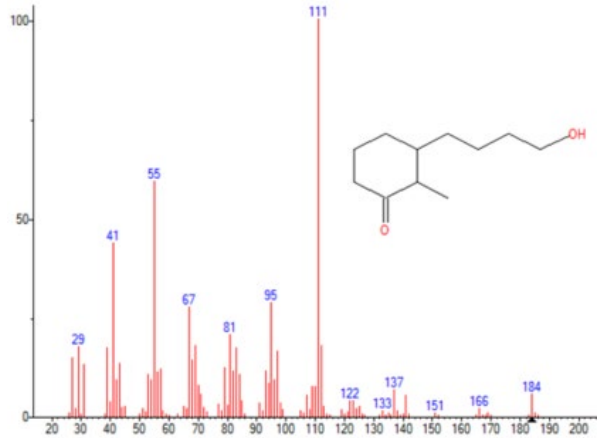	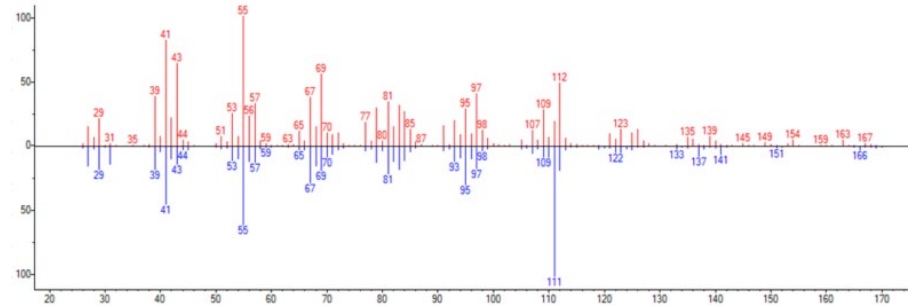
A’8	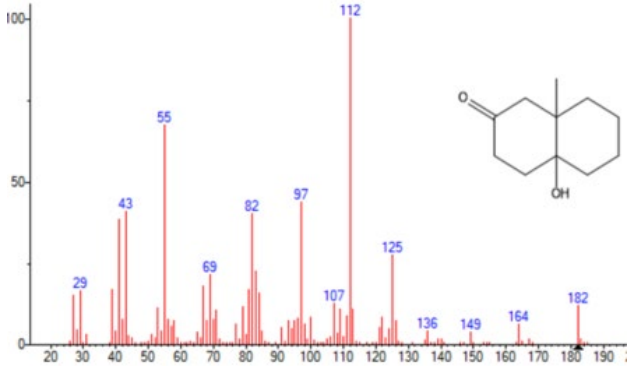	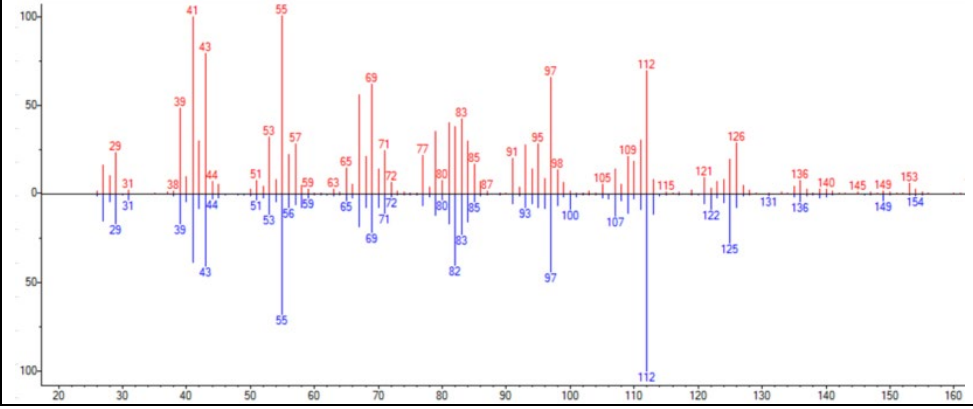

STD CONTAMINATION 1	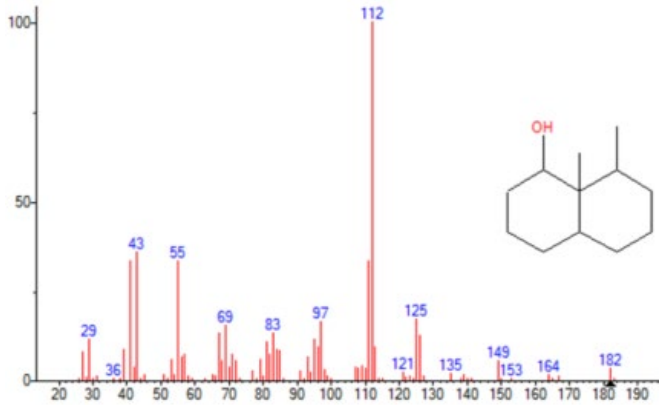	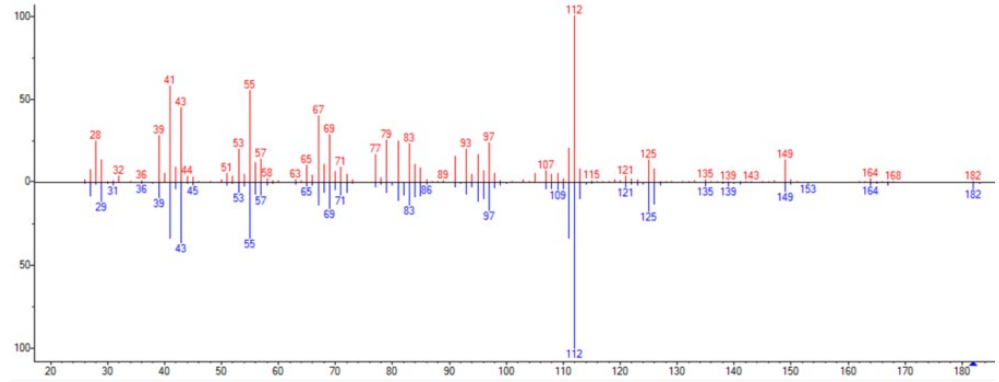
$O_2^{-\bullet}$ / $HO_2^{\bullet}$ (oxygenated)		
B'1	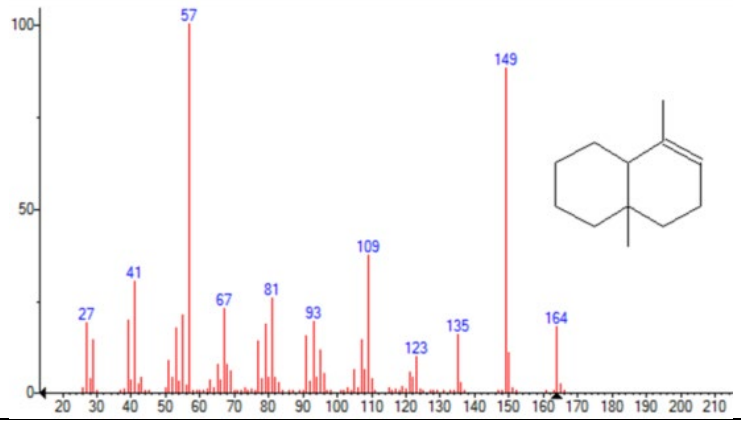	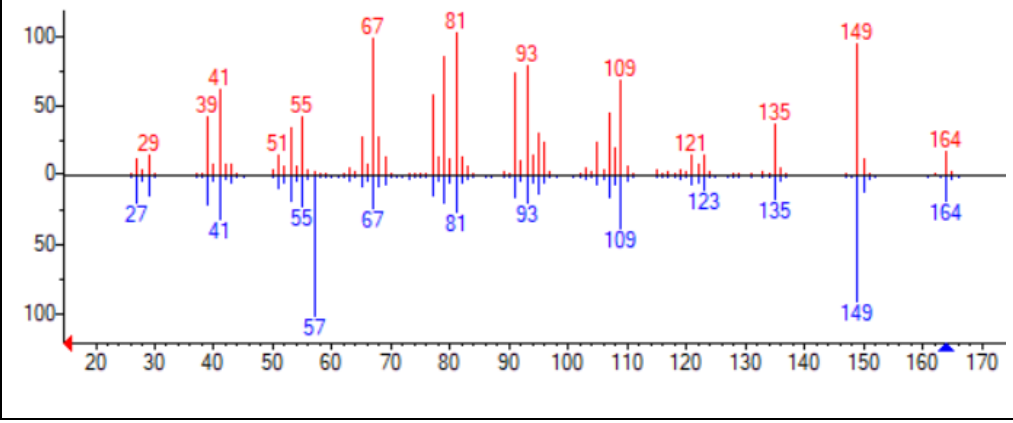

B’2	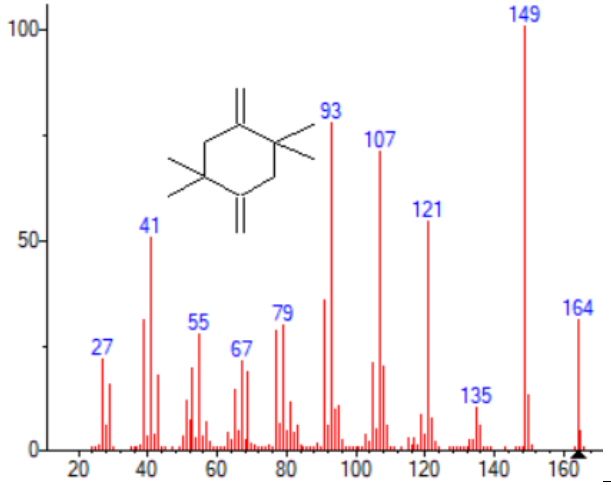	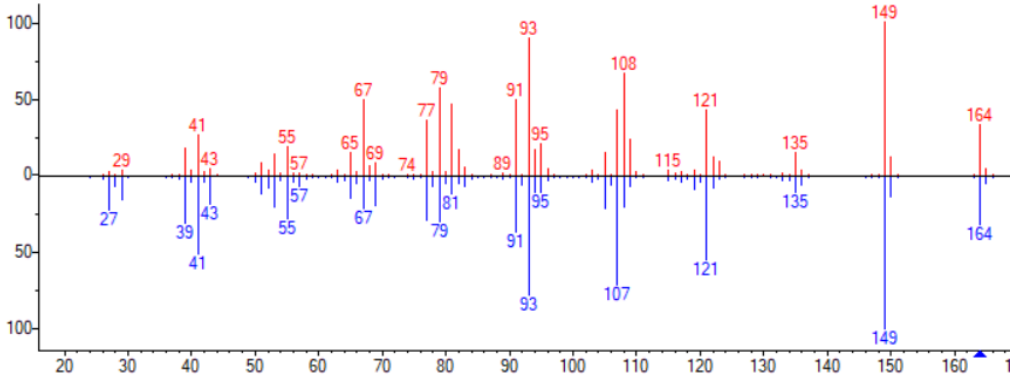
B’3	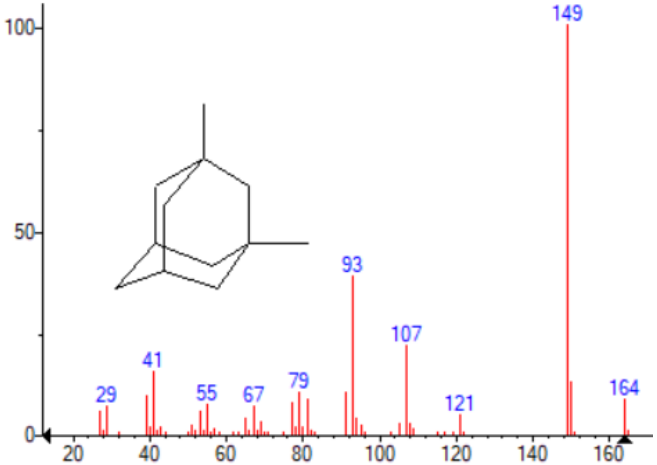	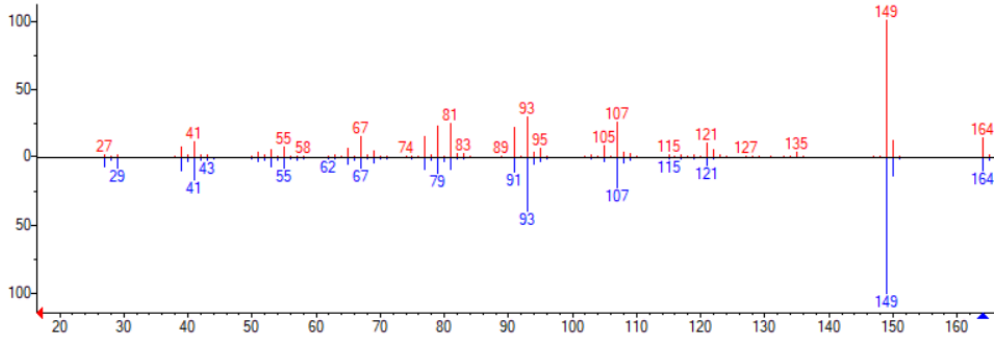

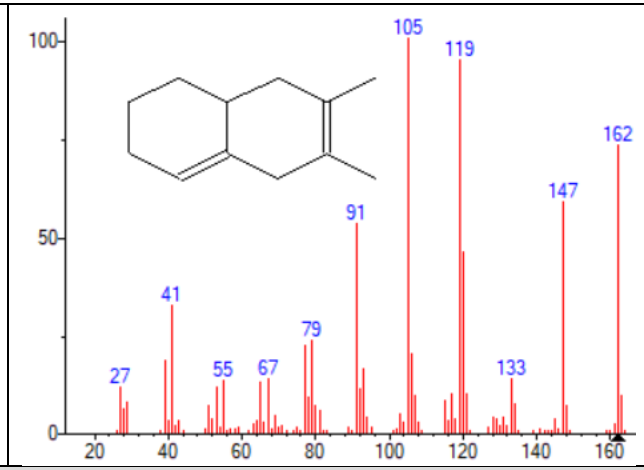

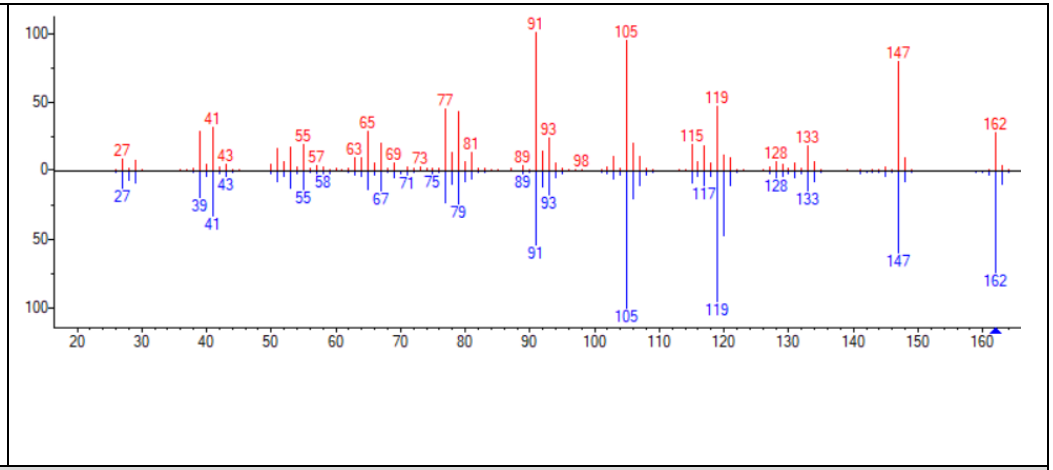

H• (deaerated / TBA /pH 1)

C'1

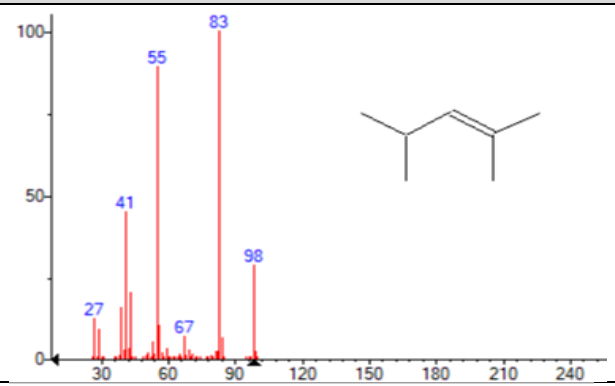

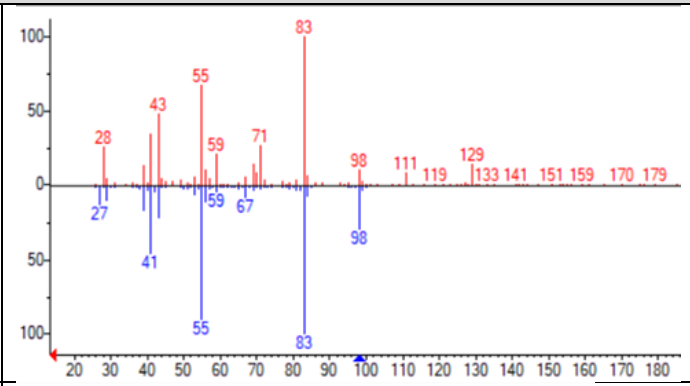

C'2

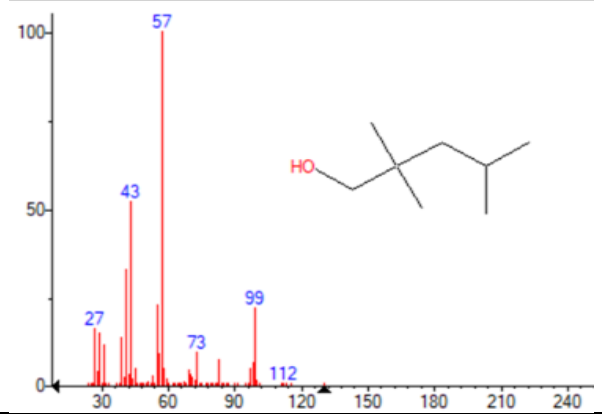

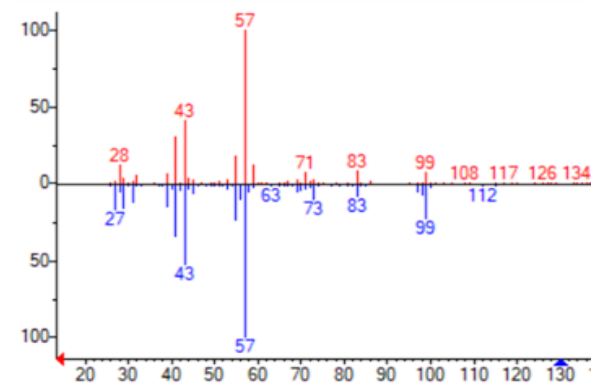

C’3	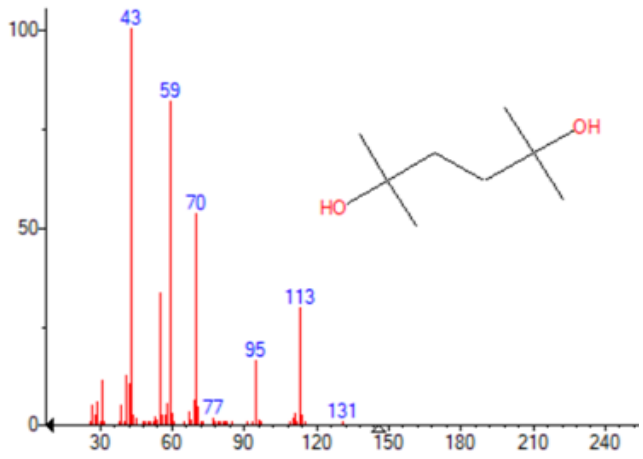 43 59 70 77 95 113 131 HO OH	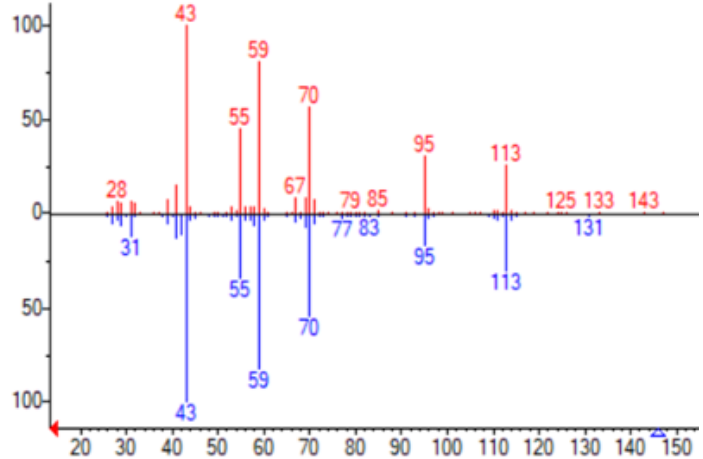 43 59 55 70 67 28 31 79 85 77 83 95 113 125 133 143 131
C’4	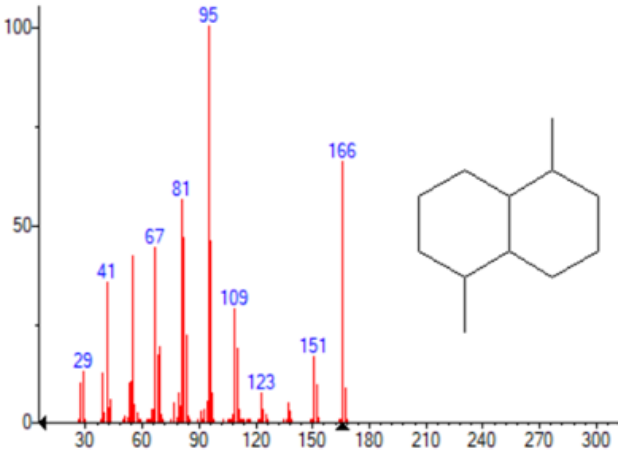 95 166 81 67 41 109 29 151 123	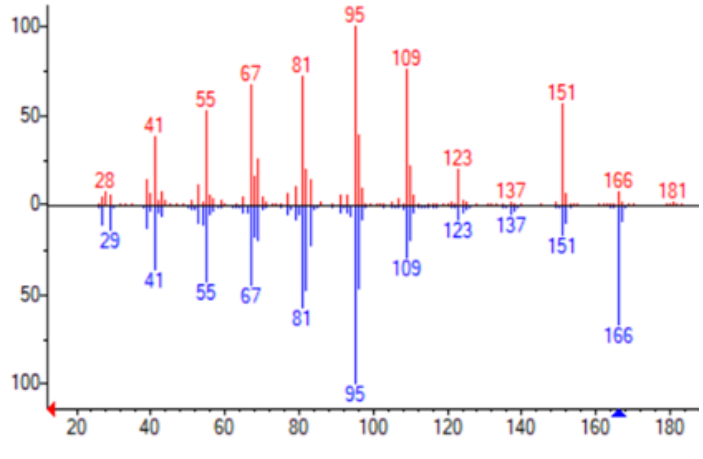 95 109 67 81 55 41 151 123 28 137 166 181 29

C’5	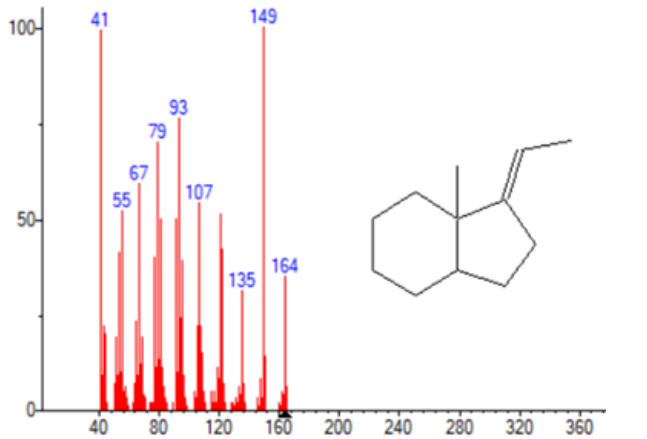	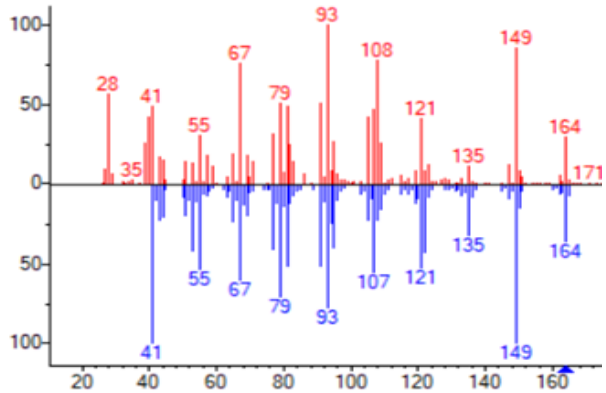
C’6	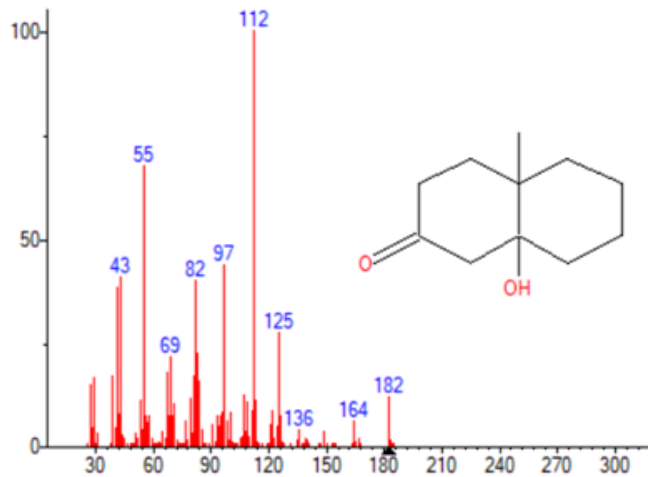	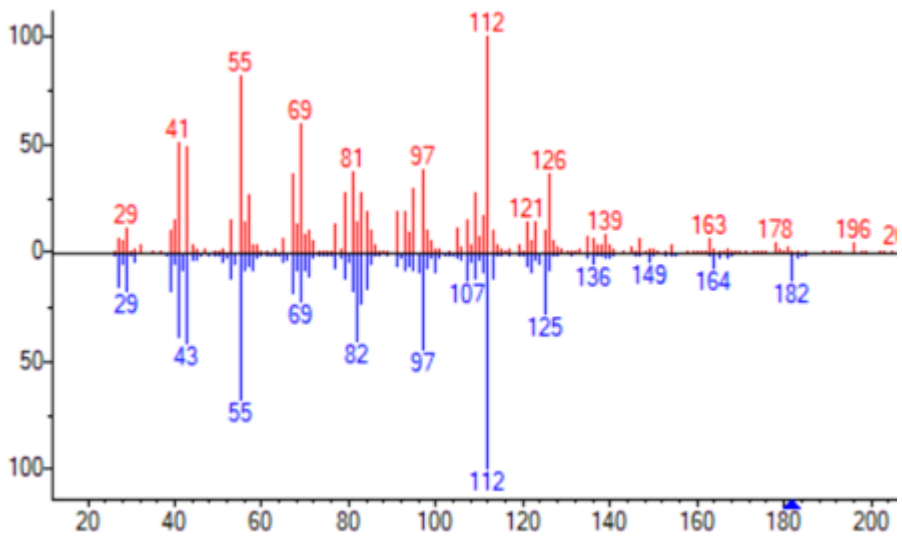
e_{aq}^- (deaerated / TBA)		

D’1

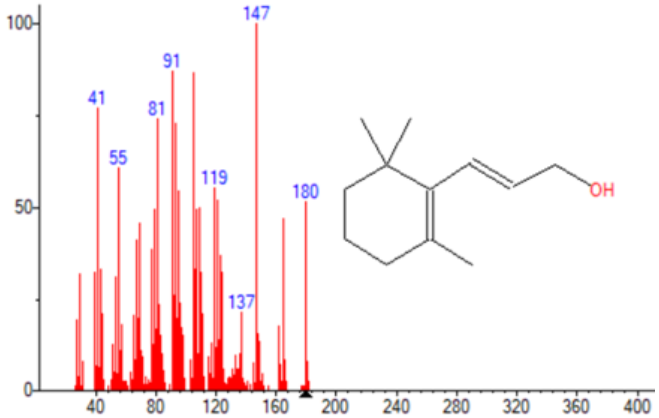
147
91
41
81
55
119
180
137
OH

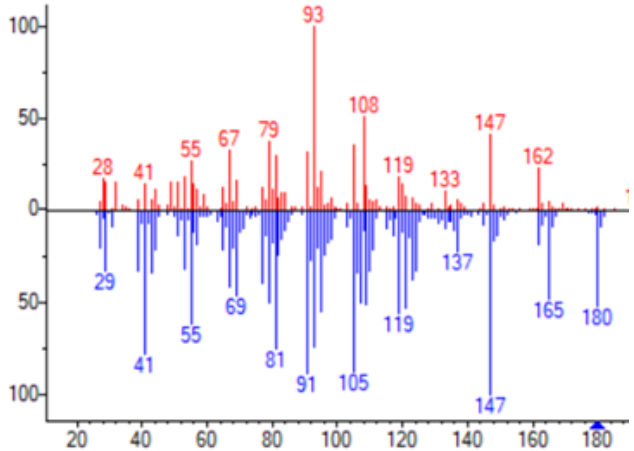
93
108
147
162
28
41
55
67
79
119
133
29
137
69
165
180
119
41
55
81
91
105
147

D’2

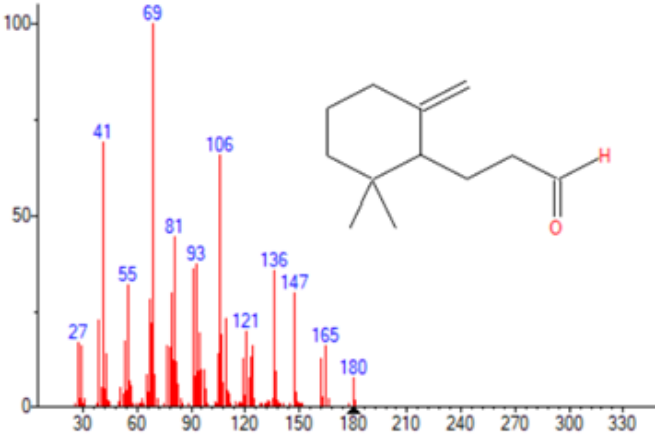
69
41
106
81
93
55
136
147
27
121
165
180
H
O

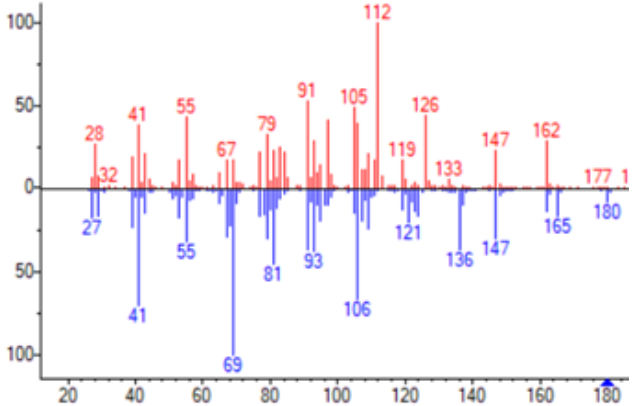
112
91
105
126
41
55
28
79
119
147
162
67
32
133
177
27
180
165
121
55
136
147
81
93
41
106
69

D’3

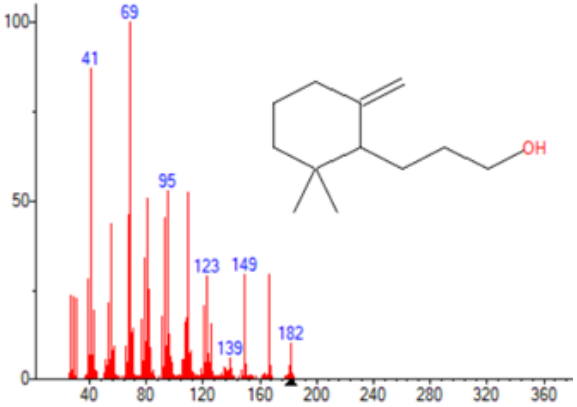
69
41
OH
95
123
149
139
182

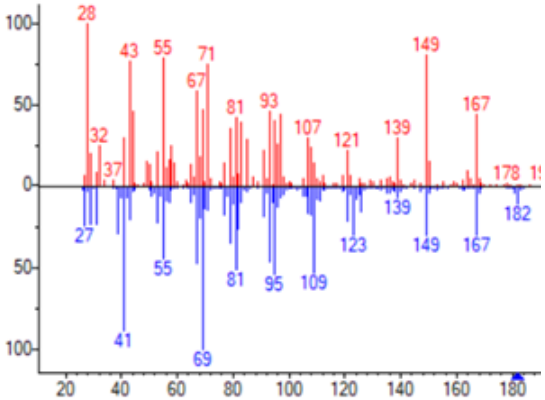
28
43
55
71
149
67
81
93
167
32
107
121
139
37
178
27
139
182
123
149
167
55
81
95
109
41
69

D’4	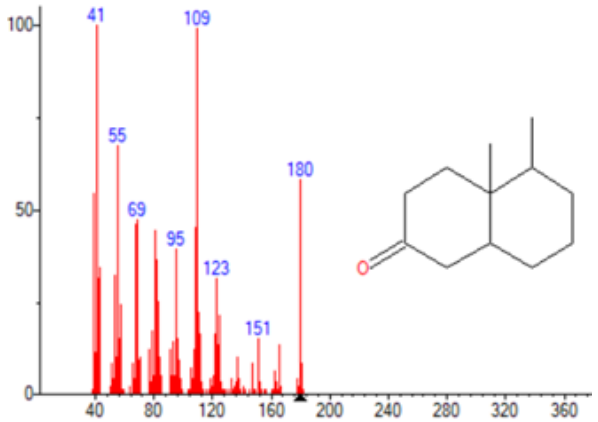	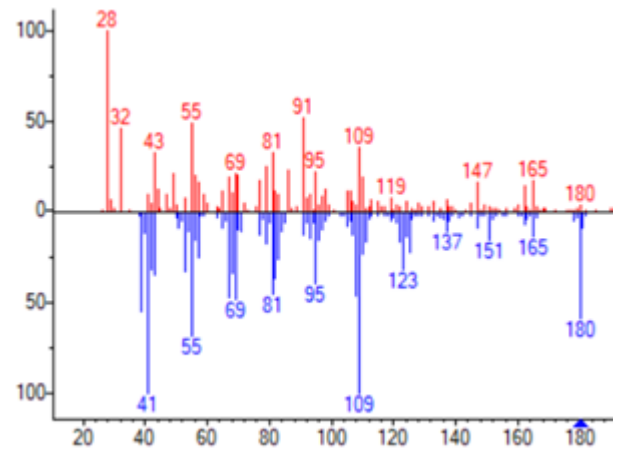
D’5	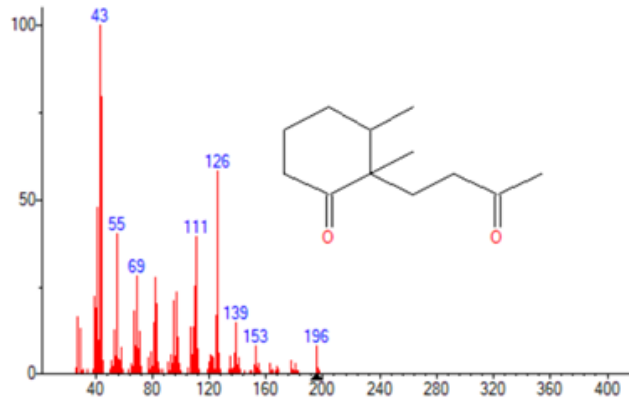	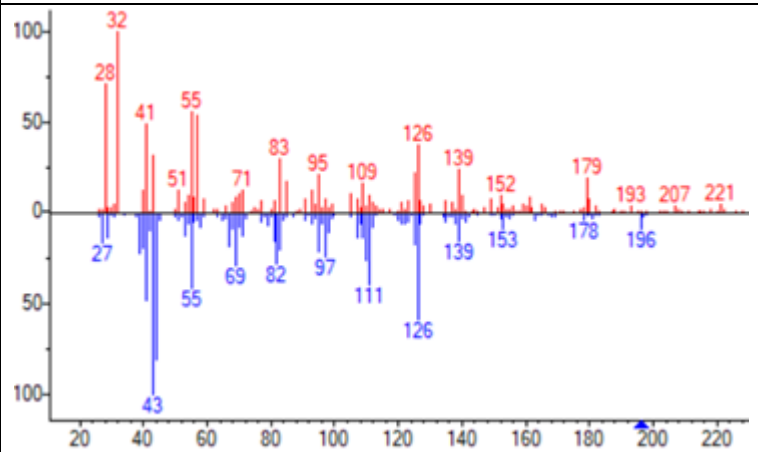
D’6	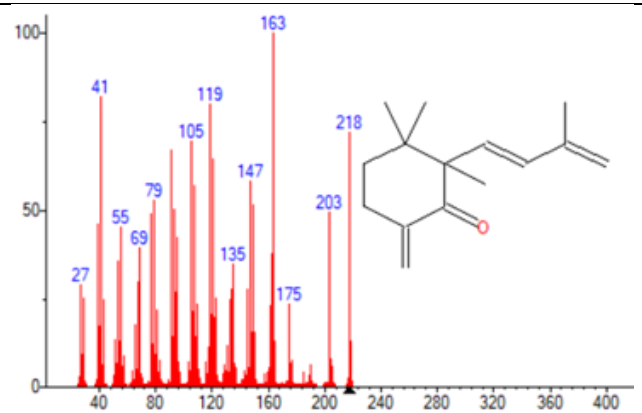	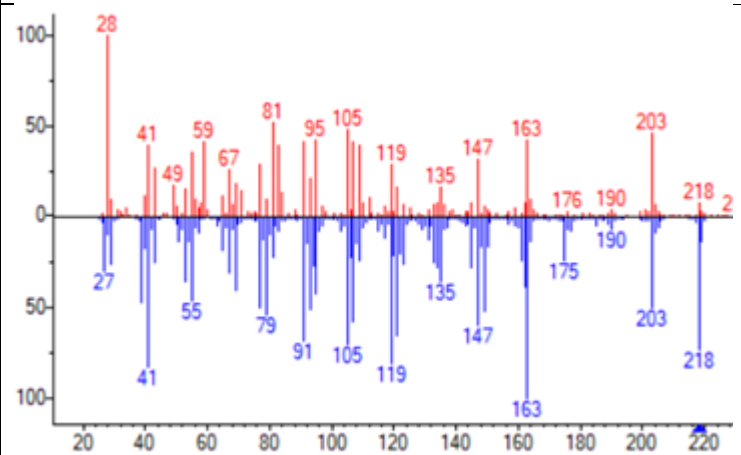

D’7	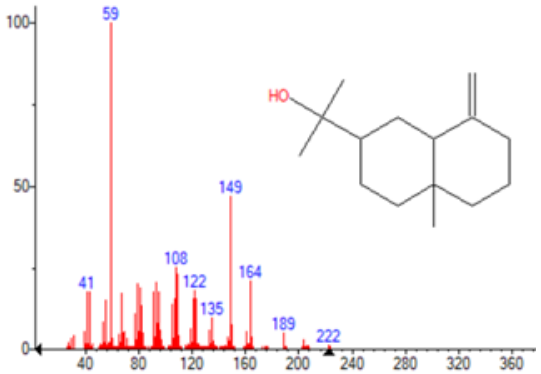	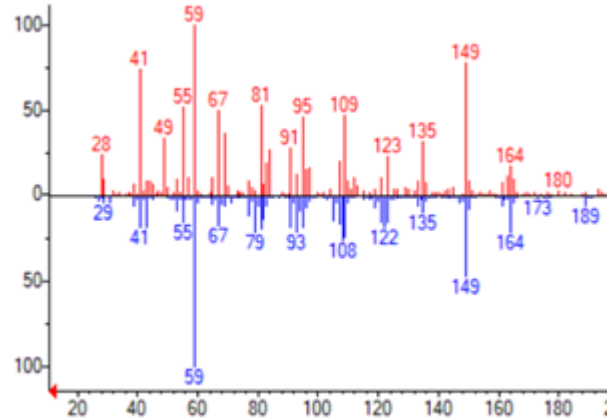
D’8	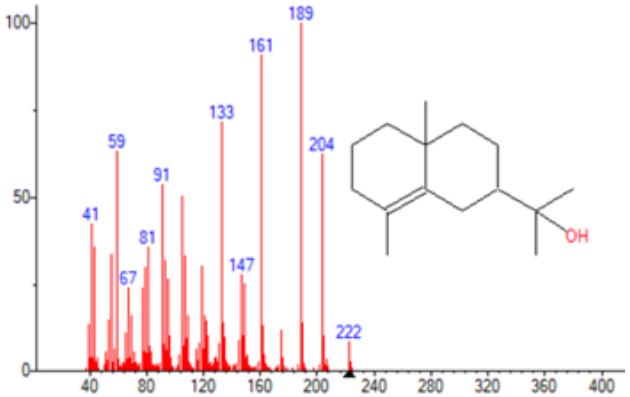	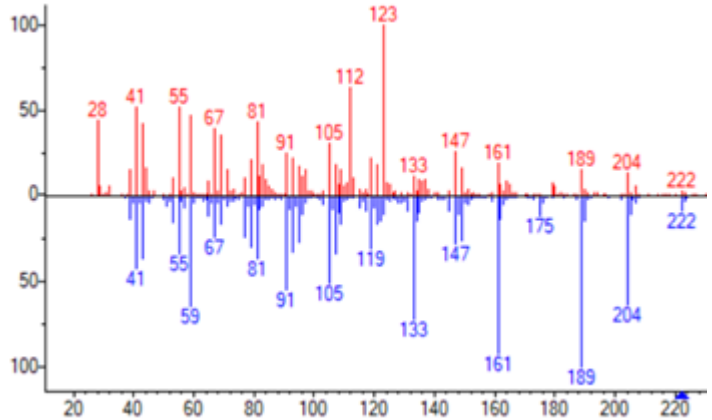
D’9	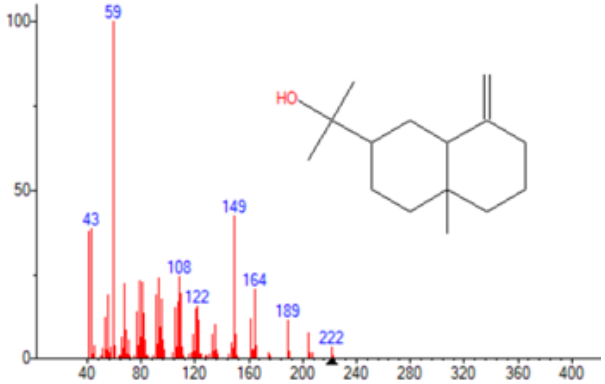	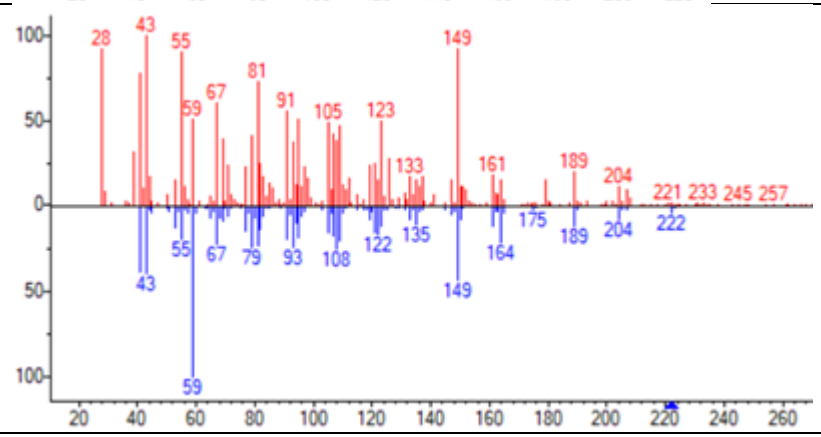

References

[1] H.W. Richter, Radiation Chemistry: Principles and Applications, in: Photochemistry and Radiation Chemistry, American Chemical Society, 1998, pp. 5-33.
[2] R.J.W. J.W.T. Spinks, 7. Water and inorganic aquesous systems, in: An introduction to radiation chemistry, John Wiley and Sons, Inc., New York, 1990, pp. 274.
[3] I. Kruk, Environmental Toxicology and Chemistry of Oxygen Species, Springer Berlin Heidelberg, 1998.